Synthesis of new thiazole-condensed germoles and their derivatives with enhanced electron-deficient properties

(電子欠損特性が向上した新規チアゾール縮環ゲルモールおよびその誘導体の合成)

September, 2023

Sun Weipeng

Hiroshima University

Contents

Chapter 1: General Introduction 1

Chapter 2: Synthesis of thiazole-condensed germoles with enhanced electron-deficient properties 8

Chapter 3: Preparation of D-A copolymers based on dithiazologermole and germaindacenodithiazole as weak electron donor units 29

Chapter 4: Dicyanovinyl-capped thiazologermoles with moderate donor-acceptor interaction as visible photoluminescence turn-on sensors for primary amines 55

Chapter 5: Conclusions 83

References 85

List of publications 99

Acknowledgements 101

Chapter 1: General Introduction

Organic π-conjugated materials have received much attention in the past decade owing to their application to organic electronic devices, such as organic solar cells (OSCs), organic field-effect transistors (OFETs), and organic light-emitting diodes (OLEDs), which exhibit several advantages including low weight, low cost, high flexibility and adjustable electronic states in comparison with inorganic material-based devices. [1-5] The development of high-performance organic semiconductors in devices, which relies on the synthesis of π-conjugated blocks with proper electronic states, is required for the progress of organic electronics. [6] The introduction of a heteroatom bridge to aromatic units such as thiophene, pyridine, furan, selenophene, and benzene is a promising method to tune the electronic state, as shown in Chart 1.1. [7-13] Heteroatom bridges can modify the electronic state not only by electronic effects of the heteroatom but also by steric effects enhancing coplanarity of the aromatic units. In addition, the introduction of substituents on the heteroatom effectively improves the solubility of the compounds in organic solvents. [14]

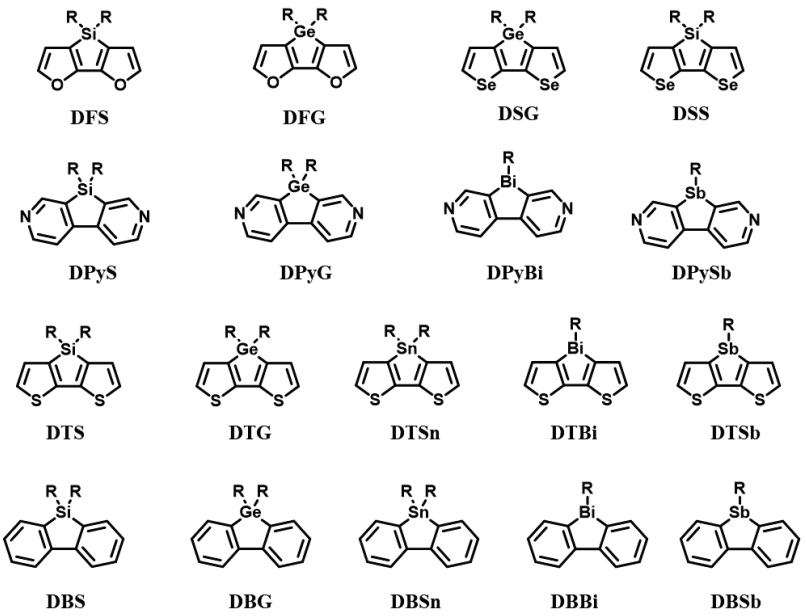

Chart 1.1. Structures of dithiophene-, difuran-, diseleophene-, dibenzene-, and dipyridine-based metalloles.

Group 14 element-bridged aromatic units have been widely reported. Silole (silacyclopentadiene) is known to exhibit lower lowest unoccupied molecular orbital (LUMO) and highest occupied molecular orbital (HOMO) energy levels than those of the carbon-bridged analogue cyclopentadiene, because of σ*-π* conjugation between the silicon σ* orbital and the butadiene π* orbital. [15] In addition, the long Si–C bonds keep the side chains away from core structures, permitting strong π-π stacking of the silole-containing π-conjugated oligomers and polymers in the solid states, which leads to the high carrier-transport properties of the polymer films in OFETs and OSCs. [16, 17]

It is well known that germoles possess electronic states similar to those of siloles; however, a longer C–Ge bond would lead to stronger molecular packing in comparison with siloles. [18] In addition, arylgermanes are more stable towards bases and nucleophiles than the corresponding arylsilanes, which is due to the low electronegativity of Ge much closer to C than that of Si, reducing the polarization of the C–Ge bond. [19] Some germole-containing compounds have been studied including dibenzogermole (DBG) [20], dithienogermole (DTG) [21] and dipyridinogermole (DPyG) [12], which exhibit different electronic properties along the variation of aromatic units, as shown in Chart 1.1. In addition, applications of germole-based π-conjugated polymers as semiconductors in OSCs and OFETs have been reported with decent device performances. [16, 22]

With the development of small aromatic molecules bearing a heteroatom-bridge, their polymerization has been studied to form conjugated polymers for the application to organic electronic devices. In particularly, since our group synthesized dithienosilole (DTS) and its germanium congener DTG for the first time, DTS and DTG-based polymers have been widely reported, because of abovementioned advantages of enhanced π-π stacking in the solid states and lower LUMO energy levels relative to cyclopentadiene-based analogue polymers. Easy chemical modification of DTS and DTG such as lithiation, halogenation and stannylation is also a reason for the fact that these units have been extensively employed as the building units for conjugated

polymers. [21, 23] In 2008, Tobin J. Marks's group [24] reported a family of silole-containing polymers (TS6, TS6T1, TS6T2, BS8, BS8T1 and BS8T2), as shown in Figure 1.1 and it was demonstrated that those polymers exhibited promising performances as active materials in OFETs. According to the theoretical and optical characterization data, it was suggested that silole-based polymers have higher degree of π-delocalization than the carbon counterparts. Christoph J. Brabec's group and our groups independently synthesized donor-acceptor (D-A) type polymers (PDTS-BT and PDTG-BT) that are composed of DTS/DTG and 2,1,3-benzothiadiazole (BT), which exhibited not only OFET performance, but also OSC performance. [19, 21, 25] On the other hand, more expanded π-conjugated structures, including silaindacenodithiophene (SIDT) [26] and germaindacenodithiophene (GIDT) [27], were also synthesized. These ladder-type SIDT- and GIDT-based copolymers generally possess strong intermolecular π-π stacking in the solid state and facile electron delocalization and hence have been applied in OFETs and OSCs. [28, 29] In particular, PSIDT-BT and PGIDT-BT copolymers exhibit higher hole mobility and power conversion efficiency in OTFTs and OSCs, respectively, than PDTS-BT and PDTG-BT copolymers.[23, 30] Structures of abovementioned polymers are shown in Figure 1.1.

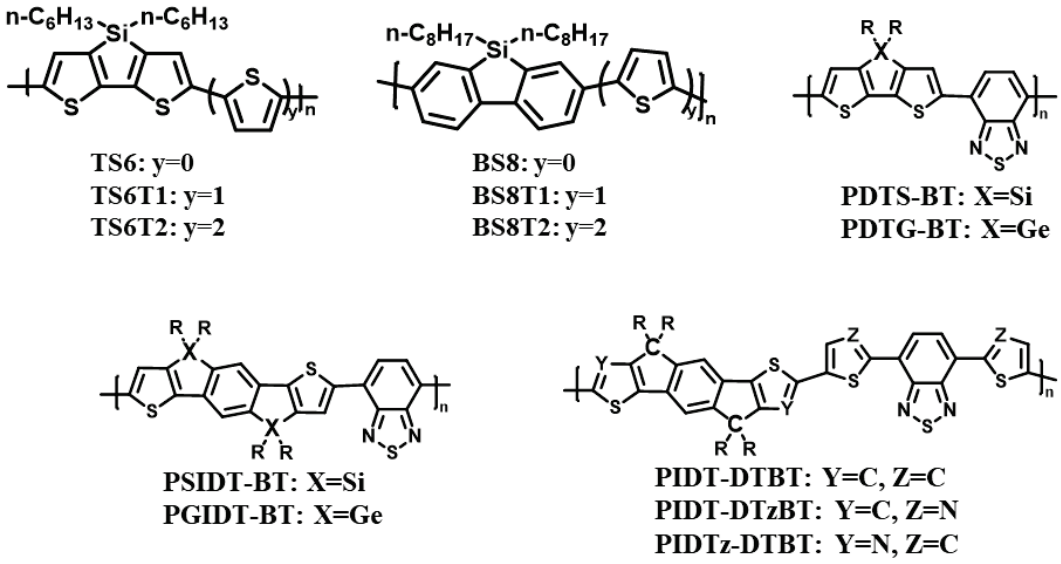

Figure 1.1. Structures of the Group 14 element-based π-conjugated polymers.

As derivatives of the electron-donating Group 14 element-bridged bithiophenes, a new class of compounds containing thiazole units have been studied as weak electron donors. These units can enhance electron-transporting properties when combined with electron acceptors, although still some donor-acceptor interaction is observed in the copolymers. Besides the advantage of enhanced electron-deficient properties, thiazole-containing compounds generally show a high degree of coplanarity, which is due to intramolecular noncovalent bond interactions such as N–H or N–S bond interactions.[31] Several thiazole-containing compounds have been reported, such as cyclopentadithiazole (CDTz) [32], indacenodithiazole (IDTz) [33], 4,7-di(thiazol-2-yl)-2,1,3-benzothiadiazole (DTzBT) [34], bithiazole imide (BTzI) [35], and dithiazolylthienothiophene bisimide (TzBI) [4], as shown in Chart 1.2. Polymers with these thiazole-containing units have been studied as semiconductors in OFEFs with high carrier mobilities. [36] For example, IDT- and IDTz-ladder-type monomers were copolymerized with 4,7-di(thien-2-yl)-2,1,3-benzothiadiazole (DTBT) or DTzBT units to obtain ambipolar polymers PIDT-DTBT, PIDT-DTzBT [37], and PIDTz-DTBT [33], as shown in Figure 1.1. Notably, these thiazole-based polymers showed improved electron-transporting properties compared with that of thiophene congeners, indicating that introducing weak donor units in D-A polymers is beneficial to generate efficient electron-transporting materials.

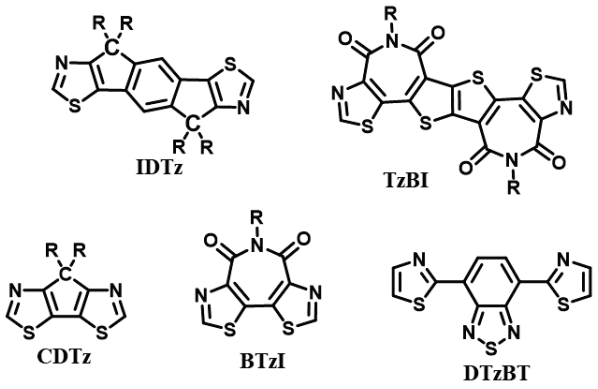

Chart 1.2. Structures of thiazole-containing compounds.

In Chapter 2, new thiazole-condensed single and double germole derivatives

(DTzG and GIDTz) were prepared as weak donor units by the reactions of respective lithiated thiazole compounds with dichlorodioctylgermane (Figure 1.2). The compound structures were verified by ^{1}H NMR, ^{13}C NMR, and mass spectral measurements. The single-crystal structure of brominated GIDTz shows high planarity of the fused ring system. The optical and electrochemical properties of DTzG and GIDTz derivatives indicate that the derivatives possess enhanced electron deficiency compared with thiophene-based germole congeners reported previously. This is supported by density functional theory (DFT) calculations that reveal lower-lying HOMO and LUMO for the thiazole-condensed germoles than the thiophene-condensed congeners.

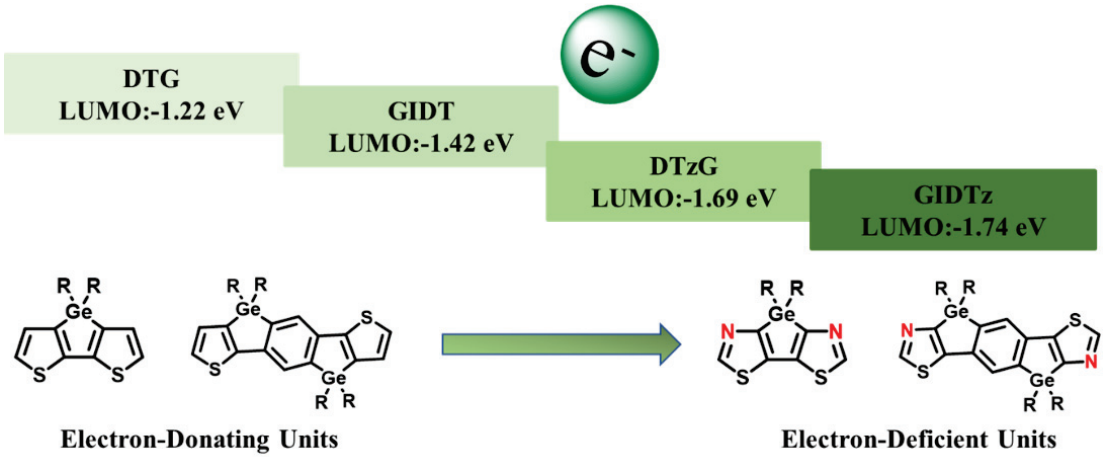

Figure 1.2. Schematic diagram of the structures and HOMOs/LUMOs of germoles compounds, described in Chapter 2.

In Chapter 3, distannylated DTzG and GIDTz were copolymerized with dibrominated 2,1,3-benzothiadiazole and 4,7-di(thiazol-2-yl)-2,1,3-benzothiadiazole to produce four new donor-acceptor conjugated copolymers (Figure 1.3). The optical, electrochemical, and thermal properties of the copolymers were characterized, and intramolecular charge transfer was evaluated on the basis of solvatochromic behavior in the photoluminescence spectra. DFT calculations revealed that these thiazole-containing copolymers exhibited lower HOMO and LUMO energy levels than those of thiophene-based congeners PDTG-BT and PGIDT-BT (Figure 1.3), and this finding agreed with the experimental results. The intramolecular noncovalent S–N and N–H

bond interactions and the effects of the bridging atom (C or Ge) on the HOMO and LUMO energy levels were also suggested by the DFT calculations.

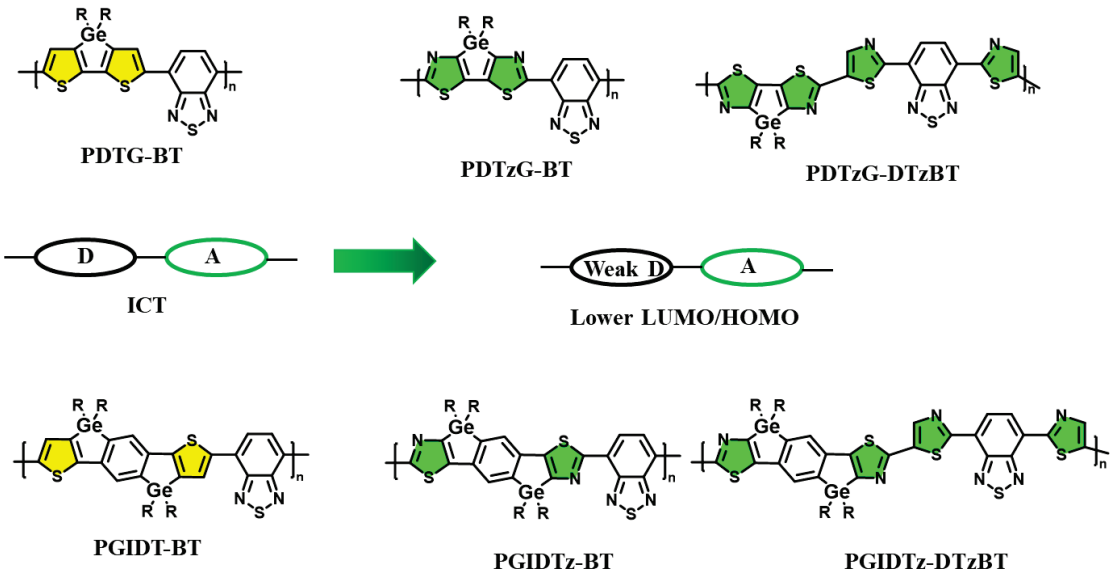

Figure 1.3. Schematic diagram of the structures of copolymers, described in Chapter 3.

In Chapter 4, dicyanovinyl-capped dithiazologermoles (DTzG-DCV and GIDTz-DCV) were synthesized (Figure 1.4), and their optical and electrochemical properties were investigated. Both DTzG-DCV and GIDTz-DCV showed solvatochromism, exhibiting red shifts of the photoluminescence (PL) bands with increasing solvent polarity from toluene to DMF, likely due to intramolecular donor–acceptor interaction. Moreover, they served as selective PL sensors, with spectral changes in the presence of amines and fluoride and iodide ions, but not other halogen ions, in solution. DTzG-DCV and GIDTz-DCV underwent a quick and high-yield reaction with *n*-butylamine to give imine derivatives, accompanied by PL color changes. Similar color changes were observed even in the solid state with *n*-butylamine and *n*-hexylamine. In contrast, reactions with secondary and tertiary alkylamines caused no obvious changes in PL color. The color changes are visible to the naked eye under irradiation with a portable UV lamp at 365 nm, and thus DTzG-DCV and GIDTz-DCV can be used for the quick and selective sensing of primary amines.

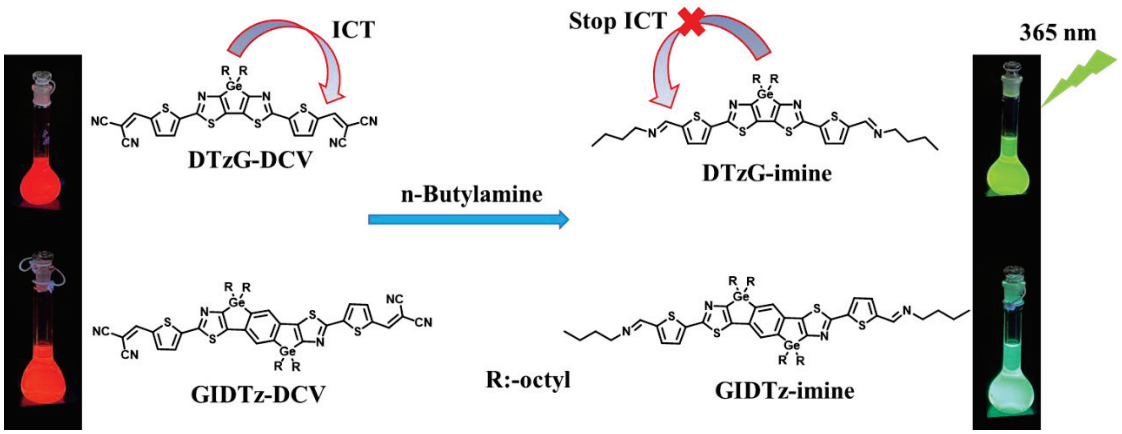

Figure 1.4. Schematic diagram of the reaction of stopping ICT, described in Chapter 4.

Chapter 2: Synthesis of thiazole-condensed germoles with enhanced electron-deficient properties

1. Introduction

Previously, we reported the first synthesis of DTS as a typical heteroatom-bridged thiophene-based compound. [38] The introduced Si atom shows distinct electronic perturbation by fixing bithiophene unit to be planar and by orbital interaction between the silicon σ* and the butadiene π* orbital, namely σ*-π* conjugation, [39, 40] which lead to the low-lying LUMO. Based on these interesting properties, DTS units are extensively used as building units of π-conjugated oligomers and polymers for the application to OLEDs, OFETs, [11, 41] and OSCs. [42-45] Our group has also synthesized several element-bridged bithiophenes with Ge, Sn, Sb and Bi, as shown in Chart 2.1. [8, 10, 11, 18, 21] For DTS and DTG, the long C-Si and C-Ge bonds keep the side chains away from DTS and DTG core structure, permitting strong π-π stacking of DTS- and DTG-containing π-conjugated polymers in the solid state, leading to high carrier-transporting properties of the polymer films in OFETs and OSCs, despite the existence of substituents on the bridging element. [16, 46, 47]

Expanded bridged π-conjugated systems with ladder structures, including indacenodithiophene [48], dipyrrole [49], digermole [29] and disilole [50] have been also studied as the components of p-type polymer semiconductors (Chart 2.2). For the development of electron-deficient components for n-type materials, introduction of electron-deficient carbonyl and dicyanovinylene as the bridging units was examined in IDD [51] and M2 [52] in Chart 2.2. Replacement of thiophene by thiazole also led to n-type π-conjugated units as for IDD and IDTz. [33]

In recent years, we synthesized dipyridinometalloles, (DPyS, DPyG, DPySb and DPyBi in Chart 2.1) with enhanced electron-deficient properties and interesting solid-state phosphorescence. [12, 13] However, dipyridinometalloles are hard to polymerize, except for coordination polymerization, as they possess no suitable reactive sites. [13]

On the other hand, thiazole-containing compounds, such as IDD and IDTz, are anticipated as promising electron-deficient building units for conjugated polymer formation. The past few years, thiazole-based compounds with N, [49] P, [53] and As [54] bridging elements have been also reported as new electron-deficient materials and their use as semiconductor materials for OFETs has been explored. However, no synthetic studies of dithiazole-condensed silole and germole have been reported, although a theoretical study predicted good photovoltaic properties of a dithiazole-containing compound. [55]

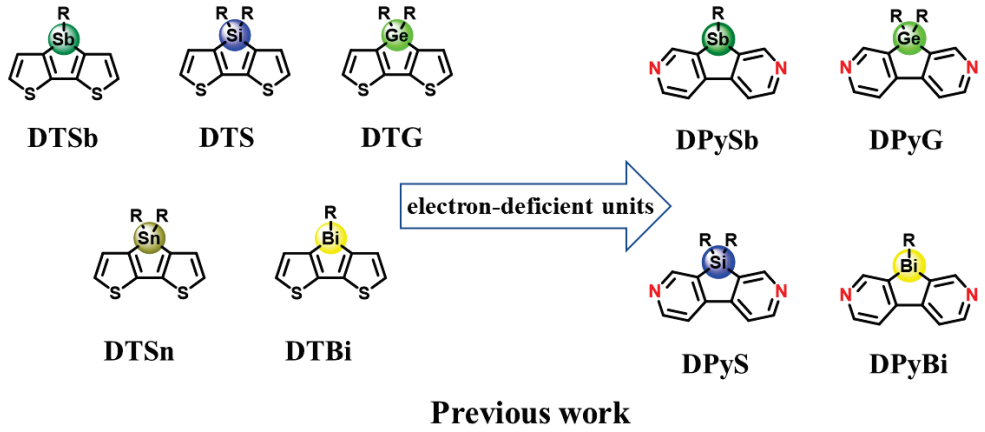

Chart 2.1. Structures of dithiophenemetalloles and dipyridinometalloles.

In this Chapter, the author reported the first synthesis of dithiazole-condensed germoles (DTzGs) and germaindacenodithiazoles (GIDTzs), which possess enhanced electron deficiency and extended conjugation. These are new germole-containing derivatives and it is interesting to us to investigate how germole affects the electronic states of these compounds and how replacement of thiophene rings of previously reported dihtienogermoles by thiazole enhance the electron deficiency. We also report the synthesis of new conjugated polymers with DTzG and GIDTz units.

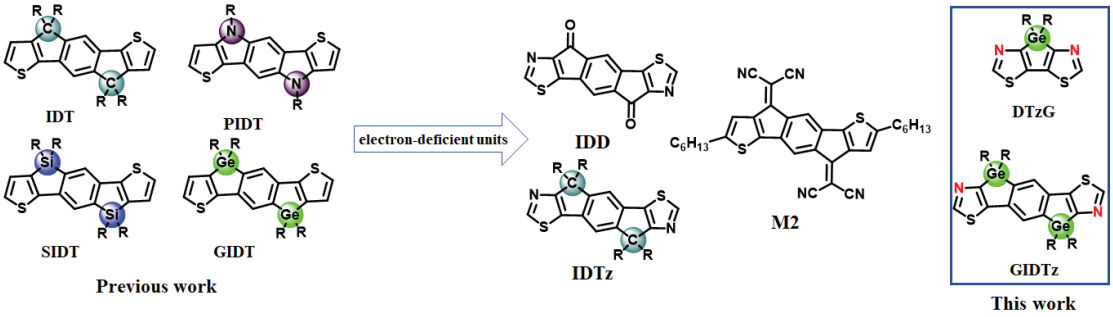

Chart 2.2. Structure of ladder π-conjugated compounds

2. Results and discussion

2.1. Synthesis and characterization

The synthesis of new compounds is presented in Scheme 2.1 and the details are given in Supporting Information and the structures of target compounds were characterized by NMR and mass spectra (Figure 2.7-2.18). 2-(triisopropylsilyl)thiazole (**2a**), 5-bromo-2-triisopropylsilylthiazole (**3a**), 2,2'-bis-triisopropylsilyl-4,4'dibromo-5,5'-bithiazole (**4a**) were obtained as reported in the literature. [56] Compound **1b** was prepared by the reaction of **3a** and LDA with halogen dance at -78 °C, [57] followed by stannylation. Compound **1b** was then subjected to Stille cross-coupling reaction with 1,4-dibromo-2,5-diiodobenzene using $Pd(PPh_3)_2Cl_2$ as the catalyst. The reaction of **4a** with *n*-butyllithium followed by treatment of the resultant dilithiated compound with dichlorodioctylgermane gave triisopropylsilyl (TIPS)-substituted TIPS-DTzG in 40% yield, which was desilylated with tetrabutylammonium fluoride (TBAF) to give DTzG in 99% yield. Ladder compounds GIDTz and TIPS-GIDTz were synthesized in the same manner as above in 96% and 50% yield, respectively. We also attempted to prepare thiazole-condensed siloles by the reactions of dilithiated **4a** and dichlorodioctylsilane under the same conditions. However, no siloles were obtained. Lowering the reaction temperature from -78 °C to -100 °C and employing difluorodioctylsilane instead of dichlorodioctylsilane did not afford siloles.

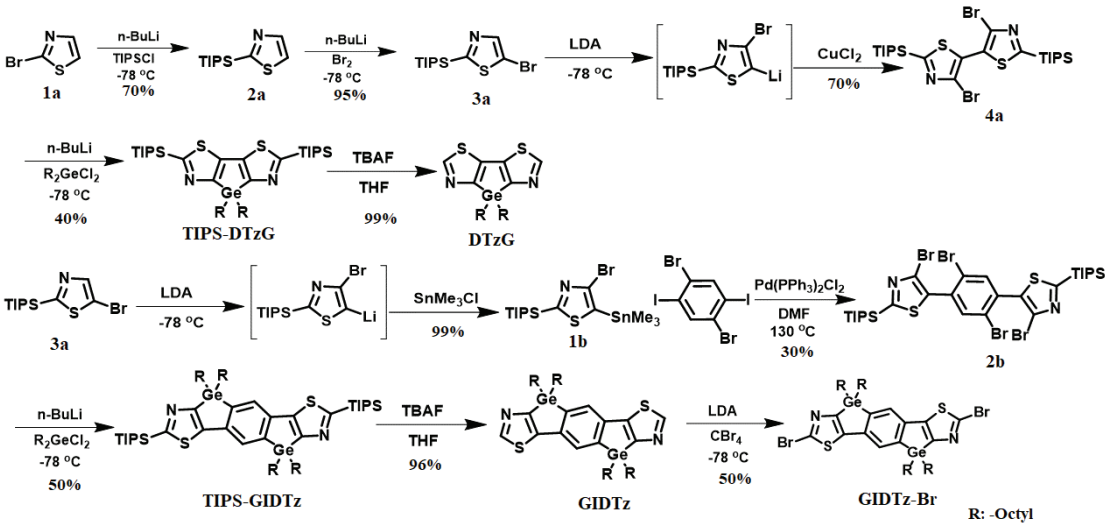

Scheme 2.1. Synthesis of thiazole-condensed germoles.

2.2. Crystal structure of brominated GIDTz

In order to study the solid packing of thiazole-condensed germoles, the single-crystal structure of brominated GIDTz (GIDTz-Br) was analyzed by an X-ray diffraction study, which was obtained by the slow solvent evaporation from the dichloromethane/methanol solution at room temperature. Figure 2.1 depicts the crystal structure and the molecular packing of GIDTz-Br. The fused five-membered rings exhibit high planarity with a small dihedral angle of 1.59° as shown in Figure 2.1(a), and the endo cyclic bond distance and angle of the germanium atom are 1.96 Å (C-Ge) and 87.24° (C-Ge-C), respectively. The molecular packing of brominated GIDTz indicates close stacking between the thiazole rings of the slipped π-units with the interplane distance of 3.66 Å, as shown in Figure 2.1(b). Crystal structures of similar carbon bridged ladder compounds, IDTO2-Br and IDTO4-Br, were reported and high planarity was demonstrated (Chart 2.3). Compounds IDTO2-Br and IDTO4-Br have no π-π stacking with intermolecular distances of 4.000 and 4.430 Å. It is likely that interdigitation of octyl chains observed in the packing structure enhances the intermolecular interaction of GIDTz-Br (Figure 2.1(c)).

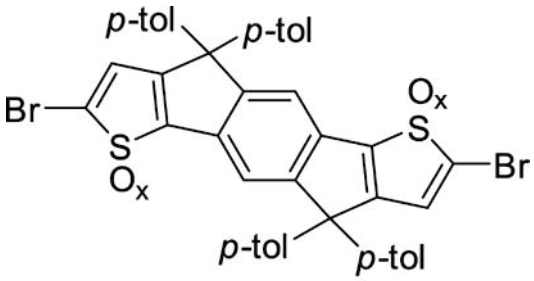

IDTO2-Br: x=1
DTO4-Br: x=2

Chart 2.3. Structures of IDTO2-Br and IDTO4-Br.

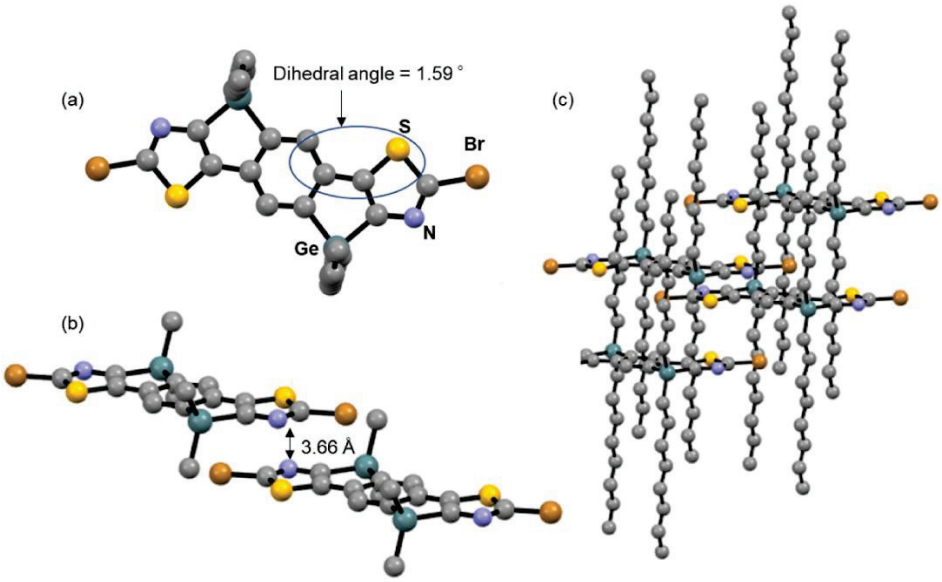

Figure 2.1. Single crystal of (a) molecular, (b) π-π stacking, and (c) packing structures of GIDTz-Br. Hydrogen atoms are omitted for clarity. In (b), only C-Ge bonds are shown for octyl groups.

2.3. Optoelectronic properties

UV-vis absorption spectra of DTzG, TIPS-DTzG, GIDTz, and TIPS-GIDTz in tetrahydrofuran (THF) are shown in Figure 2.2(a), and the data are summarized in Table 2.1. The absorption maxima are at 347, 327, 367 and 353 nm for TIPS-DTzG, DTzG, TIPS-GIDTz and GIDTz, respectively. In contrast to DTzG that has one broad absorption peak, GIDTz shows vibrationally resolved three absorption peaks, likely due to the more rigid structure of GIDTz. Higher rigidity of GIDTz than DTzG was also indicated by smaller Stokes shifts of GIDTz compounds (see below). Similar results have been reported for Si-bridged thiophene analogs. [40][58-60] The UV-vis

absorption spectrum of DTzG exhibits a slight blue shift of 6 nm relative to that of DTG (λ_{max}: 333 nm), which is due to the replacement of thiophene with thiazole lead to mildly larger bandgap. The optical bandgaps (E_g^{opt}) were estimated to be 3.45, 3.26, 3.09 and 3.22 eV for DTzG, TIPS-DTzG, GIDTz and TIPS-GIDTz from the absorption edges, respectively. TIPS-substituted compounds, showed red-shifted absorption bands from those of the TIPS-free congeners, likely due to elevation of the HOMO by electron donating TIPS groups. σ-π Interaction between the silyl substituents and the π-system may be also involved (see the computational part below). The PL spectra of thiazole-condensed germoles are shown in Figure 2.2(b). The fluorescence bands in THF are in the range of 340-540 nm, and the maxima are at 405, 388, 419 and 404 nm, with the Stokes shifts of 58, 61, 52 and 51 nm for TIPS-DTzG, DTzG, TIPS-GIDTz, and GIDTz, respectively. Absolute PL quantum yields of the compounds were also determined as listed in Table 1. It was found that TIPS-compounds exhibited higher PL quantum yields than the corresponding TIPS-free compounds. Similar effects of silyl substituents, enhancing the PL efficiencies have been reported, previously. [61]

Table 2.1. Optical and electrochemical properties of thiazole-condensed germole.

Compound	λ_{max}/ nm[a]	E_g^{opt}/eV[b]	$\varepsilon/10^4$ $M^{-1}cm^{-1}$	λ_{em}/nm /Φ[c]	HOMO[d] /LUMO[d]	HOMO[e] /LUMO[f]
TIPS-DTzG	347	3.26	1.42	405/0.55	-5.70/-1.74	-5.61/-2.35
DTzG	327	3.45	0.52	388/0.39	-5.86/-1.71	-5.72/-2.27
TIPS-GIDTz	367	3.09	1.31	419/0.26	-5.45/-1.80	-5.46/-2.37
GIDTz	353	3.22	1.61	404/0.16	-5.55/-1.78	-5.58/-2.36

[a] In THF at room temperature. [b] E_g^{opt} = 1240 / absorption edges. [c] Fluorescence quantum yield. [d] Based on DFT calculations at the B3LYP/6-31G(d,p) level of theory in CH_2Cl_2. [e] E_{HOMO} = - (E_{ox}^{onset} + 4.80) eV with E_{ox}^{onset} from F_c/F_c^+ internal standard. [f] E_{LUMO} = E_{HOMO} + E_g^{opt}.

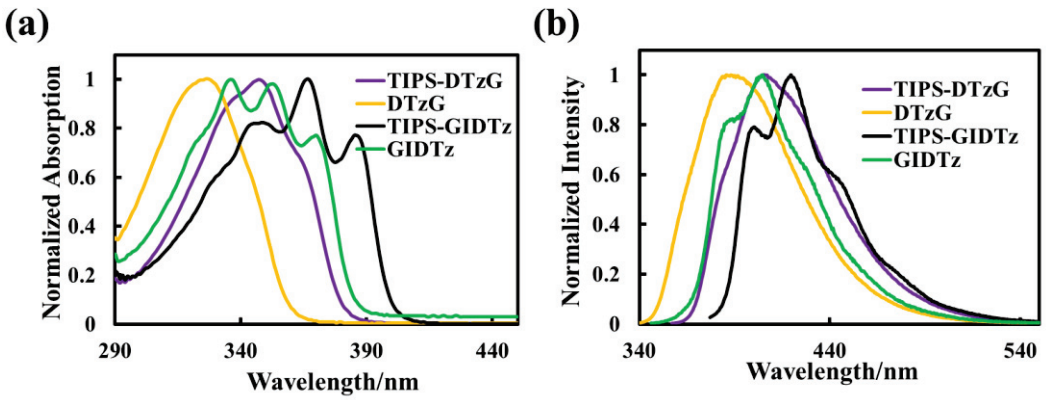

Figure 2.2. (a) UV-vis absorption spectra and (b) PL spectra of thiazole-condensed germoles in THF at room temperature.

To investigate the electrochemical characteristics, cyclic voltammetry (CV) was conducted for the thiazole-condensed germoles in dichloromethane (Figure 2.3). All compounds exhibit nonreversible anodic behaviors. However, no electrochemical reduction was observed. The HOMO and LUMO energy levels of the compounds were estimated on the basis of the anodic onset potentials and E_g^{opt}, as presented in Table 2.1. Interestingly, the differences in HOMO energy levels between DTzG and GIDTz and between TIPS-DTzG and TIPS-GIDTz are larger than the differences in LUMO energy, and are primarily responsible for the red-shifted UV-vis absorption and PL bands for ladder compounds GIDTz and TIPS-GIDTz. It is also noted that the LUMO energy levels of TIPS-substituted TIPS-DTzG and TIPS-GIDTz are slightly lower than those of TIPS-free DTzG and GIDTz. However, the HOMO energy levels of TIPS-DTzG and TIPS-GIDTz are much higher than those of DTzG and GIDTz, indicating that the TIPS substituents affect mainly the HOMO energy levels by their electron-donating property, which results in the shift of the UV-vis absorption and PL bands.

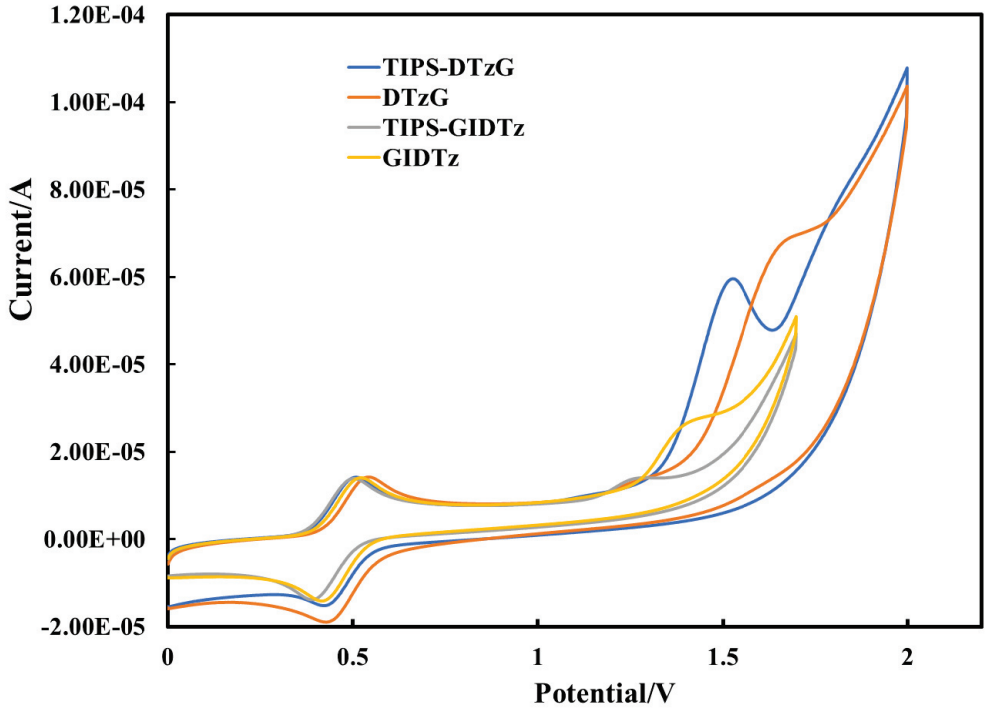

Figure 2.3. Cyclic voltammograms of TIPS-DTzG, DTzG, TIPS-GIDTz and GIDTz measured in 0.1M tetrabutylammonium hexafluorophosphate in CH_2Cl_2 solution with the Fc/Fc^+ redox couple as the internal standard, at the scan rate of 50 mV/s, using Pt disk, Pt plate, and Ag wire as the working, counter, reference electrodes, respectively.

2.4. DFT calculations

To further explore the electronic properties of thiazole-condensed germole, DFT calculations were carried out at the level of B3LYP/6-31G(d,p), in which the alkyl side chains were replaced by methyl for reducing computation time.[62] The data are summarized in Figure 2.4. Compared with the HOMO and LUMO energy levels of Tz-Tz that has no Ge bridges, those of DTzG are raised by 0.15 and 0.38 eV, respectively. It is likely that the electron-donating property of Ge raises the LUMO energy level, although the LUMO profile demonstrates clear σ*(Ge)-π*(Tz) interaction for the DTzG model, as shown in Figure 2.5. The HOMO-LUMO gap of the DTzG model is smaller than that of Tz-Tz by 0.23 eV, clearly indicating effects of the Ge bridge enhancing the conjugation. This is in good agreement with the fact that the UV-vis absorption maximum of **4a** in THF appears at 315 nm, which is shorter by 32 nm than that of TIPS-DTzG. The difference in the HOMO-LUMO gap of **4a** and TIPS-DTzG experimentally

estimated from the absorption edges is 0.20 eV, which is slightly smaller than the theoretically predicted value for Tz-Tz and the DTzG model. It is also apparent that GIDTz possesses an even smaller HOMO-LUMO gap than DTzG, reflecting the extended π-conjugation. In addition, replacing the electron-rich thiophenes by thiazole units leads to the large stabilization of the HOMO and LUMO by approximately 0.5 eV, whereas the bandgaps are not significantly affected. From these results, it is likely that the replacement of thiophene by thiazole can achieve a low LUMO system that is potentially applicable to n-type semiconductors.

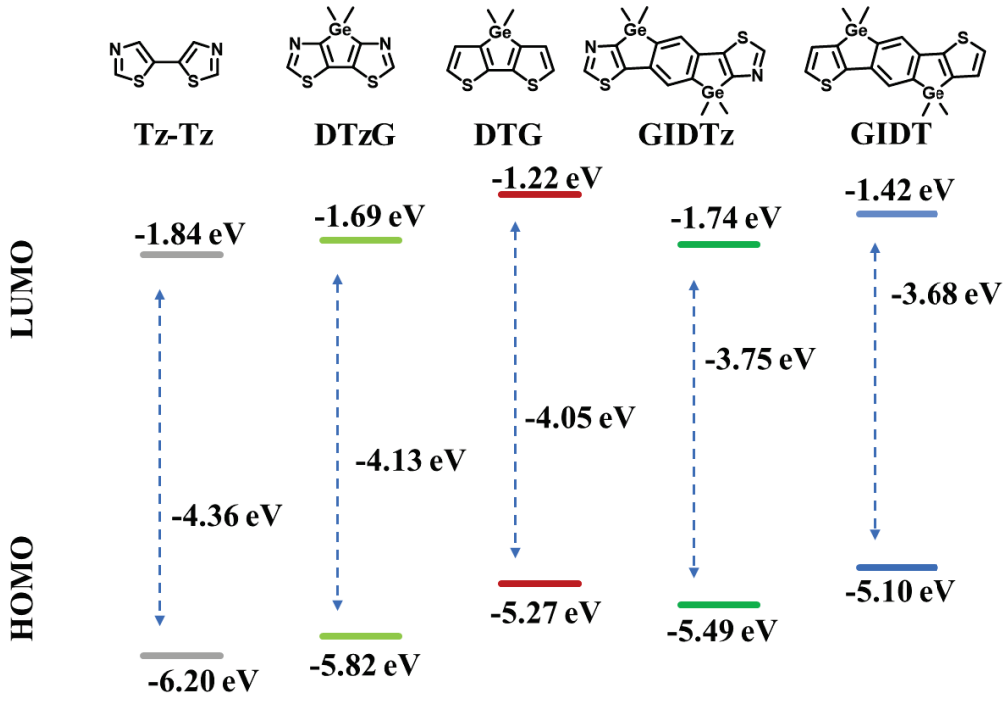

Figure 2.4. HOMO and LUMO energy levels for bridged or nonbridged bithiazole and bithiophene, derived from DFT calculations at B3LYP/6-31G(d,p) level.

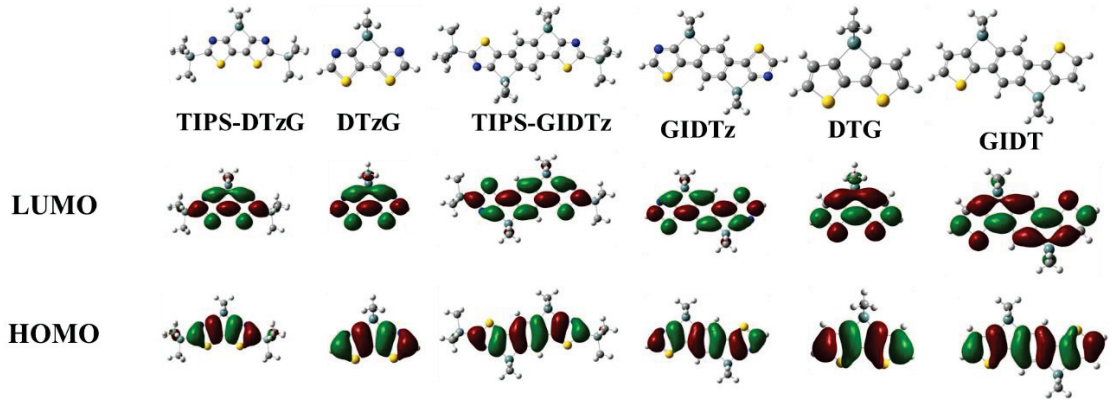

Figure 2.5. The optimized structures of dithiazole-based germole.

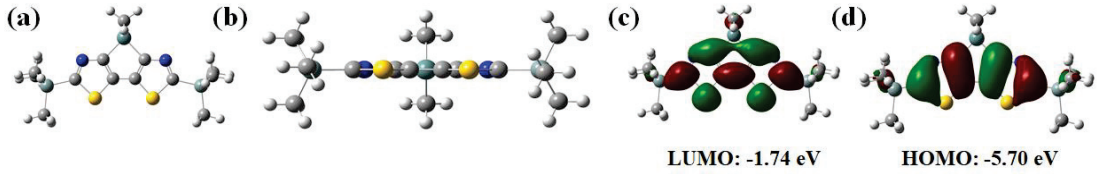

Figure 2.6. (a, b) Optimized structures of TIPS-DTzG model with different view directions. (c) LUMO and (d) HOMO profiles of TIPS-DTzG.

The optimized structures of the compounds exhibit high planarity, as shown in Figure 2.5. Figure 2.6(a) and (b) show the optimized geometries of TMS-DTzG as a typical example that indicates complete planarity including the Si atoms of the TIPS groups and the core dithiazologermole unit. Figure 2.6(c) indicates that the σ*(Ge)-π*(Tz) interaction contributes to the LUMO of TMS-DTzG. The introduction of TIPS has a larger effect on the HOMO than the LUMO. The change of HOMO is 0.16 eV, whereas that of LUMO is 0.03 eV. The TIPS orbitals contribute to elevating the HOMO, as shown in Figure 2.6(d).

3. Conclusion

In summary, the author has prepared dithiazole-condensed single germole and double germole compounds and investigated their electrochemical and optical properties. The single-crystal structure of brominated GIDTz exhibits close intermolecular stacking. DFT calculations revealed that the HOMO and LUMO energy

levels of the thiazole-condensed germoles are low in comparison with those of the thiophene-condensed germole congeners reported previously.

General consideration

All reactions were carried out in dry argon. Diethyl ether, *N*,*N*-dimethylformamide (DMF), and tetrahydrofuran (THF) that were used as the reaction solvents were distilled from CaH_2 and stored over activated molecular sieves in the dark until use. NMR spectra were recorded on a Varian 400-MR spectrometer. UV-vis absorption and PL (photoluminescence) spectra were measured on Hitachi U-2910 and HORIBA FluoroMax-4 spectrophotometers, respectively. PL quantum yields were determined on a HORIBA FluoroMax-4 spectrofluorometer using a calibrated integrating sphere system (λ_{ex} = 337, 317, 357, 343 nm for TIPS-DTzG, DTzG, TIPS-GIDTz and GIDTz, respectively). APCI-mass spectra were obtained by a Thermo Fisher Scientific LTQ Orbitrap XL spectrometer at N-BARD, Hiroshima University.

Synthesis

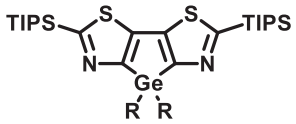

Synthesis of TIPS-DTzG

To a solution of **4a** (0.64 g, 1.0 mmol) in THF (20 mL) was added at -78 °C a solution of *n*-BuLi (2.1 mmol, 1.6 M) in hexane and the resulting mixture was stirred for 1 h at this temperature. Dichlorodioctylgermane (0.48 g, 1.3 mmol) was added to the reaction solution at -80 °C. After stirring the mixture overnight at room temperature, the solvent was evaporated under reduced pressure. The residue was purified by column chromatograph on silica gel with hexane: ethyl acetate = 10:1 as the eluent to afford TIPS-DTzG in 40% yield (0.31 g, 0.4 mmol) as a yellow oil. ^{1}H NMR ($CDCl_3$) δ 1.52-1.44 (sept, 6H), 1.44-1.16 (m, 28H), 1.16 (d, *J* = 8 Hz, 36H), 0.85 (t, *J* = 8 Hz, 6H); ^{13}C NMR ($CDCl_3$) δ 170.42, 165.60, 140.84, 32.33, 31.86, 29.23, 29.08, 25.44, 22.64, 18.54, 14.44, 14.08, 11.81. HRMS (APCI) *m/z* calcd for $C_{40}H_{76}GeN_2S_2Si_2$ [M^+] 778.4293, found 778.4200.

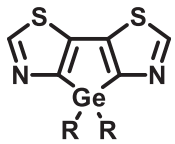

Synthesis of DTzG

To a solution of TIPS-DTzG (0.46 g, 0.6 mmol) in THF (15 mL) was added a solution of TBAF (1.2 mmol, 1 M) in THF at 0 °C and the resulting mixture was stirred for 10 min at this temperature. The solvent was evaporated under reduced pressure and the residue was purified by column chromatograph on silica gel with hexane: ethyl acetate = 5:1 as the eluent to afford DTzG in 99% yield (0.27 g, 1.0 mmol) as a yellow oil. ^{1}H NMR ($CDCl_3$) δ 8.83 (s, 2H), 1.50-1.33 (m, 8H), 1.28-1.12 (m, 20H), 0.83 (t, *J* = 8 Hz, 6H); ^{13}C NMR ($CDCl_3$) δ 162.68, 152.79, 137.90, 32.55, 31.77, 29.09, 28.96, 25.15, 22.60, 14.08, 13.91. HRMS (APCI) calcd for $C_{22}H_{36}GeN_2S_2$ [M^+] 466.1532, found 466.1588.

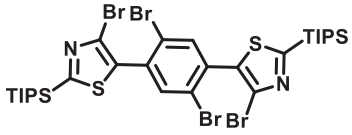

Synthesis of 5,5'-(2,5-dibromo-1,4-benzenediyl)bis(4-bromo-2-triisopropylsilylthiazole) (2b)

To a solution of **3a** (5.54 g, 17.3 mmol) in THF (40 mL) was added LDA (1 M, 20.7 mmol) at -78 °C and the resulting mixture was stirred for 30 min at this temperature. Then, trimethyltin chloride (4.12 g, 20.7 mmol) was added to the reaction solution. After stirring the mixture overnight at room temperature and quenched with sat. NaCl (aq), and extracted with dichloromethane. The combined organic layers were dried over $MgSO_4$. After filtration, the solvent was removed under reduced pressure. 4-bromo-2-(triisopropylsilyl)-5-(trimethylstannyl)thiazole (**1b**) was obtained as yellow oil. ^{1}H NMR ($CDCl_3$) δ 1.48-1.40 (sept, 3H), 1.14 (d, *J* = 8 Hz, 18H), 0.47 (s, 9H); ^{13}C NMR ($CDCl_3$) δ 176.25, 134.80, 129.77, 18.59, 18.48, -7.84. HRMS (APCI) calcd for $C_{15}H_{30}BrNSSiSn$ [M^+] 483.0134, found 483.0074.

The residue, 1,4-dibromo-2,5-diioobenzene (4.21 g, 8.6 mmol), and $Pd(PPh_3)_2Cl_2$ (0.31 g, 0.4 mmol) was dissolved in DMF (15 mL) at 80 °C for stirring 24 h. DMF were evaporated under reduced pressure and the residue was directly purified by column chromatograph on silica gel with hexane: dichloromethane = 2:1 as the eluent to afford **2b** in yield of 30% (2.20 g, 2.6 mmol) as a white powder. ^{1}H NMR ($CDCl_3$) δ 7.76 (s, 2H), δ 1.52-1.42 (sept, 6H), δ 1.19 (d, *J* = 8 Hz, 36H); ^{13}C NMR ($CDCl_3$) δ 172.64, 136.28, 134.36, 131.94, 128.88, 123.27, 18.44, 11.57. HRMS (APCI) calcd for $C_{30}H_{44}Br_4N_2S_2Si_2$ [M^+] 871.9245, found 871.9177.

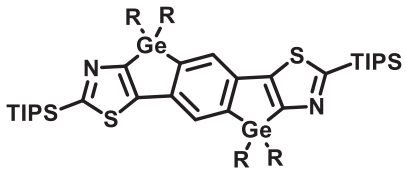

Synthesis of TIPS-GIDTz

To a solution of **2b** (1.74 g, 2.0 mmol) in THF (40 mL) was added at -78 °C a solution of *n*-BuLi (10 mmol, 1.6 M) in hexane and the resulting mixture was stirred for 1 h at this temperature then the mixture was further stirred at room temperture for 2 h. Dichlorodioctylgermane (2.22 g, 3.0 mmol) was added to the mixture at -78 °C. After stirring the mixture overnight at room temperature, the solvent was evaporated under reduced pressure and the residue was purified by column chromatograph on silica gel with hexane: ethyl acetate = 10:1 as the eluent to afford TIPS-GIDTz in 50% yield (1.15 g, 1.0 mmol) as a yellow oil. ^{1}H NMR ($CDCl_3$) δ 7.59 (s, 2H), 1.43-1.53 (sept, 6H), 1.47-1.18 (m, 56H), 1.18 (d, *J* = 8 Hz, 36H), 0.83 (t, *J* = 8 Hz, 12H); ^{13}C NMR ($CDCl_3$) δ 171.24, 163.98, 151.33, 144.55, 139.61, 128.50, 32.64, 31.83, 29.13 (2C), 25.35, 22.60, 18.55, 14.44, 14.03, 11.81. HRMS (APCI) calcd for $C_{62}H_{112}Ge_2N_2S_2Si_2$ [M^+] 1150.6263, found 1150.6238.

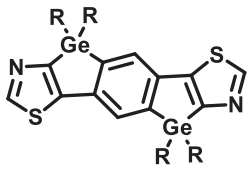

Synthesis of GIDTz

GIDTz was synthesized in a fashion similar to synthesis of and DTzG, by using TIPS-GIDTz instead of TIPS-DTzG, GIDTz in 96% yield as a yellow oil. ^{1}H NMR ($CDCl_3$) δ 8.85 (s, 2H), 7.58 (s, 2H), 1.47 (sext, J = 8 Hz, 8H), δ 1.35-1.14 (m, 48H), δ 0.84 (t, J = 8 Hz, 12H); ^{13}C NMR ($CDCl_3$) δ 161.38, 153.56, 148.60, 144.00, 139.43, 128.00, 32.82, 31.81, 29.17, 29.02, 25.27, 22.62, 14.18, 14.08. HRMS (APCI) calcd for $C_{44}H_{72}Ge_2N_2S_2$ [M^+] 838.3640, found 838.3569.

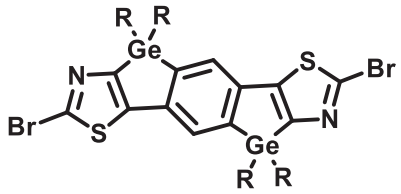

Synthesis of GIDTz-Br

To a solution of GIDTz (0.22 g, 0.26 mmol) in THF (10 mL) was added LDA (1 M, 0.55 mmol) at -78 °C and the resulting mixture was stirred for 30 min at this temperature then carbon tetrabromide (CBr_4) (0.18 g, 0.55 mmol) was added to the reaction solution. After stirring the mixture overnight at room temperature, the mixture was hydrolyzed with sat. NaCl (aq) and extracted with dichloromethane. The combined organic layers were dried over $MgSO_4$. After filtration, the solvent was removed under reduced pressure and the residue was purified by column chromatograph on silica gel with hexane: ethyl acetate = 20:1 as the eluent to afford brominated GIDTz (GIDTz-Br) in 50% yield (0.13 g, 0.13 mmol) as a yellow solid. ^{1}H NMR ($CDCl_3$) δ7.43 (s, 2H), 1.44 (sext, J = 8 Hz, 8H), δ 1.35-1.15 (m, 48H), δ 0.85 (t, J = 8 Hz, 12H); ^{13}C NMR ($CDCl_3$) δ 161.00, 151.63, 143.16, 139.36, 135.34, 127.98, 32.93, 31.96, 29.34, 29.15, 25.32, 22.79, 14.41, 14.24. HRMS (APCI) calcd for $C_{44}H_{70}Br_2Ge_2N_2S_2$ [M^+] 996.1806, found 996.1759.

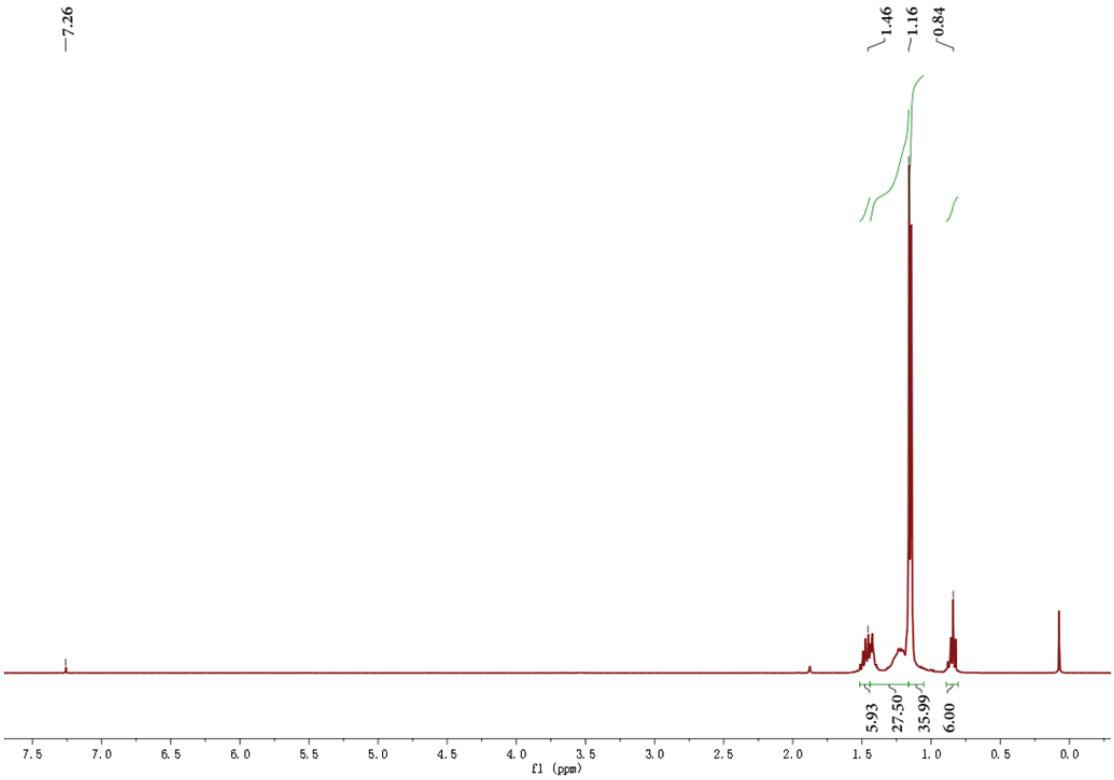

Figure 2.7. ^{1}H NMR spectrum of **TIPS-DTzG**

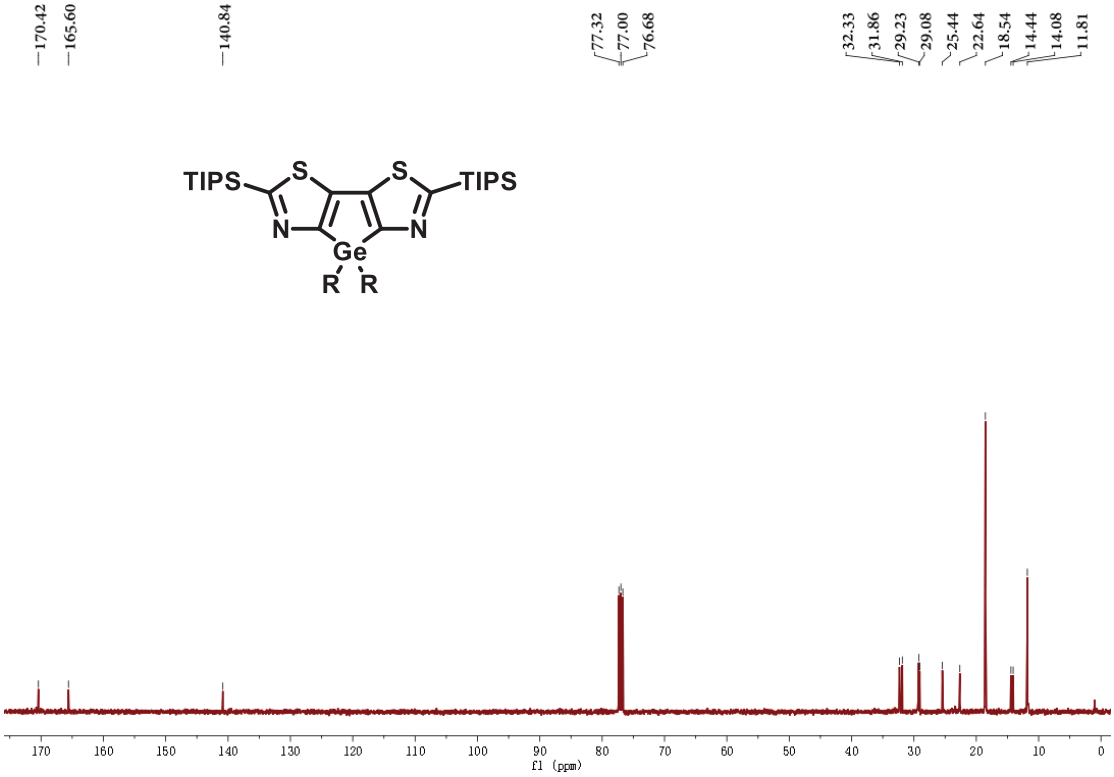

Figure 2.8. ^{13}C NMR spectrum of **TIPS-DTzG**

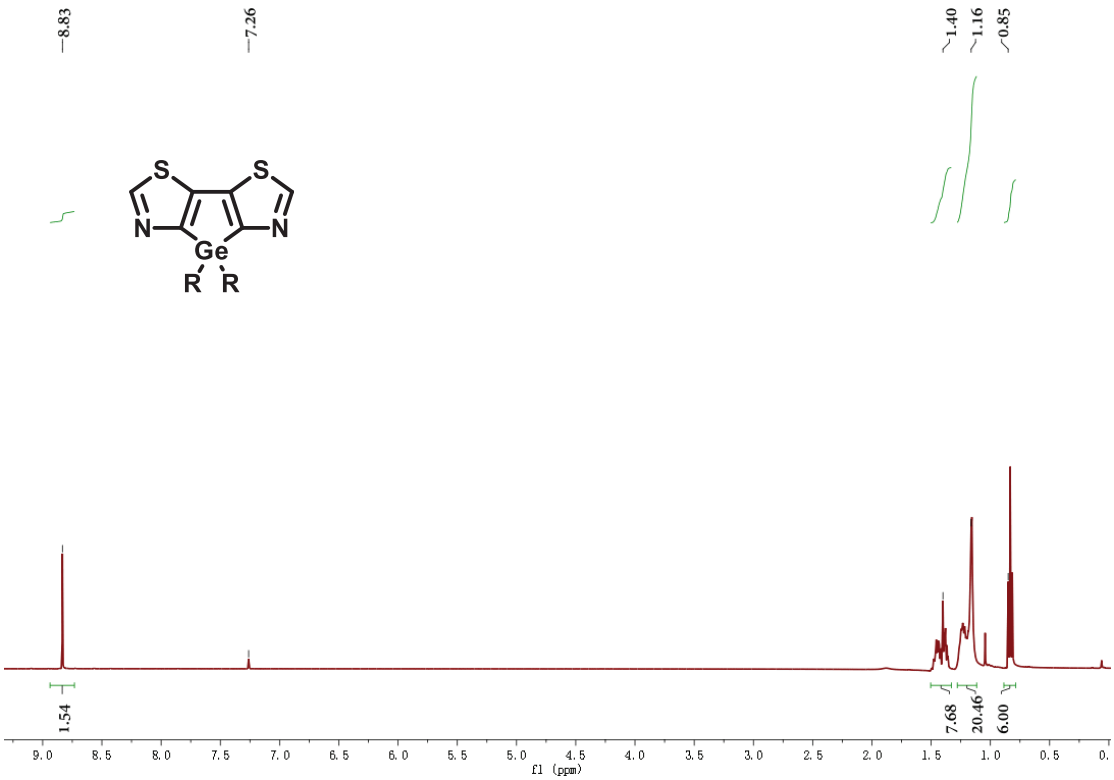

Figure 2.9. ^{1}H NMR spectrum of **DTzG**

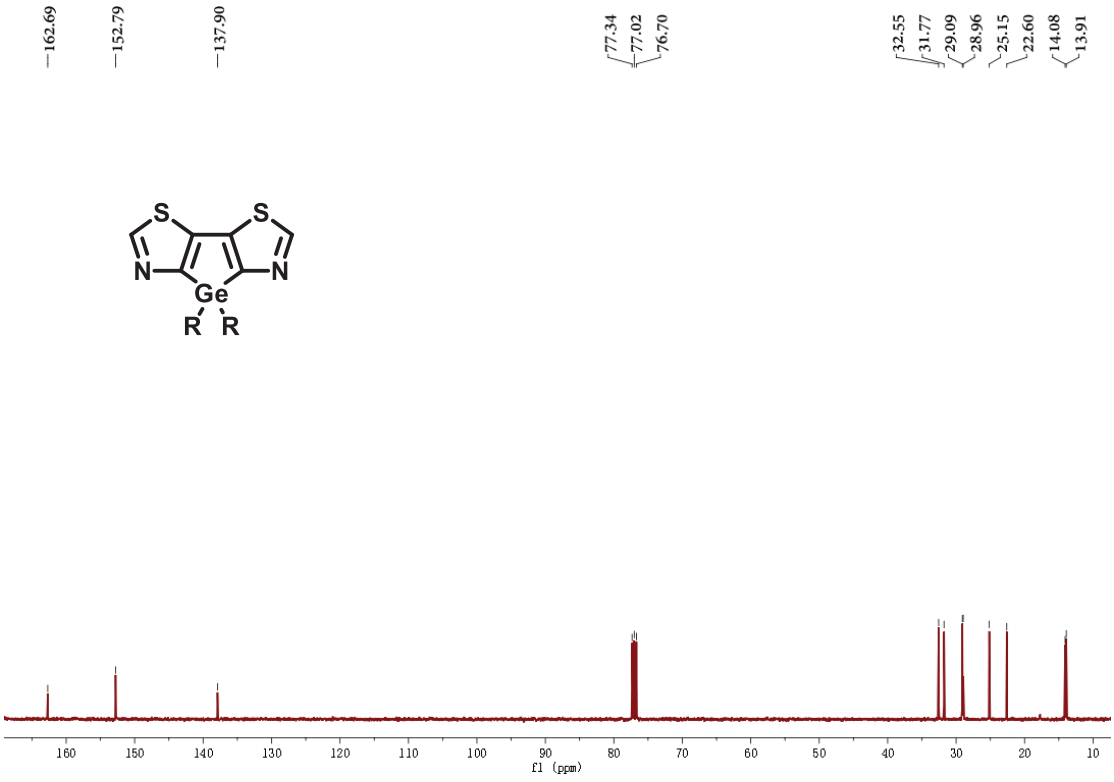

Figure 2.10. ^{13}C NMR spectrum of **DTzG**

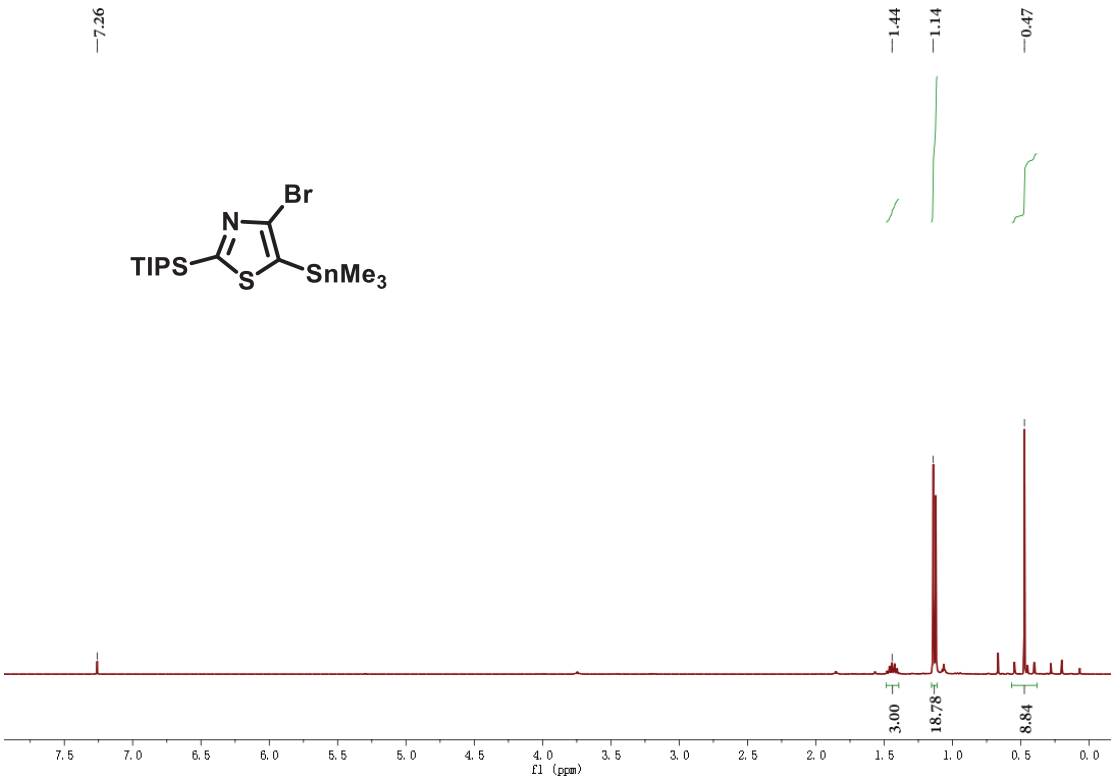

Figure 2.11. ^{1}H NMR spectrum of **1b**

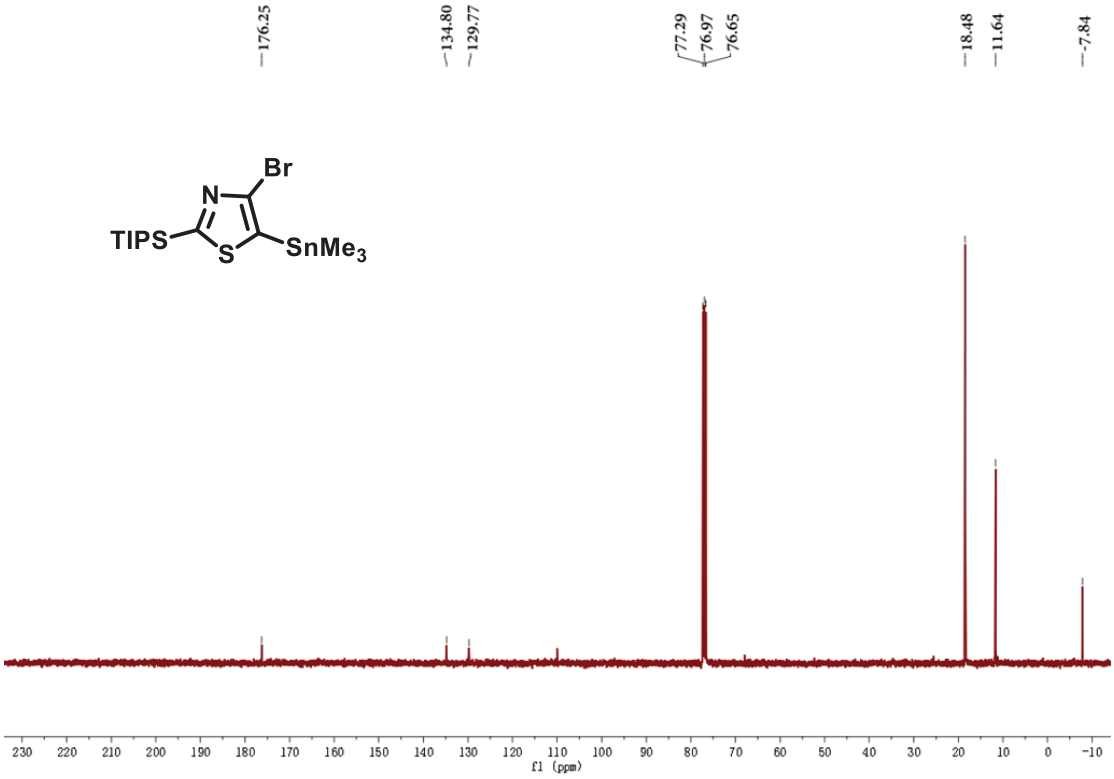

Figure 2.12. ^{13}C NMR spectrum of **1b**

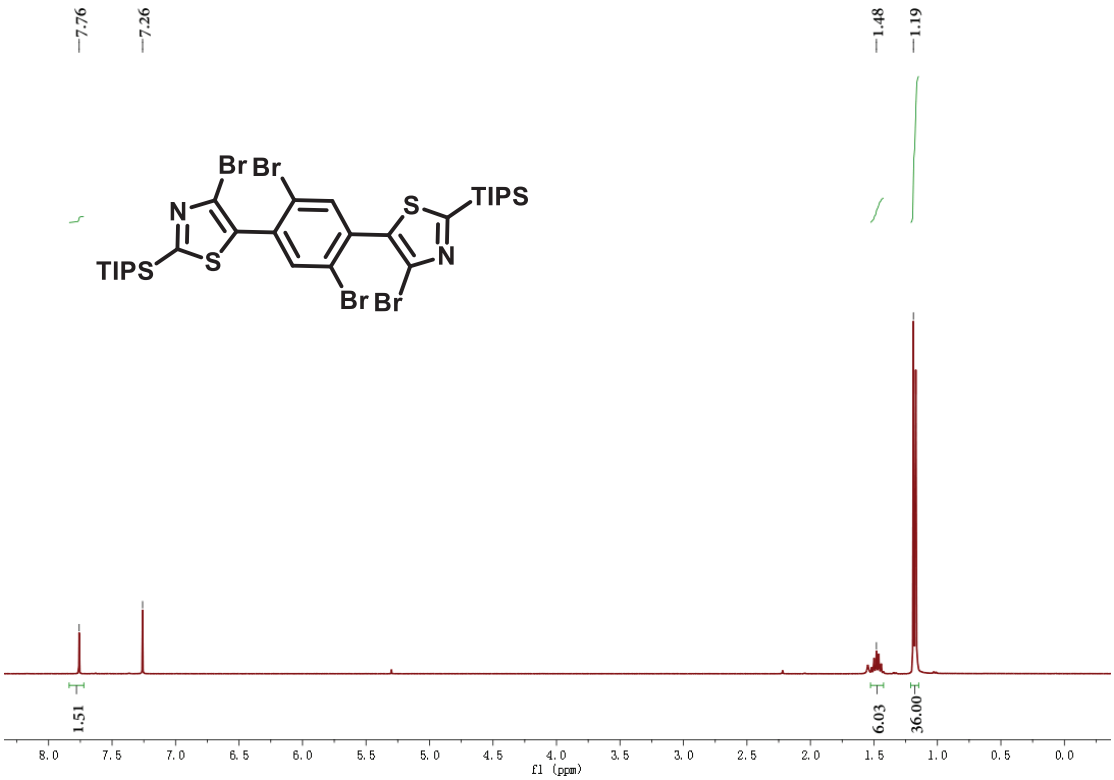

Figure 2.13. ^{1}H NMR spectrum of **2b**

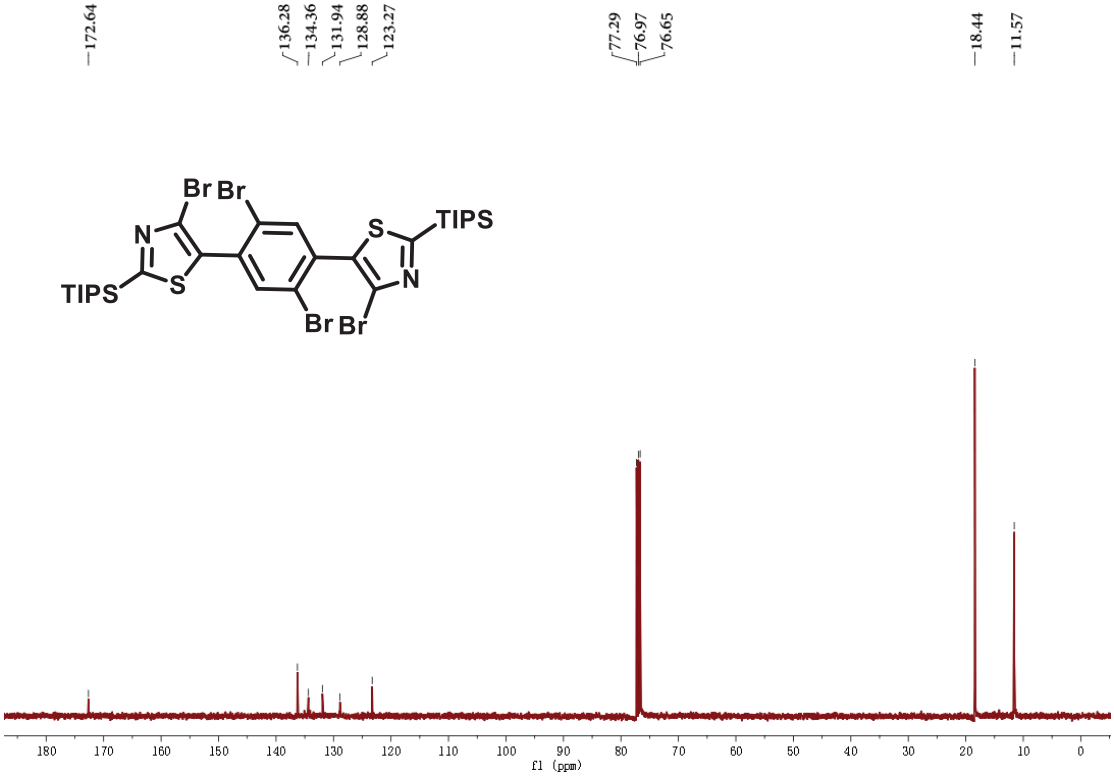

Figure 2.14. ^{13}C NMR spectrum of **2b**

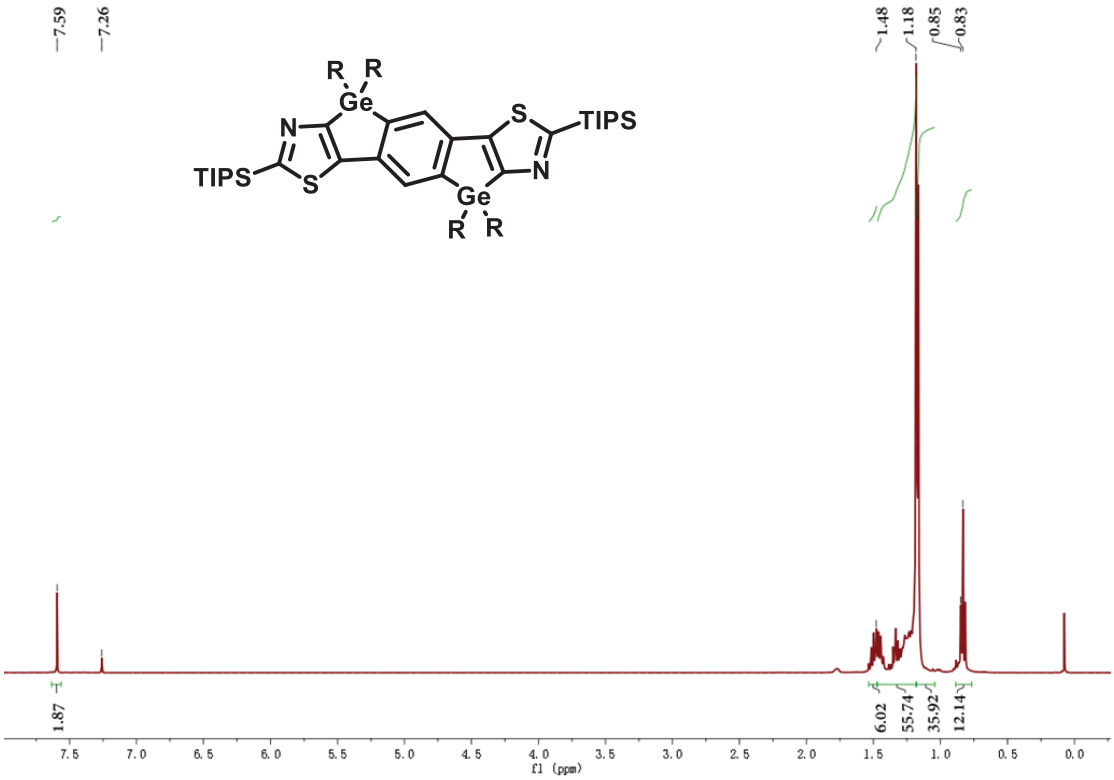

Figure 2.15. ^{1}H NMR spectrum of **TIPS-GIDTz**

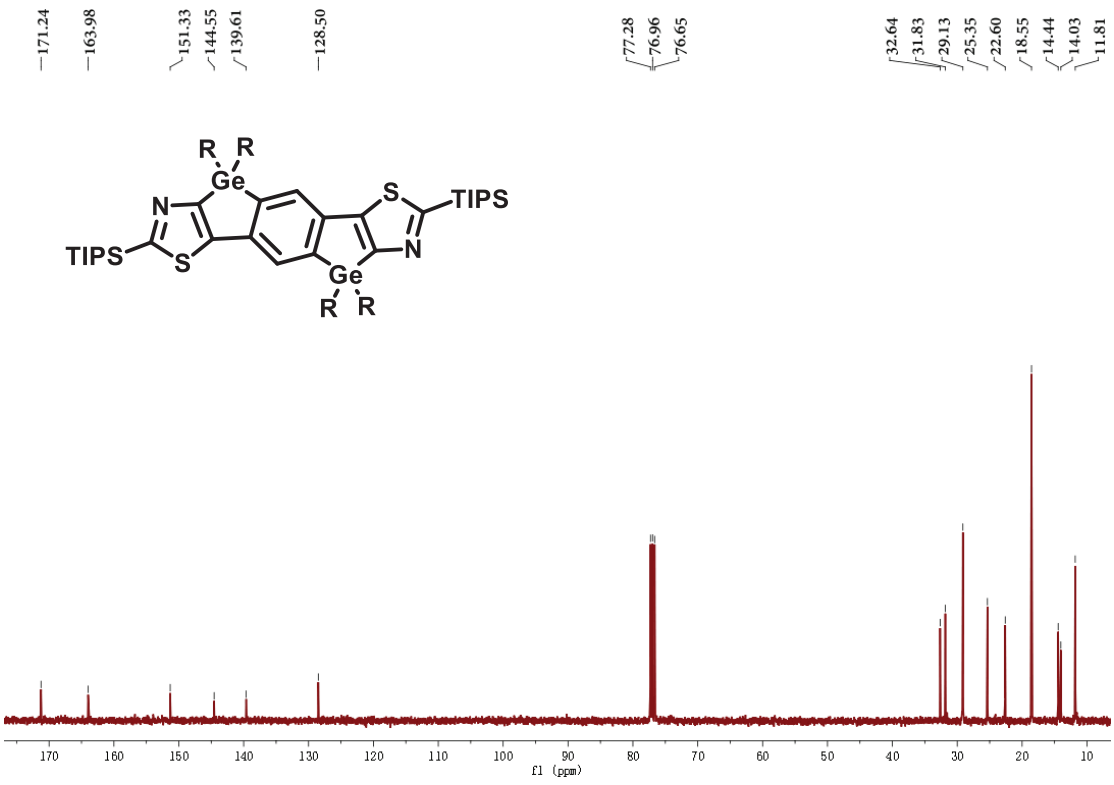

Figure 2.16. ^{13}C NMR spectrum of **TIPS-GIDTz**

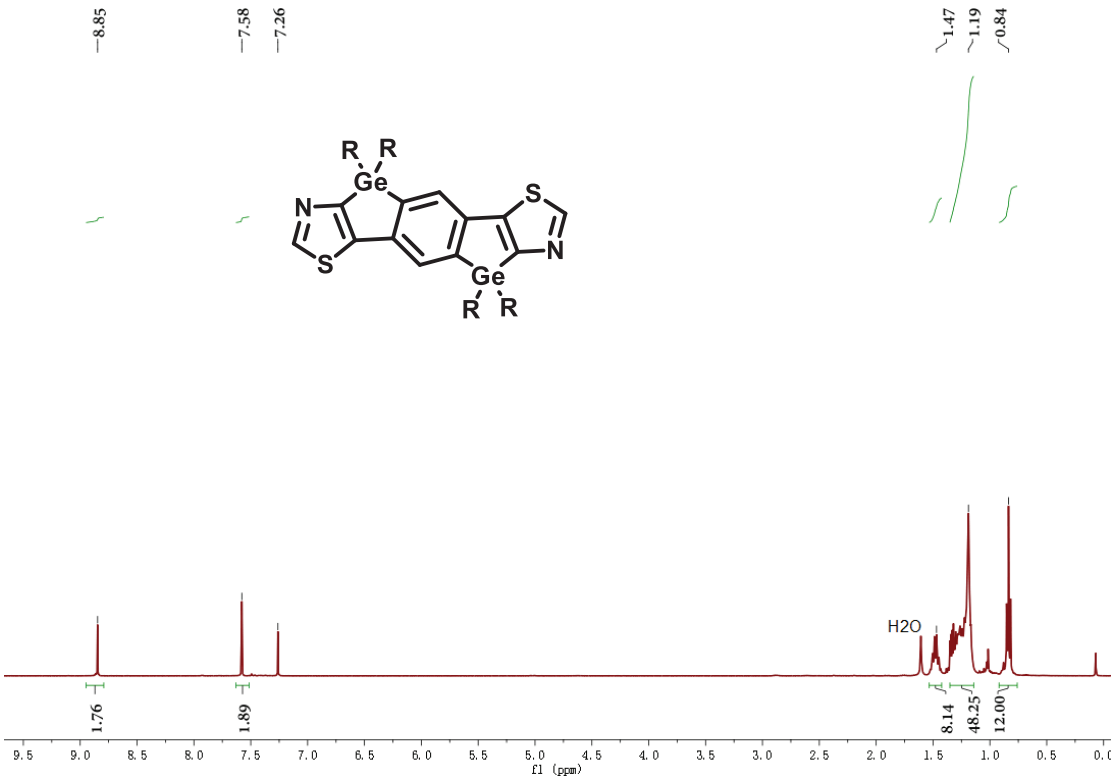

Figure 2.17. ^{1}H NMR spectrum of **GIDTz**

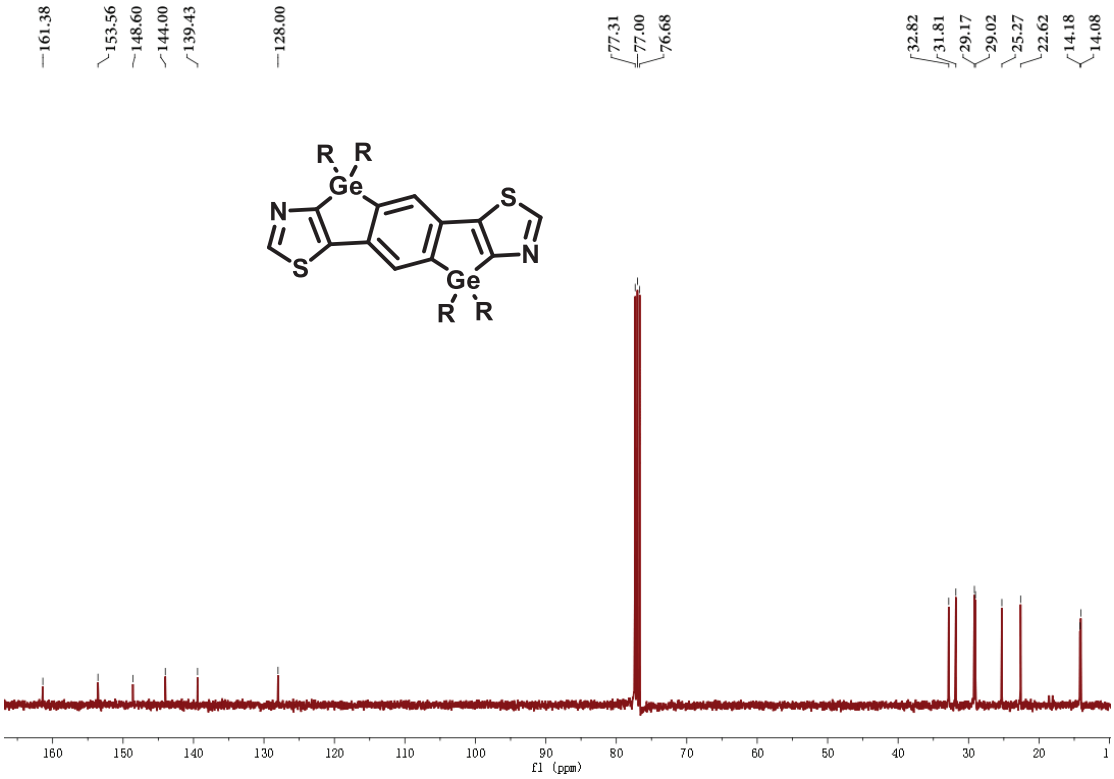

Figure 2.18. ^{13}C NMR spectrum of **GIDTz**

Chapter 3: Preparation of D-A copolymers based on dithiazologermole and germaindacenodithiazole as weak electron donor units

1. Introduction

In the past decade, much interest has been placed on π-conjugated polymer semiconductors as hole and electron transport materials because of their adjustable frontier molecular orbital (FMO) energy levels and potential applications in optoelectronic devices, such as OSCs, OFETs, and OLEDs [63-68]; in comparison with inorganic semiconductor materials, these materials exhibit several advantages, including light weight, low cost, and high flexibility [69-72]. In contrast to p-type (hole-transporting) polymers, which exhibit impressive device performances with high hole mobilities exceeding 10 cm^2 V^{-1} S^{-1} [73, 74], n-type (electron-transporting) polymers have been limited due to the presence of minority electron-deficient groups and because the synthesis process is complicated; these disadvantages have impeded the development of n-type semiconductor materials. In addition, n-type polymers show relatively low device stability because of their relatively high sensitivity to moisture in the photoexcited and carrier-doped states, and this issue has hindered their application in devices [75, 76]. Clearly, the development and design of new n-type organic semiconductors is imperative. Conjugated polymers composed of a regular alternating arrangement of D-A polymers are valuable because they show improved inter- and intramolecular interactions between the donor and acceptor units, enhancing carrier transport in their films. For the preparation of high-performance n-type D-A polymers, the polymers should also possess high electron affinity, which may be realized by introducing weak donors with low-lying LUMOs. However, weak donors may suppress the D-A interaction, and therefore, it is essential to use a donor unit with an appropriate electronic state and a moderately low-lying LUMO.

Several Group 14 element-bridged bithiophenes, such as cyclopentadithiophene (CDT) [77], DTS [7, 78], and DTG [9, 18], have been reported as typical electron donor

structures. The bithiophene unit becomes planar when bridging atoms are introduced, and the electronic effects of silicon and heavier elements used as bridging atoms have often been proposed. These monomer units have been copolymerized with BT to afford D-A type copolymers (PCDT-BT, PDTS-BT, and PDTG-BT) that present satisfactory charge-transporting behaviors in OFET devices (Chart 3.1) [19, 79, 80].

As derivatives of the abovementioned electron-donating Group 14 element-bridged bithiophenes, a new class of compounds containing thiazole units have been studied; these compounds are weak electron donor structures that can enhance electron-transporting properties while also exhibiting electron-donating properties and performing D-A interactions with strong acceptor units. For example, IDT- and IDTz-ladder-type monomers were copolymerized with DTBT or DTzBT units to obtain ambipolar polymers PIDT-DTBT, PIDT-DTzBT [37], and PIDTz-DTBT [33], as shown in Chart 3.1. Notably, these thiazole polymers showed improved electron-transporting properties compared with that of thiophene congeners, indicating that introducing weak donor units in D-A polymers is beneficial to generate electron-transporting materials. The following strategies are effective for preparing polymers with high electron-transporting properties: (1) replacing all thiophene units with thiazole units and (2) substituting silole or germole for the cyclopentadiene ring. This strategy is effective because these metalloles usually possess lower LUMO energy levels than that of cyclopentadiene, which can be ascribed to the σ*-π* conjugation between the silicon or germanium σ* and the butadiene π* orbital. Furthermore, the relatively long C-Si and C-Ge bonds function to place the side chains on these atoms far from the polymer backbone to reduce steric hindrance and enhance the intermolecular π-π stacking interaction [15-17, 21].

In this Chapter, weak electron donor units dithiazologermole (DTzG) and germaindacenodithiazole (GIDTz), which showed enhanced electron-deficient properties in our previous work [85], were copolymerized with acceptor units BT and DTzBT to form four new D-A type polymers, PDTzG-BT, PGIDTz-BT, PDTzG-DTzBT, and PGIDTz-DTzBT (Chart 3.1). Quantum chemical calculations obtained through the polymer models suggested that these thiazole-containing polymers should

possess lower-lying LUMOs and HOMOs than those of the thiophene-congener polymers. In addition, good film-forming properties were observed for the polymers, indicating potential applications as device materials.

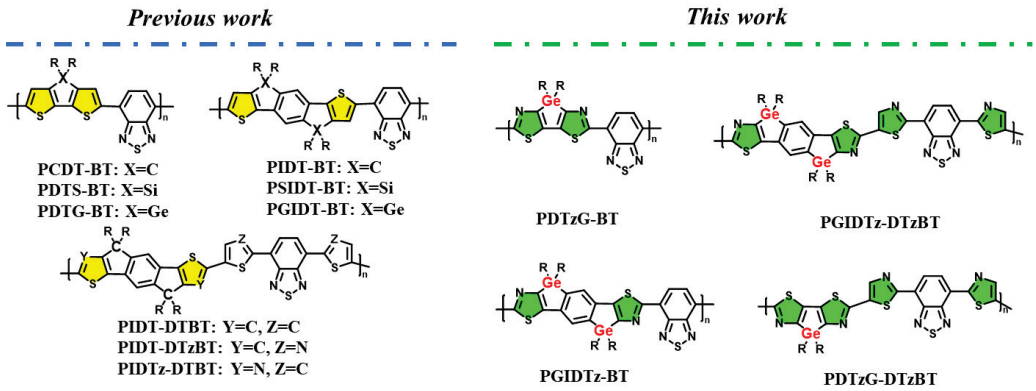

Chart 3.1. Structures of polymers based on element-bridged thiophene and thiazole units.

2. Results and discussion

2.1. Synthesis

Scheme 3.1 shows the synthetic route to distannylated monomers and copolymers. The NMR and mass spectra of target compounds were shown in Figure 3.9-3.20. Details of the experimental procedures are available in the end of this chapter. Compounds DTzG, GIDTz, and 4,7-bis(5-bromothiazol-2-yl)benzo[c][1,2,5]thiadiazole (DTzBT-Br) were prepared as reported in the literature [85, 86]. Two distannylated monomers, DTzG-Sn and GIDTz-Sn, were facilely synthesized by the lithium-hydrogen exchange reaction of DTzG and GIDTz, respectively, at -78 °C, followed by treatment of the resultant dilithium reagents with tributyltin chloride. DTzG-Sn and GIDTz-Sn were readily purified by column chromatography using neutral alumina and characterized by ^{1}H NMR, ^{13}C NMR, and mass spectral measurements.

For GIDTz, we utilized the Negishi coupling reaction to improve the synthetic route to the precursor because this reaction offers several advantages over the Stille coupling reaction, as toxic organotin is absent, the synthesis is a simple one-step process, and adequate yields are obtained.

PDTzG-BT PGIDTz-BT PGIDTz-DTzBT PDTzG-DTzBT

Figure 3.1. Photos of polymer solutions in THF (1 mg/mL).

DTzG-Sn and GIDTz-Sn were then copolymerized with BT-Br or DTzBT-Br, respectively, to afford four D-A type copolymers via the conventional Stille coupling reaction using $Pd_2(dba)_3/P(o\text{-tol})_3$ as the catalyst. After polymerization, these copolymers were purified by Soxhlet extraction using methanol, hexane, dichloromethane, chloroform, and chlorobenzene to remove salts and low molecular weight fractions. After removal of low molecular weight fractions that were soluble in methanol and hexane, PDTzG-BT and PGIDTz-BT were found to be soluble in chloroform, and chlorobenzene extraction was not carried out. Similarly, PGIDTz-DTzBT was soluble even in dichloromethane, and no further extraction with chloroform and chlorobenzene was performed. PDTzG-DTzBT was only soluble in chlorobenzene. The extracts of PDTzG-BT and PGIDTz-BT in chloroform, PGIDTz-DTzBT in dichloromethane, and PDTzG-DTzBT in chlorobenzene were concentrated and reprecipitated in methanol to yield the target polymers as solids. Although only broad signals are observed in their ^{1}H NMR spectra, the integration ratios are in good agreement with the regular alternating structures. ^{13}C NMR spectra could not be obtained because of the low solubility of the polymers. To further verify the polymer structures, we measured their MALDI-TOF mass spectra. Signals assignable to oligomers up to n = 7, 6, 4, and 4 terminated with H or Br were found in the spectra of PDTzG-BT, PGIDTz-BT, PDTzG-DTzBT, and PGIDTz-DTzBT, respectively. The molecular weights of the polymers were M_n = 8.8, 7.7, 3.1, and 8.7 kDa and PDI (polydispersity index, M_w/M_n) = 2.5, 1.6, 1.6, and 2.9 for PDTzG-BT, PGIDTz-BT, PDTzG-DTzBT, and PGIDTz-DTzBT, respectively, as determined by GPC at 50 °C with tetrahydrofuran (THF) as the eluent. The molecular weight and yield of PDTzG-DTzBT were lower than those of other polymers due to its low solubility, as high-

molecular weight polymers might be separated as insoluble materials. Currently, microwave irradiation is commonly used to heat the medium of coupling reactions, including the Stille coupling reaction, for the synthesis of conjugated polymers (see references for examples [42,46.47]). However, heating the reaction mixture by microwave irradiation resulted in the formation of a large amounts of insoluble materials for PDTzG-DTzBT, and therefore, the polymerization was performed by heating the mixture with an oil bath, which differed from other polymers that were prepared by microwave heating. In addition, compared to the other polymers in THF, PDTzG-DTzBT was less soluble, and only the soluble part was analyzed by GPC (Figure 3.1), which may also be responsible for the lower molecular weight determined by GPC. Dichlorobenzene was also examined as the GPC solvent but again showed low solubility. Other polymers also showed low solubility, which limits their molecular weights. Changing the reaction temperature did not affect the results.

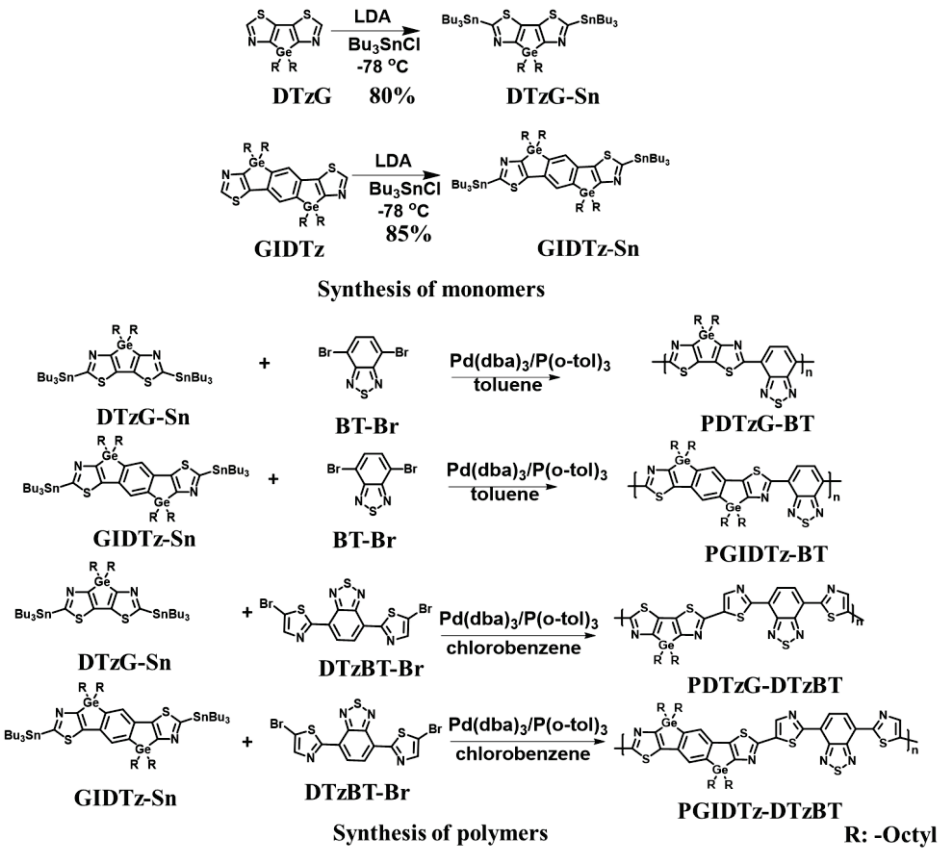

Scheme 3.1. Synthetic routes to thiazologermole-containing polymers.

2.2. Thermal properties of polymers

TGA was carried out in a nitrogen atmosphere at a heating rate of 10 °C min^{-1} to evaluate the thermal stability of the polymers. The polymers exhibited good thermal stability with temperatures of 5% mass loss T_d^5 = 366, 348, 327, and 414 °C for PDTzG-BT, PGIDTz-BT, PDTzG-DTzBT, and PGIDTz-DTzBT, respectively, as shown in Figure 3.2. DSC was also carried out from 30 °C to 250 °C to characterize the polymer crystallinity, but all polymers showed no thermal transition.

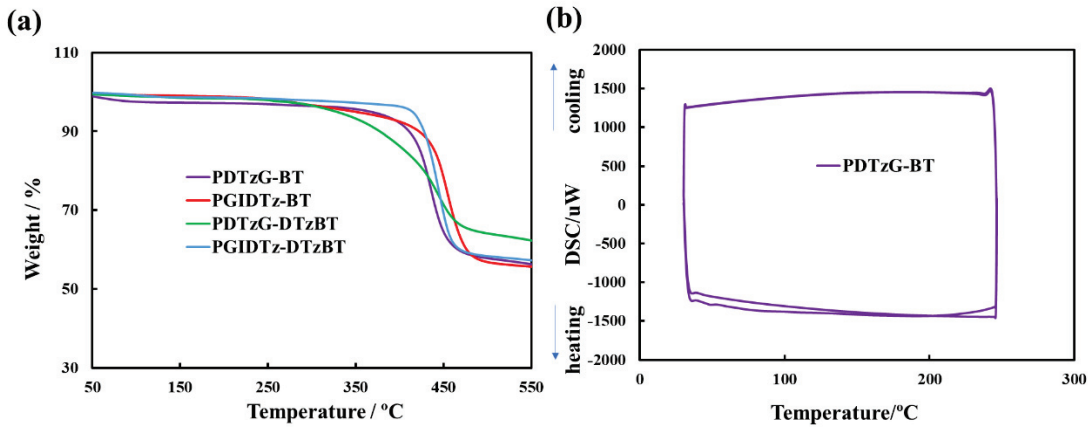

Figure 3.2. (a) TGA curves of PDTzG-BT, PGIDTz-BT, PDTzG-DTzBT and PGIDTz-DTzBT. (b) DSC curve of PDTzG-BT.

2.3. Optical and electrochemical properties of polymers

To investigate the optical properties of the polymers, UV–vis absorption spectra were measured. The normalized solution and film absorption spectra are shown in Figure 3.3(a) and (b), and the data are listed in Table 3.1. PDTzG-BT, PGIDTz-BT, PDTzG-DTzBT, and PGIDTz-DTzBT showed two major absorption peaks in chloroform solution, of which the shorter wavelength peaks appeared at 384, 388, 386, and 414 nm and the longer wavelength peaks were found at 599, 579, 526, and 554 nm, respectively. The low-energy absorption peaks of thiazologermole polymers PDTzG-BT and PGIDTz-BT were blueshifted by approximately 90 and 50 nm relative to those of their thienogermole analogs (see Chart 3.1) [17, 27], respectively, indicating that DTzG and GIDTz units are weaker electron donor units than DTG and GIDT units, thereby diminishing the D-A interaction [32]. On the other hand, the maximal

absorption peaks of all polymers in the thin films were redshifted from those in solution, suggesting that strong π-π stacking occurs in the solid state. The absorption onsets in the films (λ_{onset}^{film}) of polymers PDTzG-BT, PGIDTz-BT, PDTzG-DTzBT, and PGIDTz-DTzBT were at 829, 738, 733, and 708 nm, corresponding to optical band gaps (E_g^{opt}) of 1.50 1.68, 1.69, and 1.75 eV, respectively. The E_g^{opt} trend corresponds with the theoretical calculation results (see below), although the intermolecular interaction is not considered in the calculations. The absorption maxima were blueshifted in the order of PDTzG-BT, PGIDTz-BT, PGIDTz-DTzBT, and PDTzG-DTzBT. That the maximum of PGIDTz-DTzBT appeared at a longer wavelength than that of PDTzG-DTzBT in contrast to the absorption onsets, which may be due to the low molecular weight of PDTzG-DTzBT.

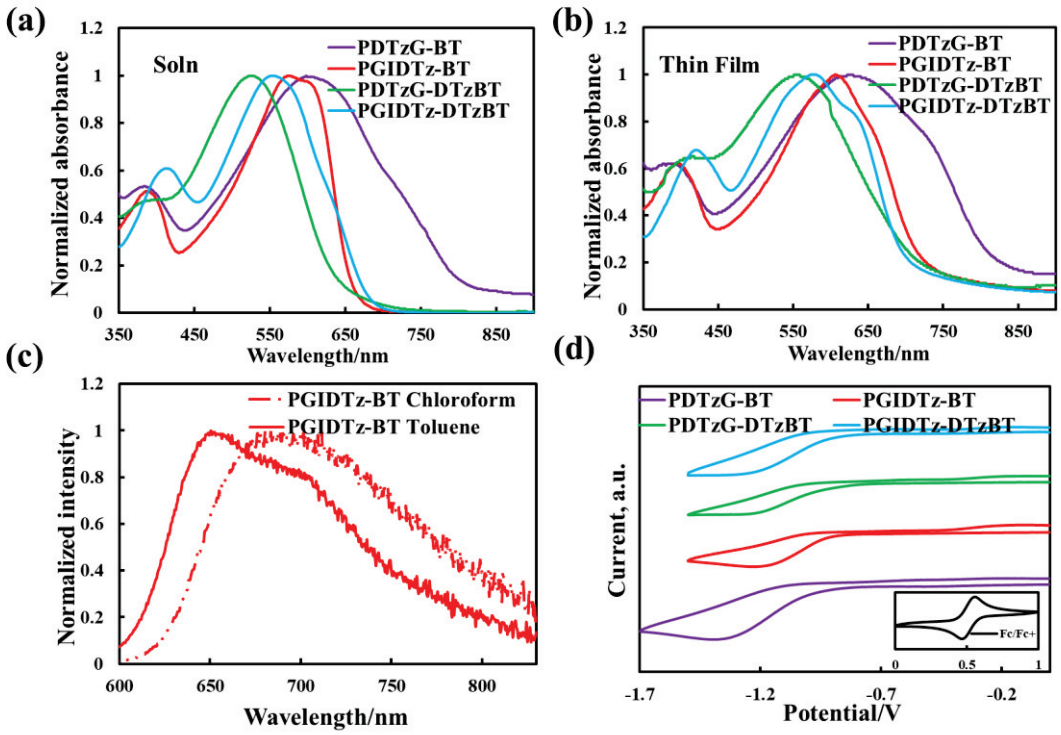

Figure 3.3. Absorption spectra of thiazologermole polymers (a) in chloroform (1 mg/10 mL) and (b) in thin films by spin-coating method; (c) PL spectra of PGIDTz-BT in toluene and chloroform (1 mg/10 mL); and (d) cyclic voltammograms of polymer thin films (0.1 M nBu_4NClO_4 in acetonitrile, with ferrocene/ferrocenium (Fc/Fc^+) as the external standard, Pt disk as the working electrode, Pt plate as the counter electrode,

and Ag wire as the pseudo-reference electrode).

To verify the intramolecular charge transfer (ICT) behaviors of these polymers, the PL spectra were measured in toluene and chloroform, and the results for PGIDTz-BT are shown in Figure 3.3(c). The maximal PL peak of PGIDTz-BT in toluene solution was located at 650 nm, which shifted to 688 nm in chloroform solution. The redshift of 38 nm caused by the increase in solvent polarity from toluene to chloroform indicates that ICT occurs between the GIDTz and BT groups, although the shift is not large. Similar redshifts were observed for the other three polymers, and the PL spectra of these polymers are shown in Figure 3.4.

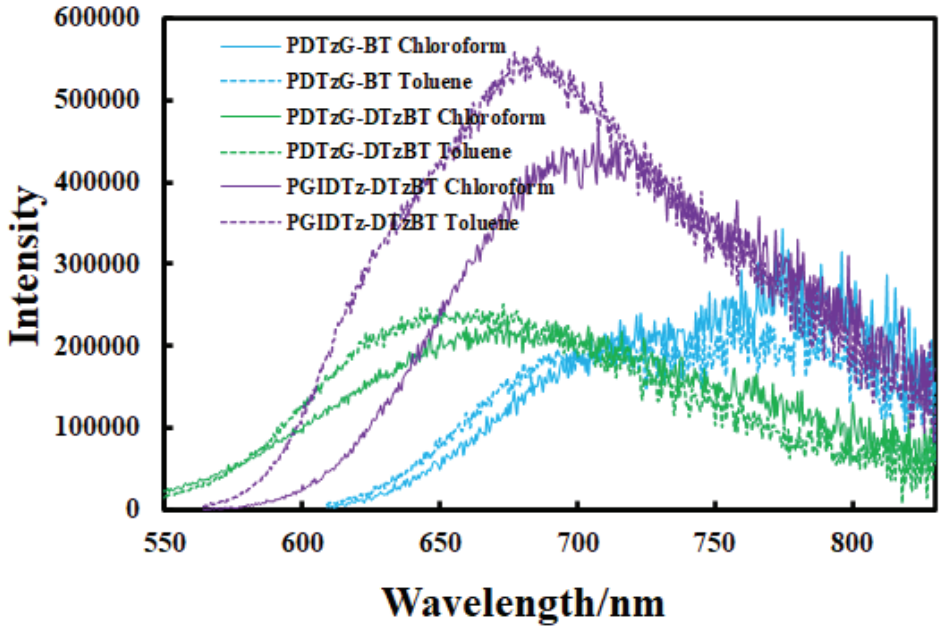

Figure 3.4. PL spectra of PDTzG-BT, PDTzG-DTzBT and PGIDTz-DTzBT.

Table 3.1 Molecular weights and optical and electrochemical properties of thiazologermole-containing copolymers.

Polymer	M_n (kDa) [a]	PDI	λ_{max}^{soln} [b] /λ_{max}^{film} [c] (nm)	λ_{onset}^{film} (nm)	E_g^{opt} [d] (eV)	E_{LUMO} [e] /$_{HOMO}$ [f] (eV)	E_{LUMO}/ $_{HOMO}$ [g] (eV)
PDTzG-BT	8.8	2.5	599/630	829	1.50	-3.55/-5.05	-3.13/-5.00
PGIDTz-BT	7.7	1.6	579/608	738	1.68	-3.55/-5.23	-2.97/-4.94
PDTzG-DTzBT	3.1	1.6	526/555	733	1.69	-3.64/-5.33	-3.26/-5.11
PGIDTz-DTzBT	8.7	2.9	554/577	708	1.75	-3.58/-5.33	-3.12/-5.07

[a] Determined by GPC at 50 °C in THF. [b] For diluted chloroform solutions at room

temperature, [c] For cast films. [d] $1240/\lambda_{onset}^{film}$. [e] $E_{LUMO} = -(E_{red}^{onset} - (E_{Fc/Fc+}) + 4.80)$ with E_{red}^{onset} from F_c/F_c^+ external standard. [f] $E_{HOMO} = E_{LUMO} - E_g^{opt}$. [g] Based on DFT calculations at the B3LYP/6-31G(d,p)/GD3BJ level of theory.

The electrochemical behaviors of the polymers were investigated by cyclic voltammetry (CV) measurements. The reduction peaks of the polymers appeared with onset potentials at -0.89, -0.89, -0.80, and -0.86 V for PDTzG-BT, PGIDTz-BT, PDTzG-DTzBT, and PGIDTz-DTzBT, respectively. The oxidation peaks of the polymers have no detected. On the basis of the reduction onsets, the LUMO energy levels were estimated to be -3.55, -3.55, -3.64, and -3.58 eV for PDTzG-BT, PGIDTz-BT, PDTzG-DTzBT, and PGIDTz-DTzBT, respectively, as shown in Figure 3.3(d). Based on previous work, LUMOs of -3.6 eV or lower are beneficial for electron transport [87]. The LUMOs of the polymers are close to -3.6 eV, which is likely to be electron transport materials. Because these polymers had indiscernible anodic peaks, the HOMO energy levels were calculated from the equation $E_{HOMO} = E_{LUMO} - E_g^{opt}$ to be -5.05, -5.23, -5.33, and -5.33 eV for PDTzG-BT, PGIDTz-BT, PDTzG-DTzBT, and PGIDTz-DTzBT, respectively. PDTzG-DTzBT and PGIDTz-DTzBT possess lower HOMO and LUMO energy levels than that of the polymers containing BT as the acceptor because of the extra thiazole units. Compared with the analogous thienogermole polymers, the present thiazoleogermole polymers exhibited enhanced electron-deficient performance with lower-lying LUMOs.

2.4. DFT calculations

To further study how the introduction of thiazole units affects the geometries and electronic states of the polymers, DFT calculations were performed on the models using the Gaussian 09 program at the B3LYP/6-31G(d,p)/GD3BJ level of theory, in which the alkyl substituents were replaced by short methyl groups, and the results are summarized in Table 3.1. The LUMO/HOMO energy levels of thiazologermole-containing polymers PDTzG-BT and PGIDTz-BT were estimated to be -3.13/-5.00 and

-2.97/-4.94, which were lower by 0.33/0.49 and 0.26/0.38 eV than those of thienogermole-containing polymers PDTG-BT and PGIDT-BT (Figure 3.5), respectively. The LUMOs of these polymers are mainly placed in the acceptor units, whereas the HOMOs are distributed in the DTzG/GIDTz units and the benzene rings of BT, as shown in Figure 3.5; this result indicates that ICT may occur from DTzG/GIDTz to acceptor unit BT or DTzBT. Figure 3.6 shows the optimized geometries of these polymer models. The polymers exhibited completely planar backbones with dihedral angles < 0.04° between DTzG (or GIDTz) and the adjacent BT or DTzBT unit as a result of intramolecular noncovalent S–N and N–H interactions [48], which are evidenced by the S–N (2.91-2.93 Å) and N–H (2.49-2.52 Å) distances, which are shorter than the sum of the van der Waals radii of S and N (3.35 Å) and H and N (2.70 Å) [88]. Although the flexibility of the polymer structures could allow for non-planar structures, the noncovalent interactions seem to enhance the polymer planarity even in real systems.

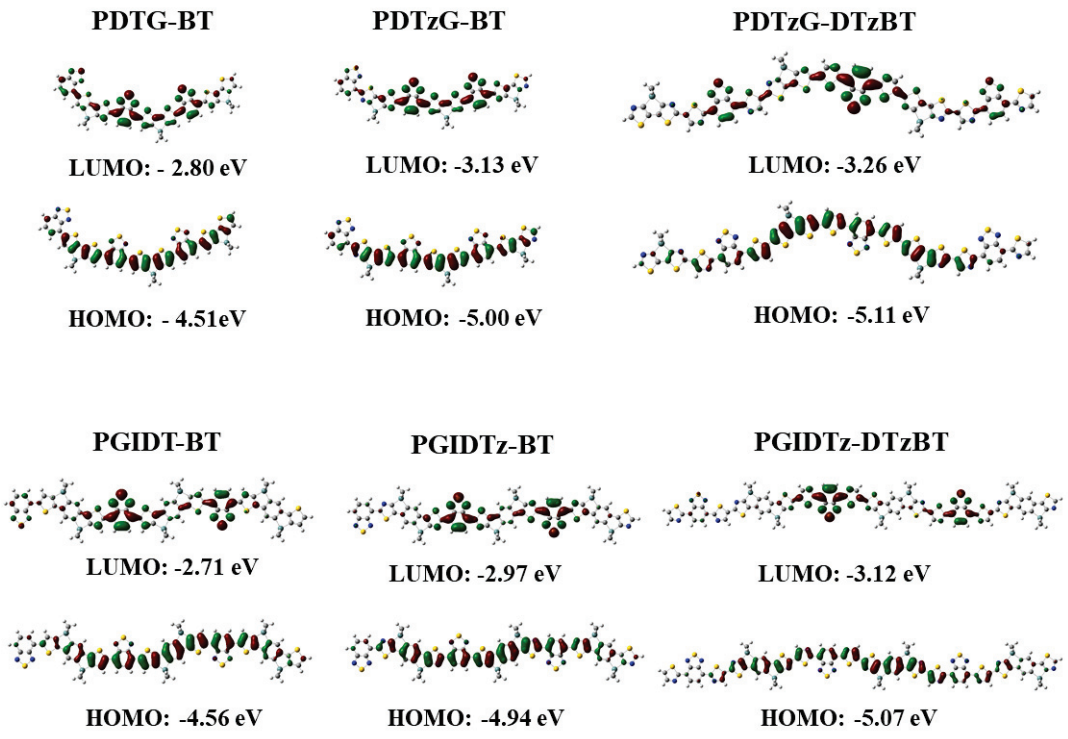

Figure 3.5. PDTG-BT, PGIDT-BT, PDTzG-BT, PGIDTz-BT, PDTzG-DTzBT and PGIDTz-DTzBT trimer with a visualization of the HOMO and LUMO distributions

and energy levels, derived from DFT calculations at B3LYP/6-31G(d,p)/GD3BJ.

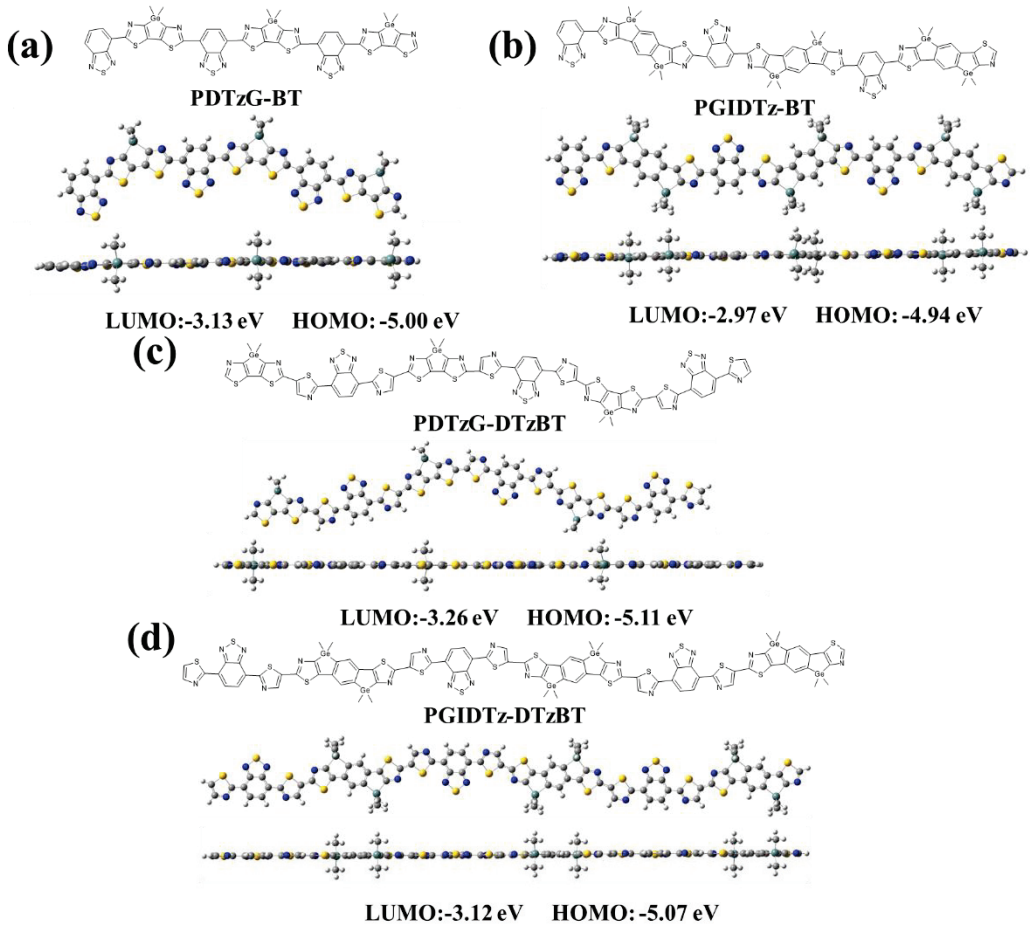

Figure 3.6. Optimized molecular geometries for three repeating units of thiazologermole-containing polymers (a) PDTzG-BT, (b) PGIDTz-BT, (c) PDTzG-DTzBT, and (d) PGIDTz-DTzBT. Calculations were performed at the B3LYP/6-31G(d,p)/GD3BJ level, and the alkyl chain was replaced by a methyl group to reduce the calculation time.

To systematically study the effects of the bridging atom in cyclopentadiene and germole and the introduction of thiazole units on the energy levels of the HOMOs and LUMOs, smaller models were also examined by DFT calculations at B3LYP/6-31G(d,p). In a previous work that compared thiophene- and thiazole-fused cyclopentadiene and germole molecules by DFT calculations, it was found that germole

compounds exhibited lower HOMO and LUMO energy levels [33]. Indeed, the LUMO energy levels of CDTz/IDTz and DTzG/GIDTz are at -1.56/-1.59 and -1.69/-1.74 eV, whereas their HOMO energy levels are at -5.72/-5.37 and -5.82/-5.49 eV, respectively. This is due to the σ*(Ge) - π*(Tz) conjugation in the LUMOs and the reduced anti-bonding interaction between Tz rings in the HOMOs, as shown in Figures 3.7 and 3.8. The negative HOMO and LUMO energy levels of IDT-DTzBT and IDTz-DTBT agree with the experimental results that IDT-DTzBT and IDTz-DTBT contain higher electron mobilities than that of IDT-DTBT. In this work, the DTzG-BT and GIDTz-BT models show HOMO and LUMO energy levels that are lower by 0.31–0.50 eV and 0.13–0.19 eV, respectively, than those of DTG-BT and GIDT-BT; this result clearly indicates the effects of thiazole in lowering these energy levels, as shown in Figures 3.7 and 3.8. It was also found that substituting DTzBT for BT to furnish DTzG-DTzBT and GIDTz-DTzBT lowered the LUMO energy levels.

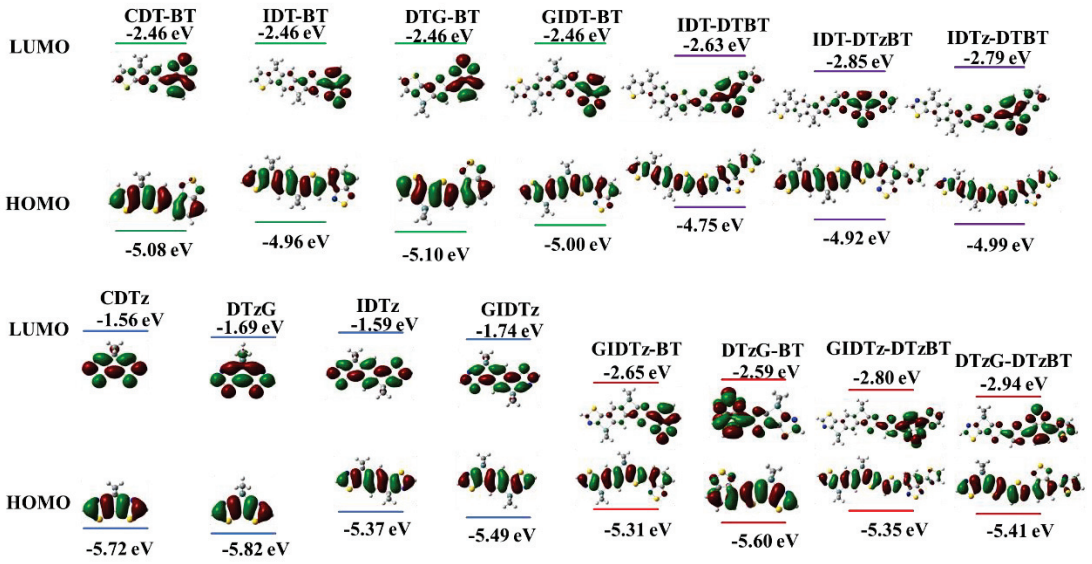

Figure 3.7. Computational spatial electron distributions of monomers and polymers of a repeating unit, derived from DFT calculations at B3LYP/6-31G(d,p).

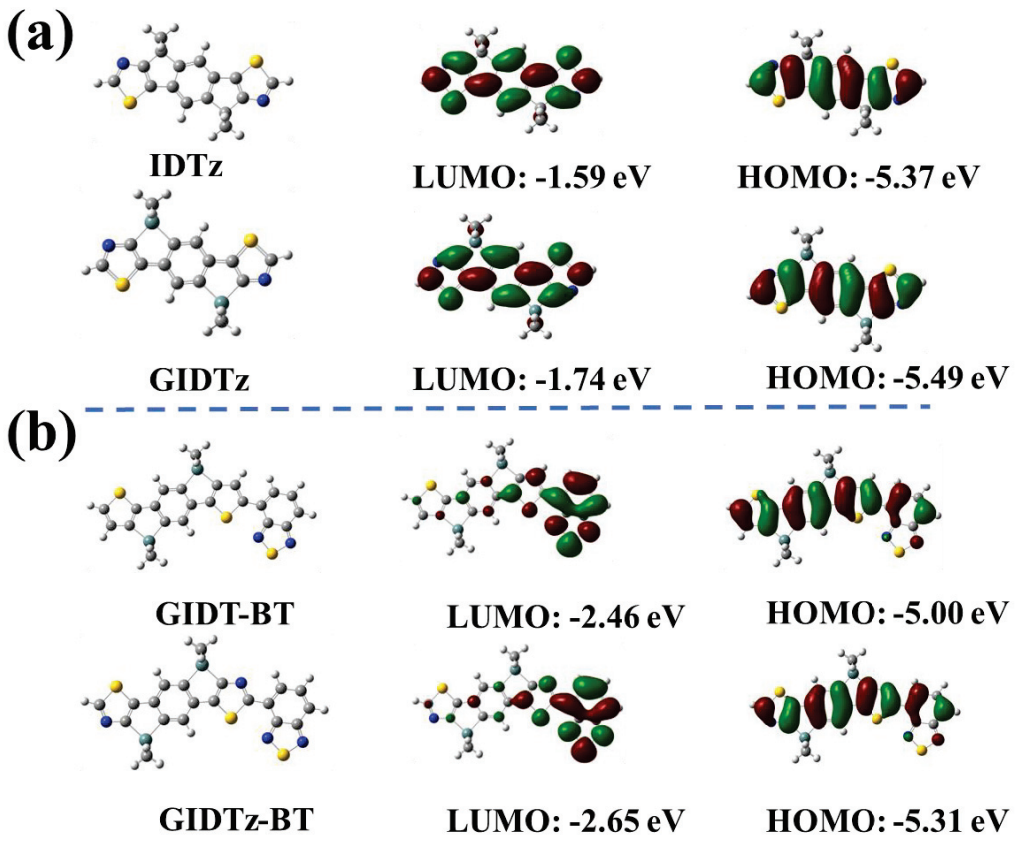

Figure 3.8. Computational spatial electron distributions of monomers (a) and polymers of a repeating unit (b).

3. Conclusions

We prepared new D-A type polymers containing thiazole-condensed germoles as the donor and BT and DTzBT as the acceptor and investigated their optical and electrochemical properties. The ICT behaviors of these polymers were also examined by PL measurements in different solvents. DFT calculations revealed that the HOMO/LUMO energy levels of DTzG- and GIDTz-based polymers are lower than those of previously reported thiophene-based congeners. In addition, DTzG/GIDTz and the adjacent BT unit exhibited high coplanarity because of intramolecular noncovalent S–N and N–H interactions. It was also indicated that replacing cyclopentadiene by germole and introducing thiazole units in place of thiophene units markedly lowered the HOMO/LUMO energy levels, revealing the possible tuning of the electronic states of the polymers by element-based molecular design. PGIDTz-BT, PDTzG-BT,

PGIDTz-DTzBT, and PDTzG-DTzBT with low-lying FMOs are excellent candidates for n-type semiconductor materials. These polymers were also demonstrated to exhibit good film-forming properties and thermal stability. Applications of polymers, such as for OTFT active layers, are being studied and will be reported elsewhere.

General consideration

All reactions were carried out in dry argon. Toluene and chlorobenzene used as the reaction solvents were distilled from CaH_2 and stored over activated molecular sieves in the dark until use. Monomers were prepared as described in below. NMR spectra were recorded on a Varian 400-MR spectrometer. UV-vis absorption and PL (photoluminescence) spectra were measured on Hitachi U-2910 and HORIBA FluoroMax-4 spectrophotometers, respectively. APCI-mass spectra were obtained by a Thermo Fisher Scientific LTQ Orbitrap XL spectrometer at N-BARD, Hiroshima University. MALDI-TOF mass spectra were obtained on a Bruker Ultraflextreme instrument in positive mode, using trans-2-[3-(4-tert-butylphenyl)-2-methyl-2-propenylidene] malononitrile as the matrix. Gel permeation chromatography (GPC) was performed on a Shimadzu LC-20AD system equipped with an SPD-20Adetector. Melting point (mp) was carried out Yanaco MP-500P. Microwave was performed on Biotage initiator+. Thermogravimetric analysis (TGA) was conducted using an SII EXSTARTG-DTA6200 thermal analyzer in the temperature range of 30 -600 ˚C with a heating rate of 10 °C min^{-1} in a nitrogen atmosphere. Differential scanning calorimetry (DSC) measurements was performed on a HITACHI DSC7000X analyzer under a nitrogen atmosphere, in which heating and cooling were performed at a rate of 10 °C min^{-1} in the temperature range of 30-250 °C.

Synthesis

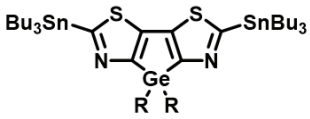

Synthesis of DTzG-Sn

To a solution of DTzG (0.38 g, 0.82 mmol) in THF (20 mL) was added a THF solution of LDA (1.8 mL, 1.8 mmol, 1.0 M) at -78 °C and the resulting mixture was stirred for 1 h at this temperature. Tributyltin chloride (0.62 g, 1.9 mmol) was then added into this solution at -78 °C. After stirring the mixture overnight at room

temperature, the solvent was evaporated under reduced pressure. The residue was directly purified by neutral alumina column chromatography with hexane: ethyl acetate = 10:1 as the eluent to afford DTzG-Sn in 80% yield (0.68 g, 0.66 mmol) as a yellow oil. ^{1}H NMR ($CDCl_3$) δ 1.69-1.49 (m, 12H), 1.43-1.11 (m, 52H), 0.95-0.75 (m, 24H); ^{13}C NMR ($CDCl_3$) δ 174.10, 164.51, 141.05, 32.05, 31.83, 29.14, 29.10, 28.90, 27.17, 25.28, 22.63, 14.31, 14.09, 13.64, 11.32. HRMS (APCI) m/z calcd for $C_{46}H_{88}GeN_2S_2Sn_2$ [M^+] 1044.3639, found 1044.3744.

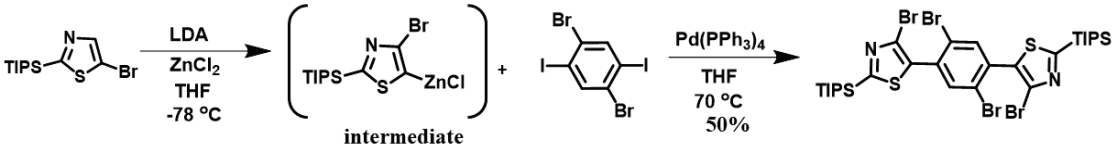

Synthesis of 5,5'-(2,5-dibromo-1,4-benzenediyl)bis(4-bromo-2-triisopropylsilylthiazole)

To a solution of 5-bromo-2-triisopropylsilyl thiazole (6.42 g, 20.0 mmol) in THF (50 mL) was added LDA (24.0 mmol, 1 M) at -78 °C and the resulting mixture was stirred for 30 min at this temperature. Zinc chloride (24 mmol, 1 M) was added to the reaction solution and further stirred at -78 °C for 1 h. Then, the reaction mixture was warmed to room temperature. After 1h stirring, 1,4-dibromo-2,5-diioobenzene (4.40 g, 9.0 mmol) and $Pd(PPh_3)_4$ (1.14 g, 1.0 mmol) were added and the mixture was heated at 70 °C overnight. The solvent was removed in vacuo and the residue was directly purified by column chromatography on silica gel with hexane: dichloromethane = 2:1 as the eluent to afford the target compound in 50% yield (4.36 g, 5.0 mmol) as a white powder; mp = 170-172 °C. ^{1}H NMR ($CDCl_3$) δ 7.76 (s, 2H), δ 1.52-1.42 (sept, J = 7.6 Hz, 6H), δ 1.19 (d, J = 7.6 Hz, 36H); ^{13}C NMR ($CDCl_3$) δ 172.64, 136.28, 134.36, 131.94, 128.88, 123.27, 18.44, 11.57. HRMS (APCI) calcd for $C_{30}H_{44}Br_4N_2S_2Si_2$ [M^+] 871.9177, found 871.9293.

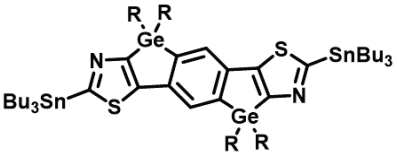

Synthesis of GIDTz-Sn

GIDTz-Sn was synthesized in a manner similar to the synthesis of DTzG-Sn, by using GIDTz instead of DTzG in 85% yield as a yellow oil. ^{1}H NMR ($CDCl_3$) δ 7.56 (s, 2H), 1.73-1.52 (m, 12H), 1.50-1.03 (m, 80H), 0.98 (t, J = 7.2 Hz, 18H), 0.83 (t, J = 6.8 Hz, 12H); ^{13}C NMR ($CDCl_3$) δ 175.29, 163.62, 151.57, 144.00, 139.52, 128.57, 32.82, 31.84, 29.20, 29.09, 28.92, 27.20, 25.33, 22.63, 14.39, 14.09, 13.66, 11.28. HRMS (APCI) calcd for $C_{44}H_{72}Ge_2N_2S_2$ [M^+] 1416.5677, found 1416.5730.

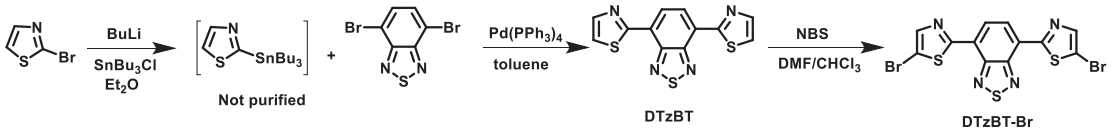

Synthesis of 4,7-Di(thiazol-2-yl)benzo[*c*][1,2,5]thiadiazole (DTzBT)

To a solution of 2-bromothiazole (3.28 g, 20.0 mmol) in Et_2O (50 mL) was added a solution of *n*-BuLi (22.0 mmol, 1.6 M) in hexane at -78 ºC and the mixture was stirred for 1 h at this temperature. Tributyltin chloride (7.80 g, 24.0 mmol) was added to the mixture. After stirring for 1 h, the resulting mixture was warmed to room temperature and stirred overnight. The solvent was evaporated under reduced pressure to give crude tributylstannylthiazole that was used for the following reaction without purification. A mixture of tributylstannylthiazole thus prepared, 4,7-dibromo-2,1,3-benzothiadiazole (2.5 g, 10 mmol), $Pd(PPh_3)_4$ (0.65 g, 0.03 mmol), and toluene (40 mL) was heated to reflux overnight. The mixture was then cooled to room temperature, and the solvent was evaporated under reduced pressure. The residue was directly purified by column chromatography (eluent chloroform) to give the title compound as a yellow solid (0.78 g, 25.8%); mp = 140-142 °C; ^{1}H NMR ($CDCl_3$) δ 8.76 (s, 2H), 8.07 (d, 2H), 7.63 (d, 2H). ^{13}C NMR ($CDCl_3$): δ 161.89, 151.96, 143.40, 127.39, 126.54, 122.36.

Synthesis of 4,7-Bis(5-bromothiazol-2-yl)benzo[c][1,2,5]thiadiazole (DTzBT-Br)

To a solution of 4,7-di(thiazol-2-yl)benzo[*c*][1,2,5]thiadiazole (0.78 g, 2.6 mmol) in chloroform (50 mL) and DMF (50 mL), NBS (1.1 g, 5.7 mmol) was added in several portions and the mixture was heated at 60 ºC for 24 h. The mixture was cooled to room

temperature and poured into 50 mL water. The aqueous phase was extracted with chloroform. Then the organic phases were dried with anhydrous sodium sulfate. The solvent was removed under reduced pressure and the crude products were washed using chloroform (10 mL) to give the title compound as a light red solid (0.8 g, 66.9%); mp = 268-270 °C; ^{1}H NMR ($CDCl_3$) δ 8.69 (s, 2H), 7.94 (s, 2H). HRMS (APCI) calcd for $C_{12}H_4Br_2N_4S_3$ [M^+] 459.7944, found 459.8013.

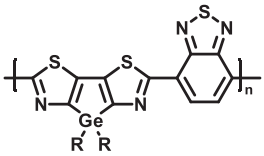

Synthesis of PDTzG-BT

A toluene (4 mL) solution of DTzG-Sn (0.40 g, 0.383 mmol), BT-Br (0.11 g, 0.383 mmol), $Pd_2(dba)_3$ (8 mg, 0.007 mmol) as the catalyst, and P(*o*-tolyl)$_3$ (0.014 g, 0.046 mmol) as the ligand was sealed in a glass tube with a rubber stopper. The sealed tube was put into a microwave reactor and heated at 140 °C for 3 h. The reaction mixture was poured into 100 mL methanol, and the resultant precipitates were collected by filtration. The precipitates were washed by Soxhlet extraction with methanol, hexane, and dichloromethane. Finally, the residue was extracted with chloroform, and the chloroform solution of polymer was concentrated to 5 mL and reprecipitated in methanol. The polymer was collected by filtration and dried in vacuo (black solid, 156 mg, 67.8% yield). ^{1}H NMR ($CDCl_3$) δ 9.03-8.64 (br, 2H), 2.03-0.96 (br, 28H), 0.93-0.43 (br, 6H). The ^{13}C NMR spectrum was not obtained because of the low solubility of the polymer.

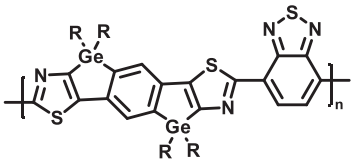

Synthesis of PGIDTz-BT

A toluene (4 mL) solution of GIDTz-Sn (0.37 g, 0.26 mmol), BT-Br (0.076 g, 0.26 mmol), $Pd_2(dba)_3$ (5.3 mg, 0.005 mmol) as the catalyst, and P(*o*-tolyl)$_3$ (9.2 mg, 0.0312

mmol) as the ligand was sealed in a glass tube with a rubber stopper. The sealed tube was heated at 140 °C for 3 h in a microwave reactor. The reaction mixture was poured into 100 mL methanol, and the resultant precipitates were collected by filtration. The precipitates were washed by Soxhlet extraction with methanol, hexane, and dichloromethane. Finally, the residue was extracted with chloroform, and the chloroform solution of polymer was concentrated to 5 mL and reprecipitated in methanol. The polymer was collected by filtration and dried in vacuo (black solid, 146 mg, 57.9% yield). ^{1}H NMR ($CDCl_3$) δ 8.85 (br s, 2H), 7.81 (br s, 2H), 1.54-0.94 (br m, 56H), 0.90-0.75 (br s, 12H). The ^{13}C NMR spectrum was not obtained because of the low solubility of the polymer.

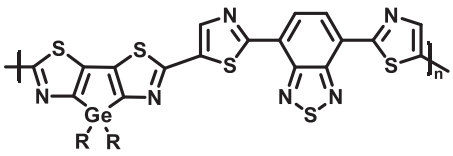

Synthesis of PDTzG-DTzBT

A chlorobenzene (10 mL) solution of GIDTz-Sn (0.19 g, 0.18 mmol), DTzBT-Br (83 mg, 0.18 mmol), $Pd_2(dba)_3$ (3.3 mg, 0.0036 mmol) as the catalyst, and $P(o\text{-tolyl})_3$ (6.6 mg, 0.0216 mmol) as the ligand were put into a three-necked flask under argon, and the flask was heated at 110 °C for 1 h in an oil bath. The reaction mixture was poured into 100 mL methanol, and the resultant precipitates were collected by filtration. The precipitates were washed by Soxhlet extraction with methanol, hexane dichloromethane, and chloroform. Finally, the residue was extracted with chlorobenzene, and the chlorobenzene solution of polymer was concentrated to 5 mL and reprecipitated in methanol. The polymer was collected by filtration and dried in vacuo (black solid, 30 mg, 21.8% yield). ^{1}H NMR ($CDCl_3$) δ 8.81 (br s, 2H), 8.43 (br s, 2H), 1.52-1.50 (br m, 8H), 1.41-1.08 (br s, 20H), 0.92-0.80 (br t, 6H). The ^{13}C NMR spectrum was not obtained because of the low solubility of the polymer.

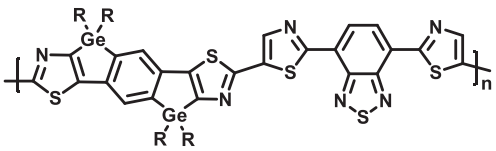

Synthesis of PGIDTz-DTzBT

A chlorobenzene (5 mL) solution of GIDTz-Sn (0.103 g, 0.073 mmol), DTzBT-Br (0.034 g, 0.073 mmol), $Pd_2(dba)_3$ (4.3 mg, 0.0036 mmol) as the catalyst, and P(*o*-tolyl)$_3$ (3.2 mg, 0.0087 mmol) as the ligand was sealed in a glass tube with a rubber stopper. The sealed tube was heated at 140 °C for 3 h in a microwave reactor. The reaction mixture was poured into 100 mL methanol, and the resultant precipitates were collected by filtration. The precipitates were washed by Soxhlet extraction with methanol and hexane. Finally, the residue was extracted with dichloromethane, and the dichloromethane solution of polymer was concentrated to 5 mL and reprecipitated in methanol. The polymer was collected by filtration and dried in vacuo (black solid, 55 mg, 66.3% yield). ^{1}H NMR ($CDCl_3$) δ 8.79 (br, s, 2H), 8.41 (br s, 2H), 7.58 (br s, 2H), 1.65-1.03 (br m, 56H), 0.93-0.52 (br m, 12H). The ^{13}C NMR spectrum was not obtained because of the low solubility of the polymer.

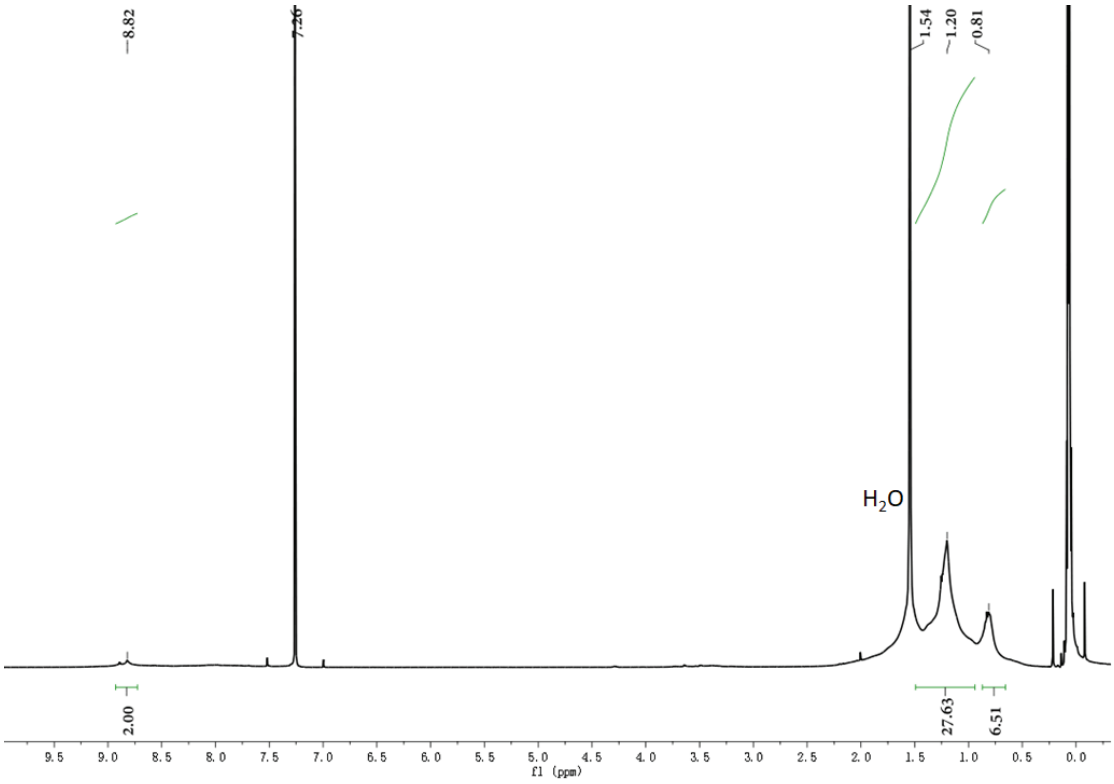

Figure 3.9. ^{1}H NMR spectrum of PDTzG-BT

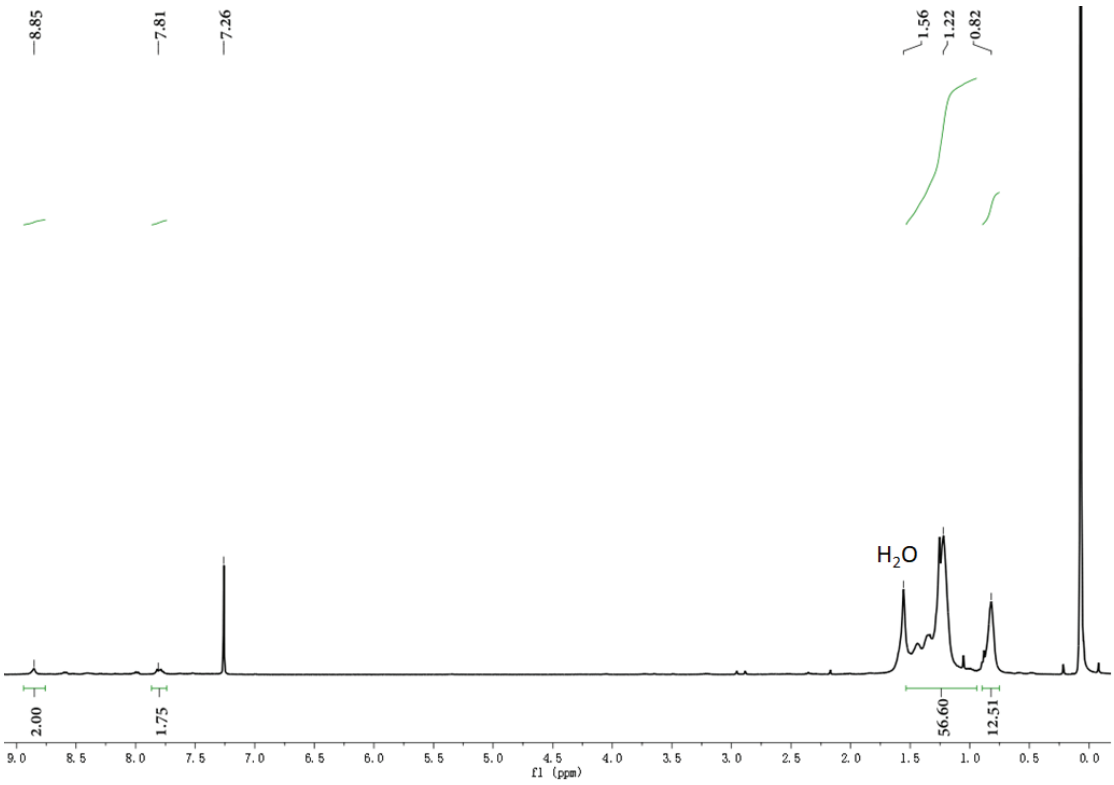

Figure 3.10. [1]H NMR spectrum of PGIDTz-BT

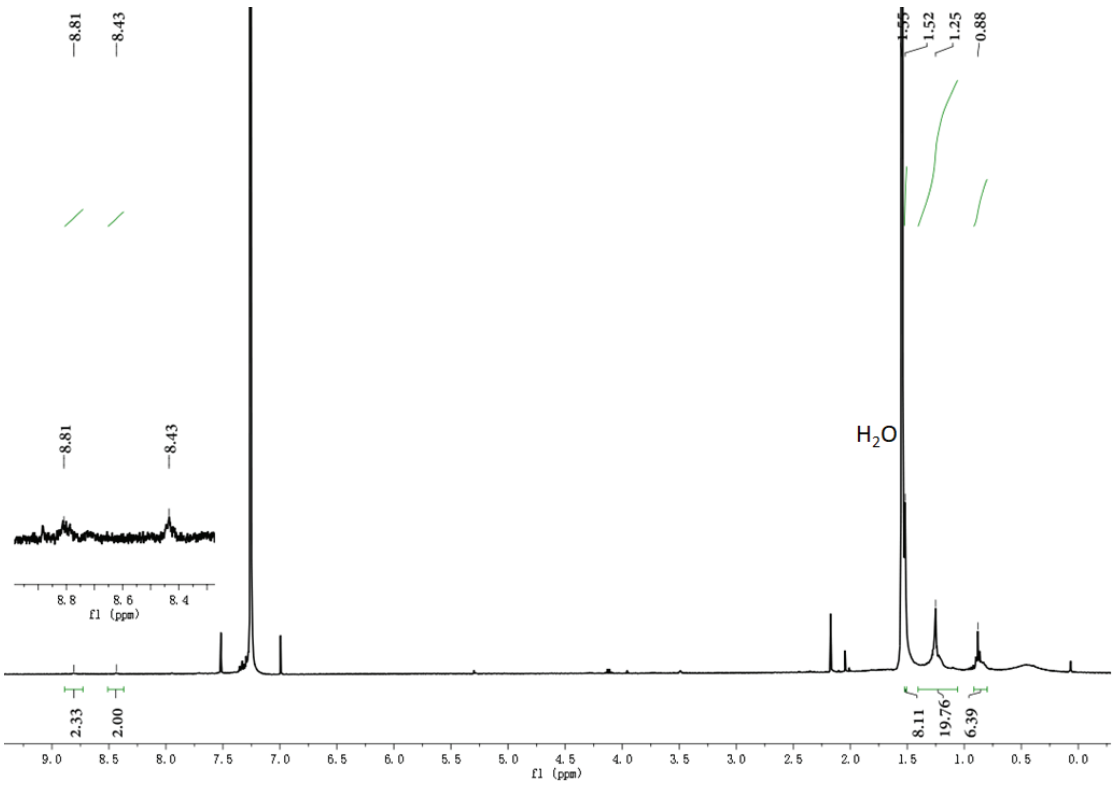

Figure 3.11. [1]H NMR spectrum of PDTzG-DTzBT

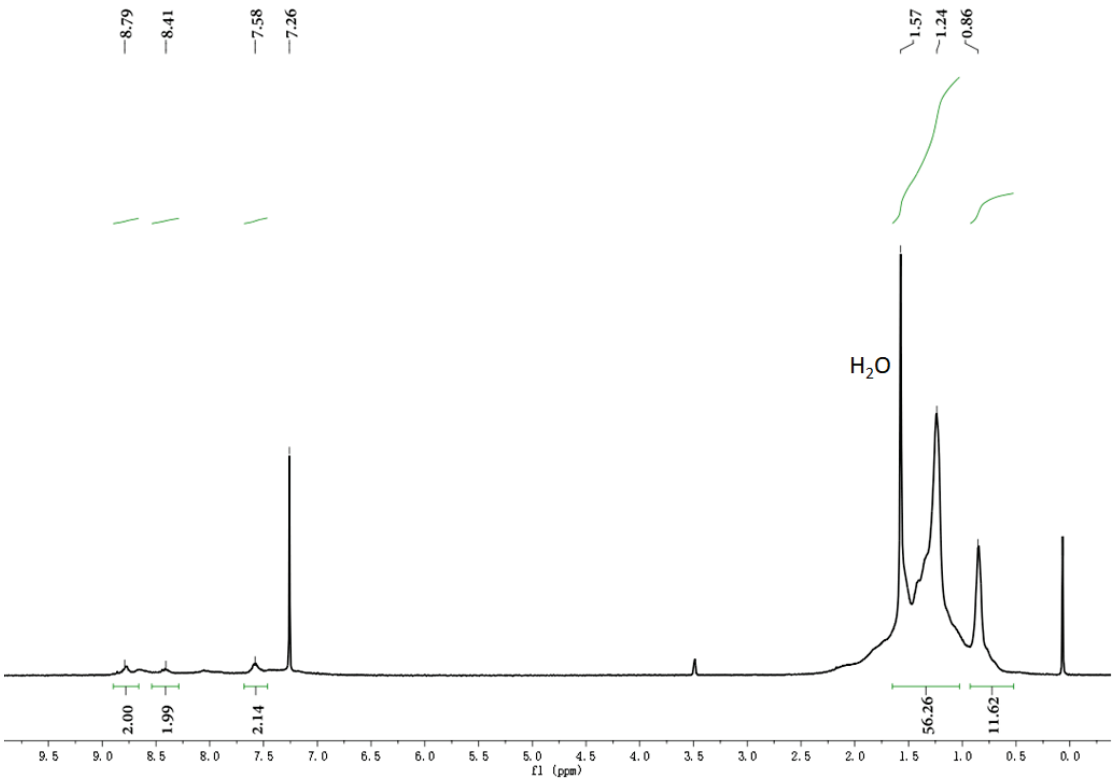

Figure 3.12. ^{1}H NMR spectrum of PGIDTz-DTzBT

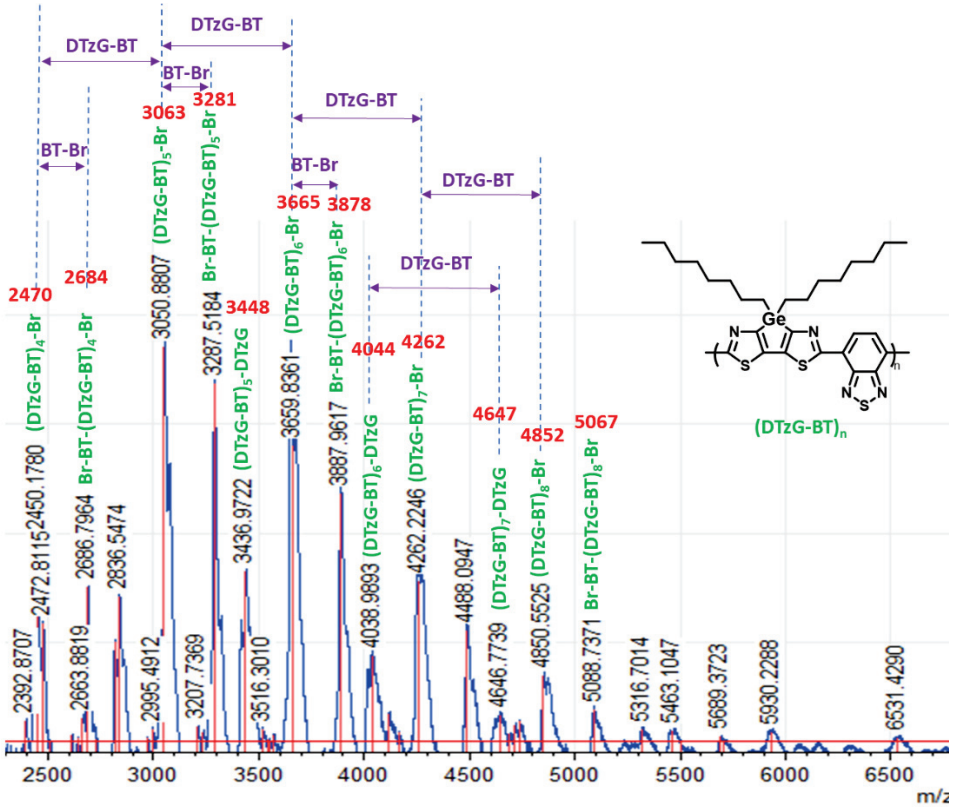

Figure 3.13. MALDI-TOF mass spectrum of PDTzG-BT (The red numbers represent the theoretical mass)

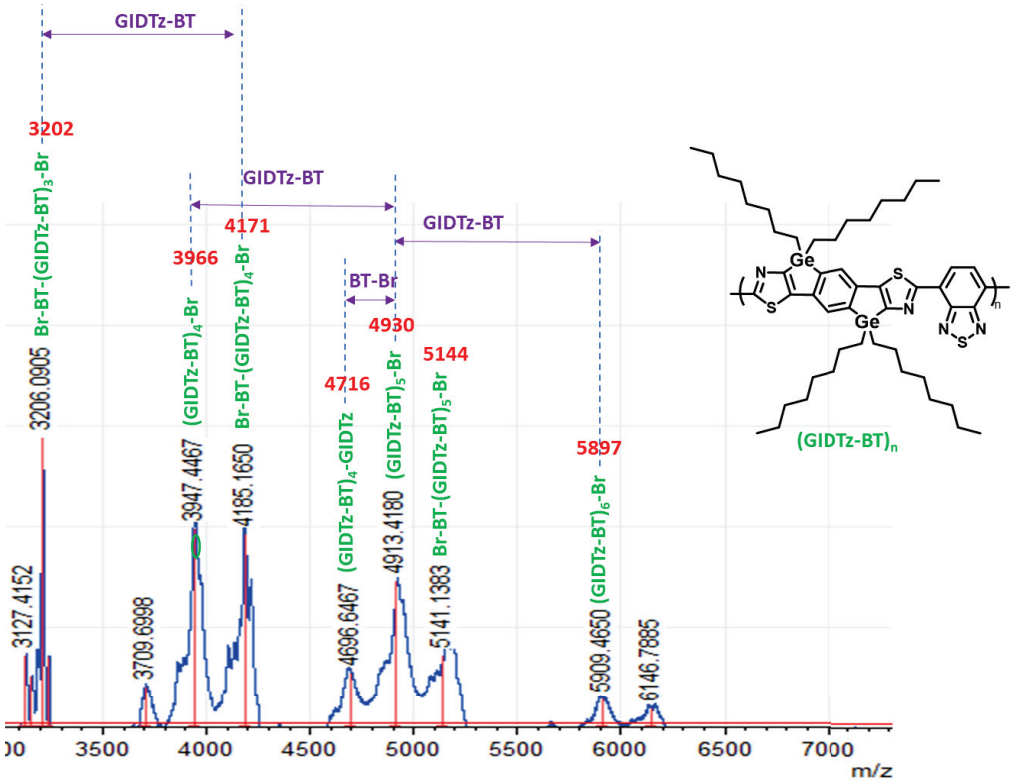

Figure 3.14. MALDI-TOF mass spectrum of PGIDTz-BT (The red numbers represent the theoretical mass)

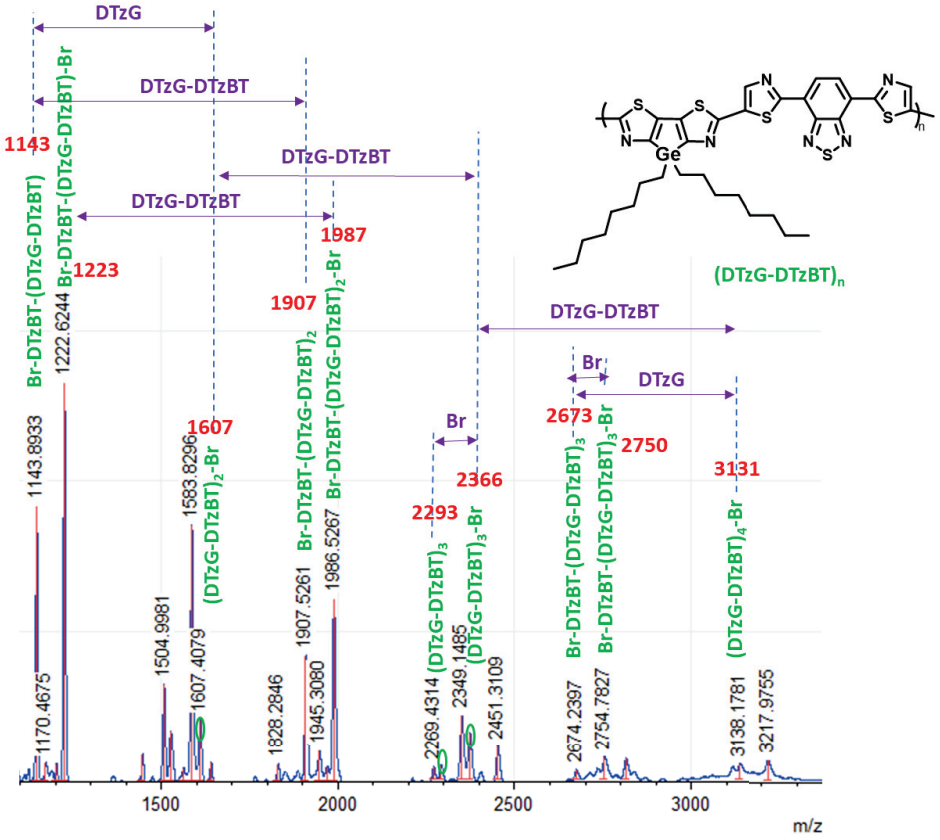

Figure 3.15. MALDI-TOF mass spectrum of PDTzG-DTzBT (The red numbers represent the theoretical mass)

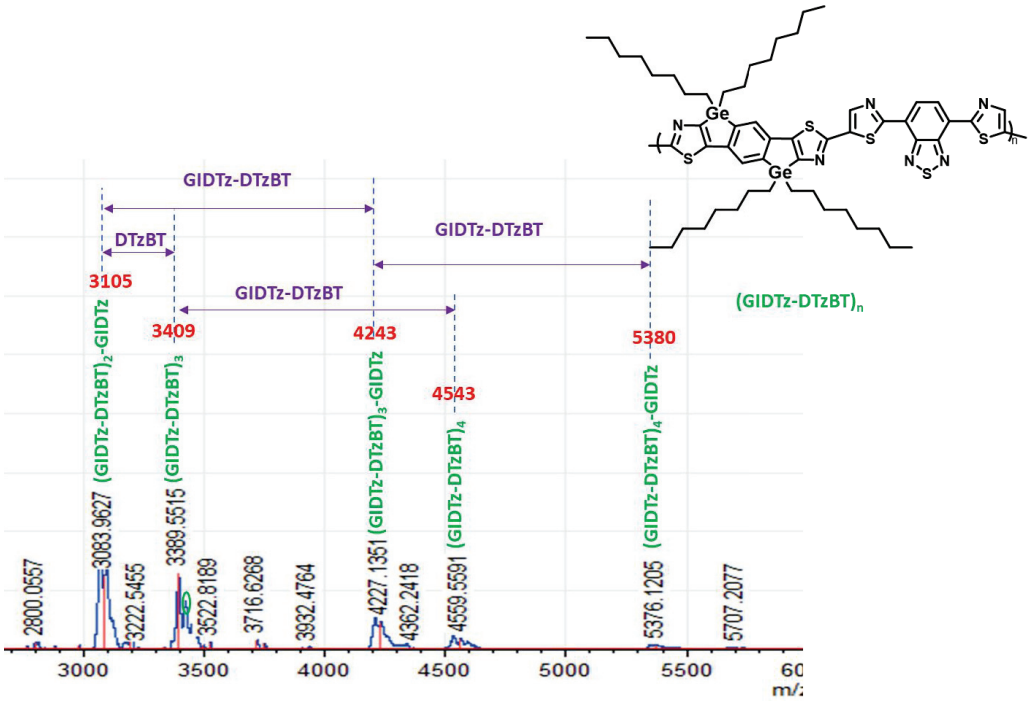

Figure 3.16. MALDI-TOF mass spectrum of PGIDTz-DTzBT (The red numbers represent the theoretical mass)

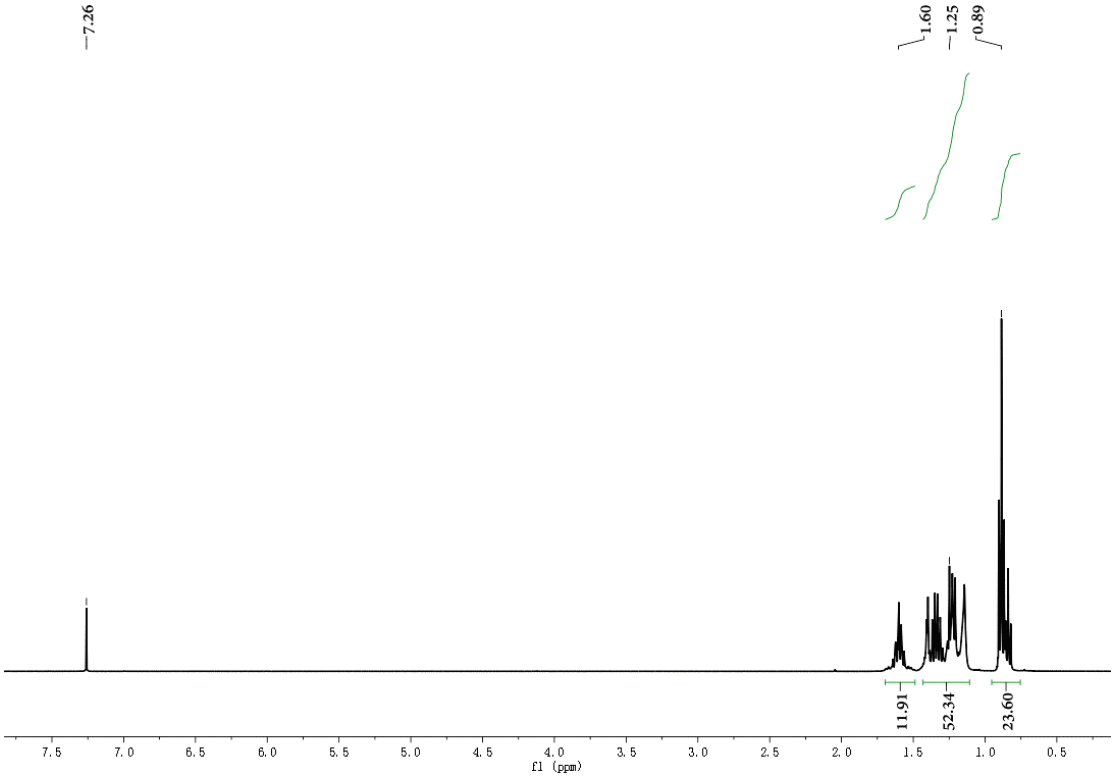

Figure 3.17. ^{1}H NMR spectrum of **DTzG-Sn**

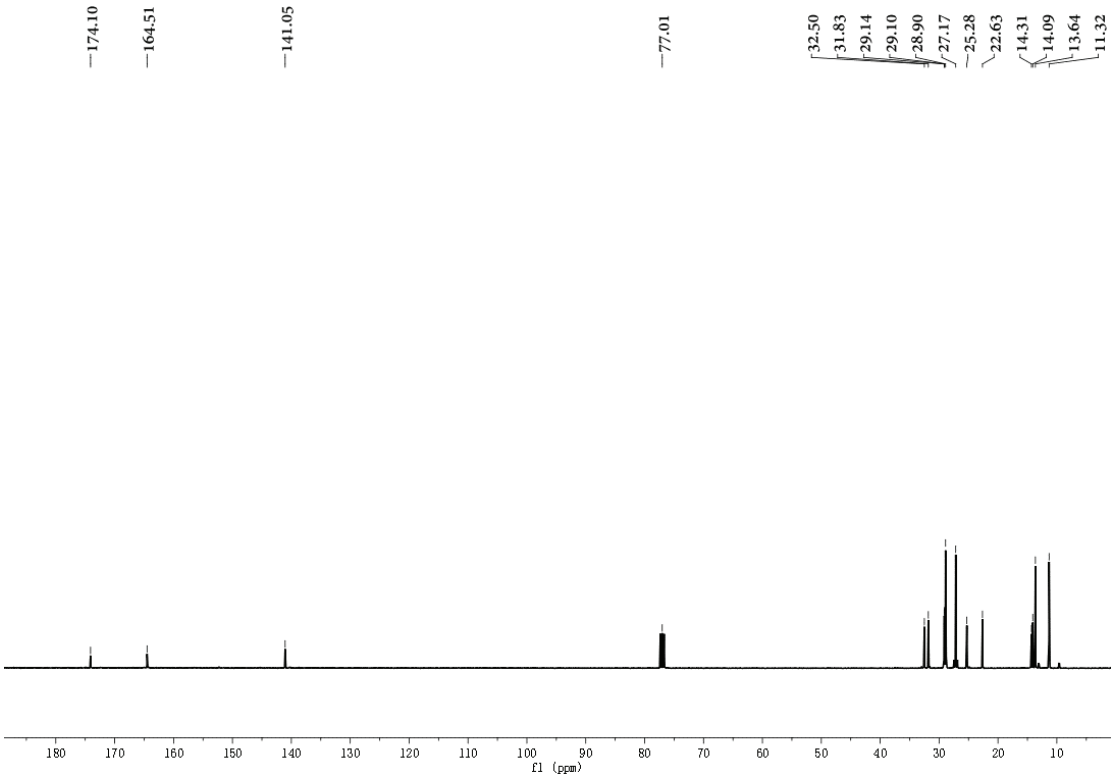

Figure 3.18. ^{13}C NMR spectrum of **DTzG-Sn**

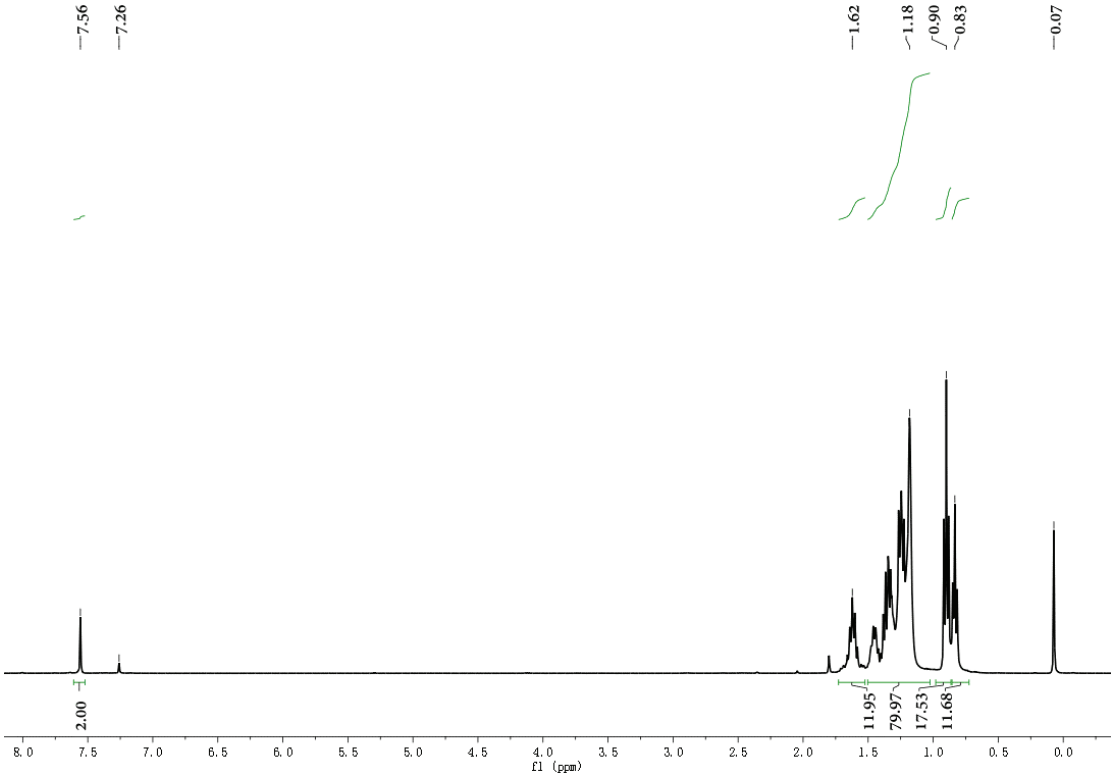

Figure 3.19. ^{1}H NMR spectrum of **GIDTz-Sn**

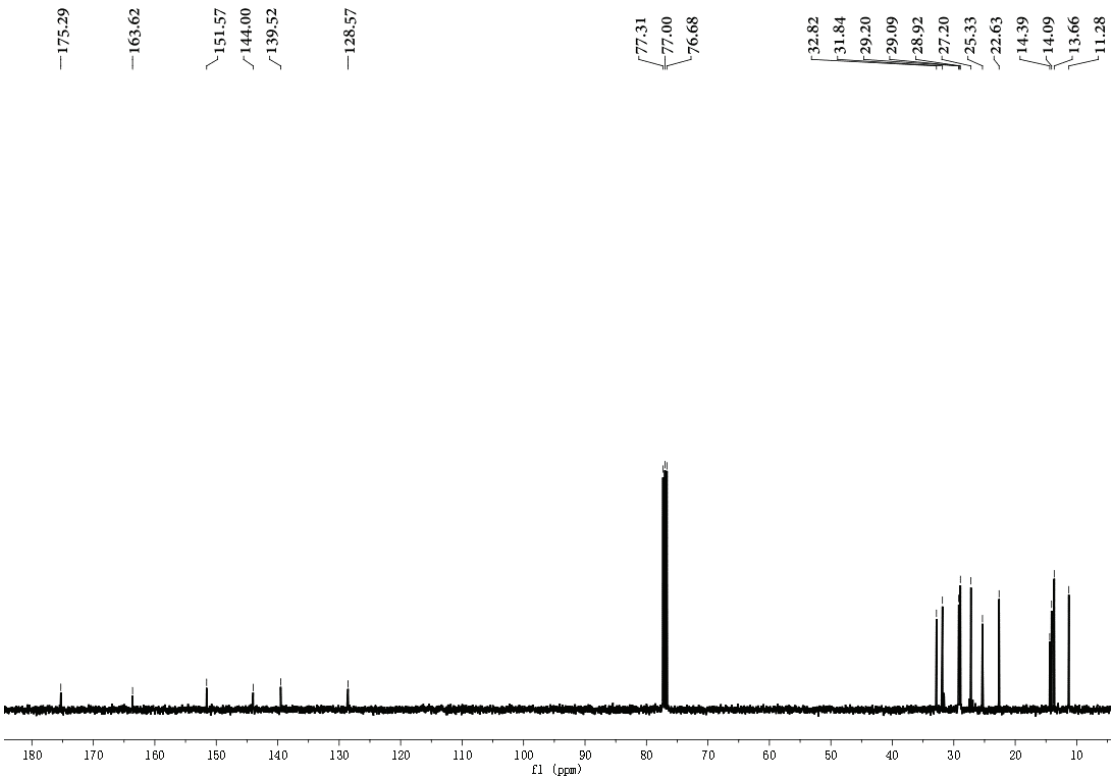

Figure 3.20. ^{13}C NMR spectrum of **GIDTz-Sn**

Chapter 4: Dicyanovinyl-capped thiazologermoles with moderate donor-acceptor interaction as visible photoluminescence turn-on sensors for primary amines

1. Introduction

Detecting amines has been an important topic in sensing technology research in the past decades, owing to widespread applications of amines in the field of materials and pharmaceutical chemistry, biology, and environmental science [89, 90]. Amines play a key role as catalysts, organic bases, solvents, and raw materials in chemical reactions [91], and large amounts of amines are produced and used to meet these demands. However, amines in general are toxic compounds that can cause headaches, skin burns, and eye irritation upon contact or ingestion [92, 93]. Thus, leakage of excess amines into the atmosphere is detrimental to public health and the environment [94]. In particular, some primary amines are known to modulate the essential metabolic and physiological functions of living organisms, and their contamination in food and drinking water is a serious concern [95, 96]. For these reasons, new materials for the detection of amines, in addition to some anions such as I^-, F^-, and CN^- that are also harmful to human health [97-99], are highly desired.

PL sensing of amines and some halide ions using organic π-conjugated materials has been well studied as a low-cost, rapid-response, and susceptible and selective sensing method [100-102]. An effective strategy for designing PL sensor materials is based on intramolecular D–A interaction to promote ICT. Interactions of amines and halide ions with a D–A unit of PL materials cause the change of ICT behavior, which leads to susceptible changes in PL color and intensity [103, 104]. π-Conjugated compounds functionalized by a dicyanovinyl (DCV) group have been examined for use as n-type organic semiconductors and PL materials [105-108]. The DCV group is a strong electron acceptor and can be readily introduced to π-conjugated systems to promote ICT behavior. Based on these properties, some compounds containing DCV groups have been applied in organic electroluminescence [109], organic thin-film

transitions [52], organic-light emitting diodes [110] and organic solar cells [111, 112]. In addition, some compounds also exhibit aggregation-induced emission behaviors for the application in biological imaging [113]. Moreover, the DCV group readily reacts with nucleophiles, leading to a less electron–accepting group. This suppresses the ICT behavior, changing photophysical properties, thereby responding to nucleophilic anions and amines [105, 114-116]. Some DCV-based compounds, such as 2-([5'-(piperidin-1-yl)(2,2'-bithiophen)-5-yl]methylene)malononitrile [93], (2-[4'-(7,8,13,14-tetrahydrodibenzo[a,i]phenanthridin-5-yl)(1,10-biphenyl)-4-yl]methylene)malononitrile [117], and dibromophenylaminobenzylidenemalononitrile [118], have been reported to serve as selective PL sensors that react only with primary amines. Given their selectivity, DCV-based compounds are useful for identifying primary amines from secondary and tertiary amines [91, 119, 120].

Enhanced ICT causes spectral shifts to longer wavelengths; this usually decreases the PL quantum efficiency owing to the dominant non-radiative decay [121]. It is thus worth paying attention to the decrease in D–A interaction appropriately to obtain PL materials with a sufficient quantum efficiency for sensitive sensing. Previous studies have disclosed that employing thiazole, which has weak electron-donating properties, instead of thiophene as the donor can efficiently weaken the intramolecular D–A interaction [35, 122, 123]. For instance, CDTz- and IDTz-based compounds have been reported to show blue shifts in the absorption spectra, compared with CDT- and IDT-based congeners by suppressing the D–A interactions [32, 33, 37]. The structures of CDT, CDTz, IDT, and IDTz units and copolymers based on these units are shown in Chart 4.1.

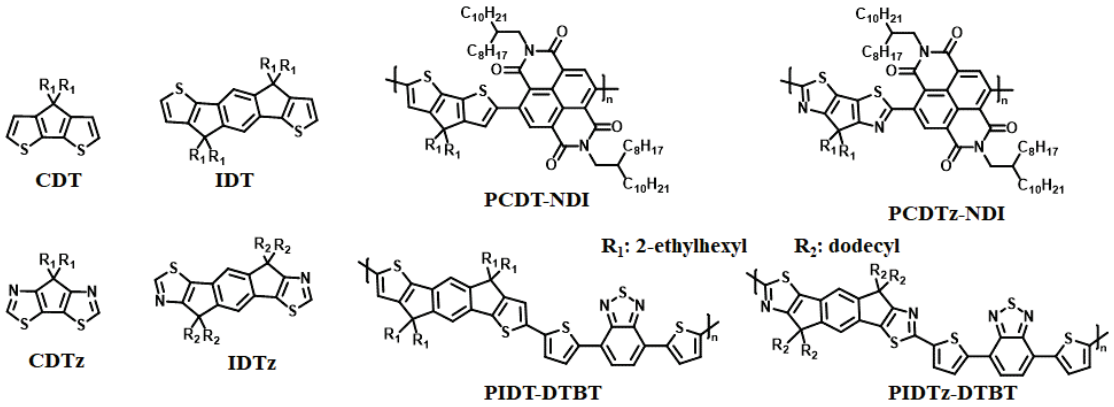

Chart 4.1. Structures of monomers CDT-, CDTz-, IDT-, IDTz, and their copolymers.

The author previously reported that DTzG and GIDTz have high planarity and weak electron-donating properties [85]. In the Chapter, the author designed and prepared DCV-capped DTzG and GIDTz (DTzG-DCV and GIDTz-DCV, respectively) as new D–A PL materials. As expected, both DTzG-DCV and GIDTz-DCV exhibited the photo-induced ICT from the thiazologermole unit to the DCV group with moderately high PL quantum efficiencies, and served as selective sensors for fluoride and iodide ions as well as primary amines.

2. Results and discussion

2.1. Synthesis and characterization

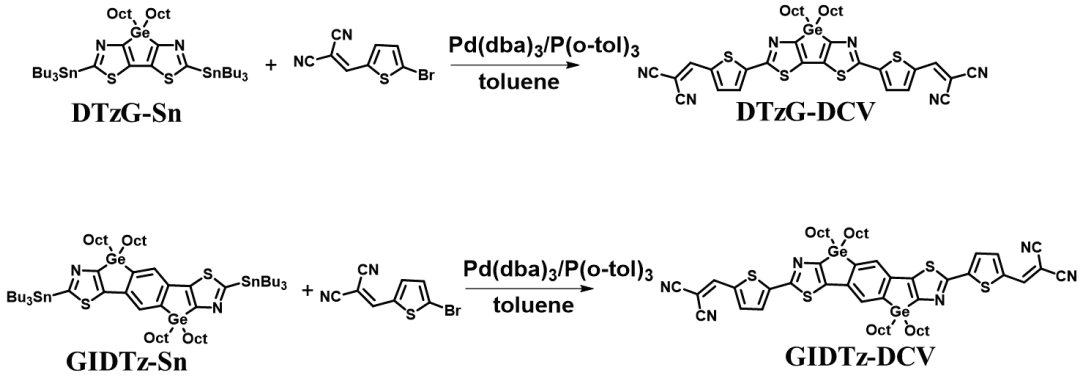

Scheme 4.1. Synthesis of DCV-capped thiazologermoles.

DTzG-DCV and GIDTz-DCV were synthesized by the Stille coupling reactions of DTzG-Sn and GIDTz-Sn [124] with 5-bromo-2-dicyanovinylthiophene [125] in 50%

and 70% yields, respectively (Scheme 4.1). Their NMR and mass spectra were shown in Figures 4.16-4.19 and 2.24-2.25, respectively. Detailed synthetic procedures and characterization are described in the Supporting Information. TGA of DTzG-DCV and GIDTz-DCV at a heating rate of 10 ºC/min from room temperature to 550 ºC in a nitrogen atmosphere revealed good thermal stability with a 5% mass loss, at T_d^5 = 375 ºC and 414 ºC, respectively (Figure. 4.1).

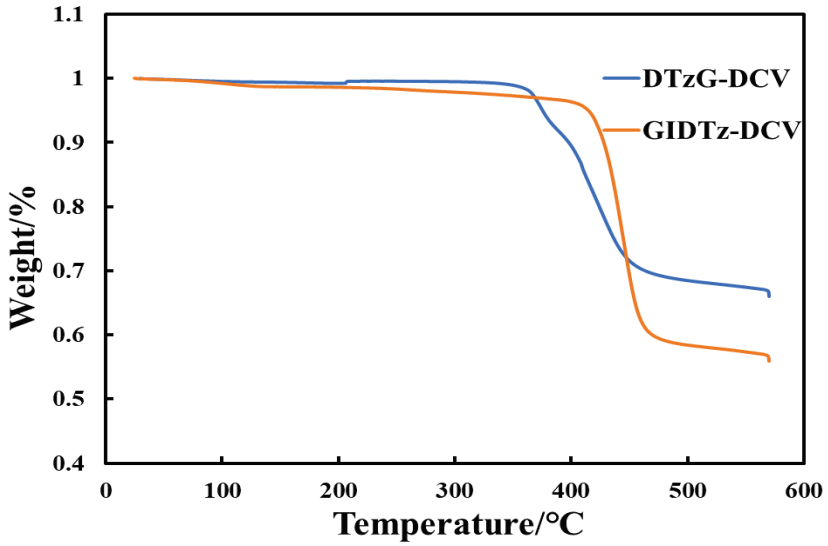

Figure 4.1. TGA curves of DTzG-DCV and GIDTz-DCV in nitrogen.

2.2. Optoelectronic properties

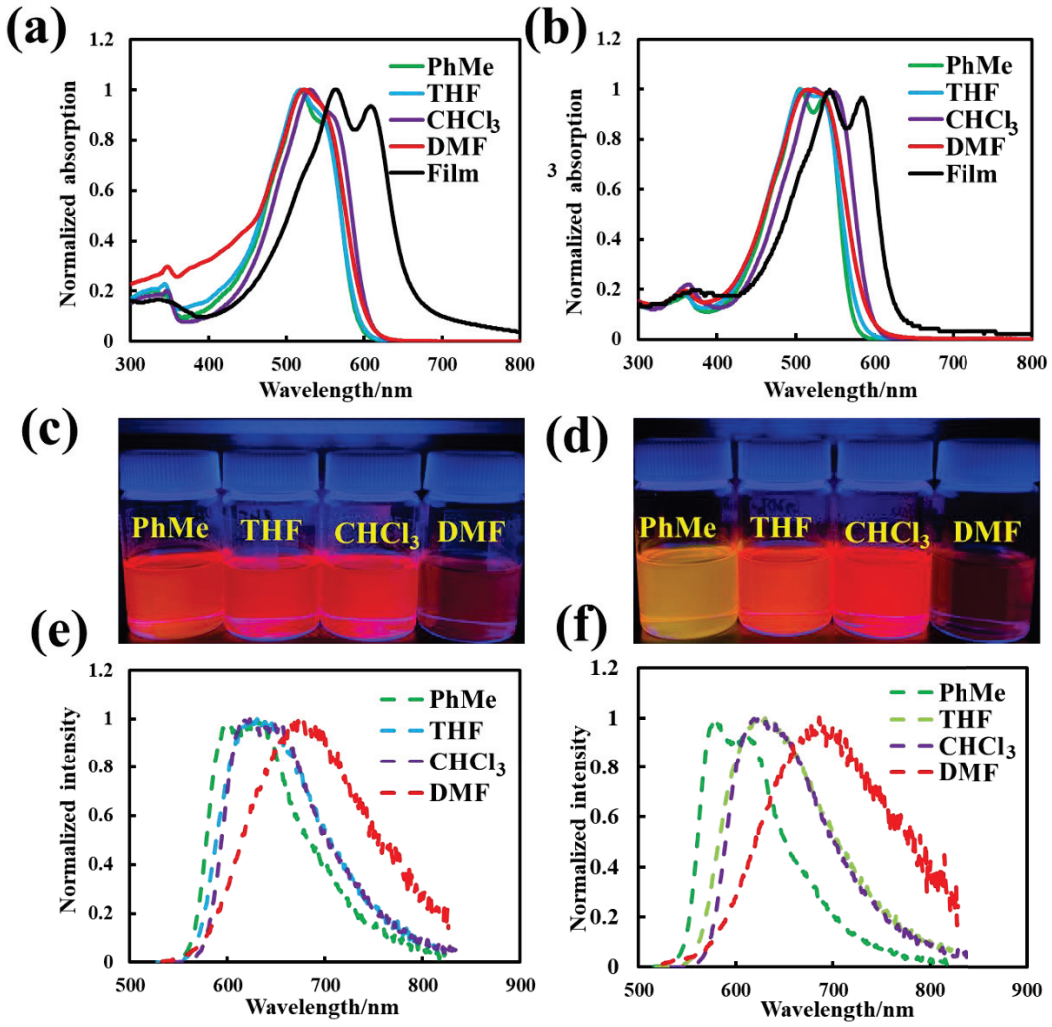

Figure 4.2. UV-vis absorption spectra of DTzG-DCV (a) and GIDTz-DCV (b) in various solvents (1×10^{-5} M), color changes of DTzG-DCV (c) and GIDTz-DCV (d) under irradiation with a portable UV lamp at 365 nm, and PL spectra of DTzG-DCV (e) and GIDTz-DCV (f) in various solvents.

The UV-vis spectra of DTzG-DCV and GIDTz-DCV are presented in Figures. 4.2(a) and (b), respectively. In all solvents, the major absorption bands were observed around 500 nm, which were ascribed to the HOMO–LUMO transition as confirmed by time-dependent density functional theory (TD-DFT) calculations at the B3LYP/6-31G level (Figure 4.3). In $CHCl_3$, the absorption edges of DTzG-DCV and GIDTz-DCV were observed at 613 and 601 nm, respectively, with optical band gaps (E_g^{opt}) of 2.02 and 2.06 eV (as shown in Table 4.1), respectively. These findings were also consistent

with the results of DFT calculations predicting a smaller HOMO–LUMO gap for DTzG-DCV, as described below. The absorption maximum of DTzG-DCV in $CHCl_3$ is blue-shifted by 29 nm from that of a dithienosilole analogue (Chart 4.2), which is due to the introduction of DTzG weakening D-A interaction [44]. The absorption maxima (λ_{max}) of DTzG-DCV and GIDTz-DCV in the cast film were red-shifted by 45 and 37 nm, respectively, relative to those in toluene, suggesting enhanced planarity in the solid state. No clear solvatochromic behaviors were observed in the DTzG-DCV and GIDTz-DCV absorption spectra.

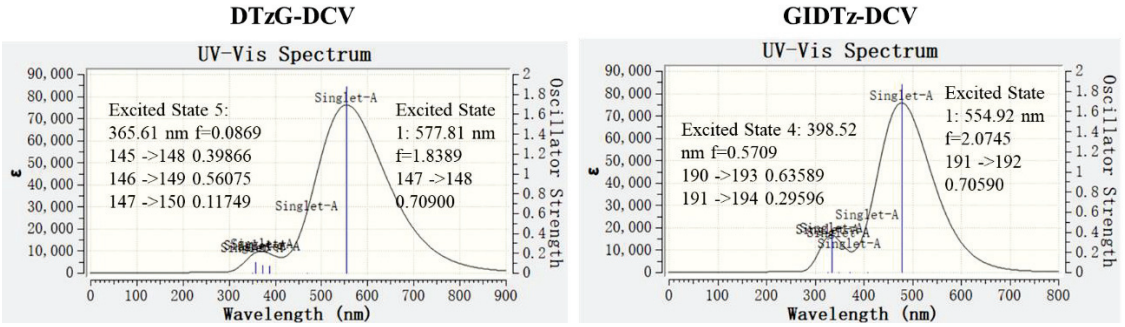

Figure 4.3. Result of TD-DFT calculation of GIDTz-DCV.

Table 4.1

Optical and electrochemical properties of thiazologermole-based derivatives.

Compound	λ_{max}/nm[a]	λ_{em}/nm[a]	Φ[b]	E_g^{opt}/eV[c]	E_{LUMO}/eV[d]	E_{HOMO}/eV[e]
DTzG-DCV	530	616	0.15	2.02	-3.68	-5.70
GIDTz-DCV	524	626	0.41	2.06	-3.55	-5.61
DTzG-imine	453	546	0.34	2.42	/[f]	/
GIDTz-imine	446	531	0.73	2.43	/[f]	/

[a]In $CHCl_3$ at room temperature.

[b]Fluorescence quantum yield.

[c]E_g^{opt} = 1240/absorption edge.

[d]E_{LUMO} = - (E_{red}^{onset} + 4.80) eV with Fc/Fc^+ as external standard.

[e]$E_{HOMO} = E_{LUMO} - E_g^{opt}$.

[f]No cathodic peaks were detected.

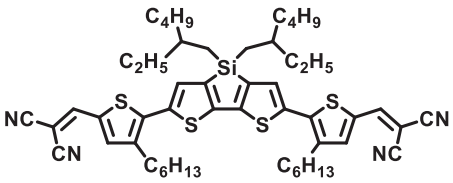

λ_{max} = 559 nm

Chart 4.2. Structure of DCV-substituted dithienosilole.

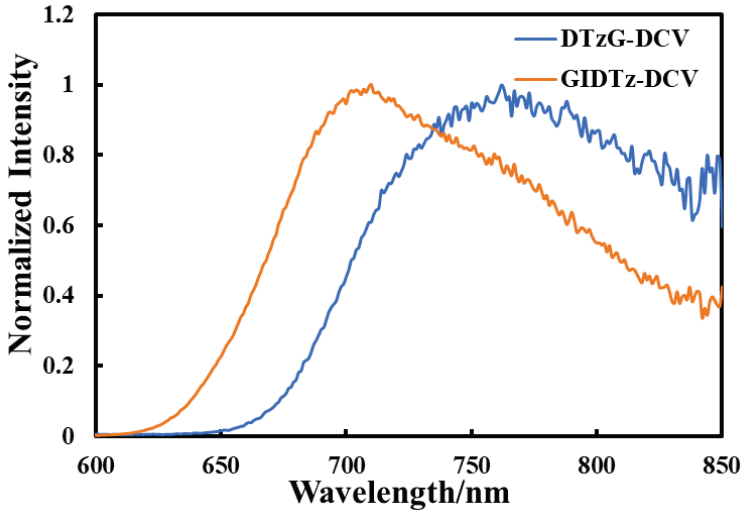

Figure 4.4. PL spectra of DTzG-DCV and GIDTz-DCV in solid states.

DTzG-DCV and GIDTz-DCV displayed different PL colors depending on the solvent under irradiation with a portable UV lamp at 365 nm, as shown in Figures. 4.2(c) and (d), respectively. The corresponding PL spectra are shown in Figures. 4.2(e) and (f) and the data are summarized in Table 4.2. Apparent red shifts of the emission maxima (λ_{em}) were observed with increasing solvent polarity (toluene < THF < $CHCl_3$ < DMF), demonstrating the ICT properties of DTzG-DCV and GIDTz-DCV in the photo-excited state. The differences in PL wavelength between toluene and DMF were 41 and 108 nm for DTzG-DCV and GIDTz-DCV, respectively, suggesting that GIDTz-DCV shows more enhanced ICT behavior than DTzG-DCV. Similar to the absorption spectra, the emission maxima of DTzG-DCV and GIDTz-DCV in the solid state appeared in the longer wavelength region than in the solution state, at 762 and 710 nm, respectively (Figure 4.4). This again indicated the packing effects of these compounds in the solid

state. The PL quantum efficiencies of DTzG-DCV and GIDTz-DCV were also determined, as listed in Table 1. GIDTz-DCV exhibited a higher PL quantum yield than DTzG-DCV, likely reflecting the higher skeletal rigidity of GIDTz-DCV compared with DTzG-DCV.

Table 4.2. PL quantum yield, emission and absorption maxima of thiazologermole-based derivatives in different solvents.

Compound	λ_{max}/ nm[a]				λ_{em}/ nm[a] (Φ[b])			
	PhMe	THF	$CHCl_3$	DMF	PhMe	THF	$CHCl_3$	DMF
DTzG-DCV	518	518	530	523	628 (0.38)	638 (0.32)	616 (0.15)	669 (0.03)
GIDTz-DCV	506	508	524	516	578 (0.55)	630 (0.46)	626 (0.41)	686 (0.05)
DTzG-imine	454	452	453	453	543	538	546 (0.34)	544
GIDTz-imine	444	442	446	444	527	528	531 (0.73)	529

[a] At room temperature.

[b] Fluorescence quantum yield.

Table 4.3

UV–Visible absorption and fluorescence properties of DTzG-DCV and GIDTz-DCV in various solvents.

Solvent	Δ_f[a]	DTzG-DCV			GIDTz-DCV		
		λ_{em} /nm	λ_{max} /nm	Stoke's Shift[b] /cm^{-1}	λ_{em} /nm	λ_{max} /nm	Stoke's Shift[b] /cm^{-1}
CH_2Cl_2	0.22	647	529	3447	651	522	3796
THF	0.21	638	518	3631	630	508	3812
$CHCl_3$	0.15	616	530	2634	626	524	3109
EtOAc	0.20	629	513	3594	623	504	3789
Acetone	0.28	651	516	4018	672	509	4765
DMF	0.27	669	523	4172	686	516	4802

[a] Orientation Polarizability.

[b] Stoke's shift = $1/\lambda_{max} - 1/\lambda_{em.}$

In order further understand the difference of ICT behaviors between DTzG-DCV and GIDTz-DCV, the Lippert-Mataga plots were obtained as shown in Figure 4.5 based

on optical parameters listed in Table 4.3. From the slopes of the Lippert-Mataga plots, the difference of the dipole moments in the excited (μ_E) and the ground state (μ_G) were estimated to be $\Delta(\mu_E - \mu_G)$ = 14.5 D and 23.0 D for DTzG-DCV and GIDTz-DCV, respectively, using Lippert-Mataga equation [126], suggesting that GIDTz-DCV has a stronger D-A interaction than DTzG-DCV [117].

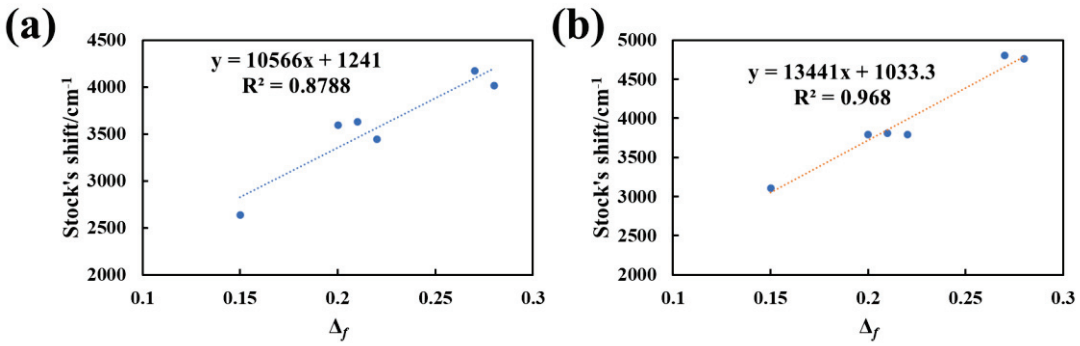

Figure 4.5. Lippert-Mataga plots for DTzG-DCV (a) and GIDTz-DCV (b). Onsager cavity radii were obtained from DFT calculations at the B3LYP/6-31G level to be 5.86 Å for DTzG-DCV and 7.35 Å for GIDTz-DCV.

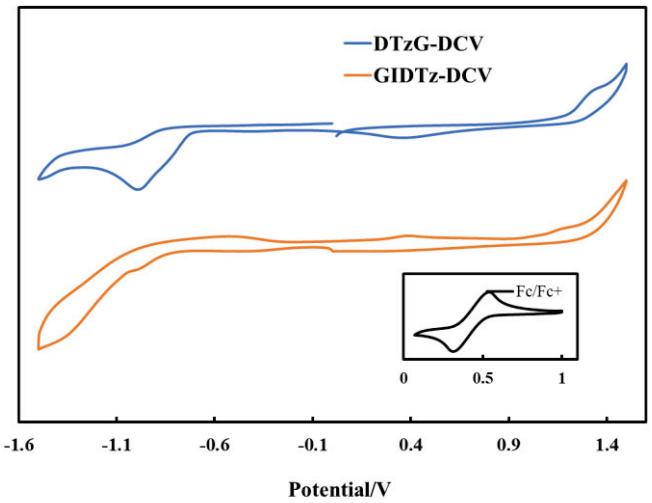

Figure 4.6. Cyclic voltammograms of DTzG-DCV and GIDTz-DCV (0.1 M $^{n}Bu_4NClO_4$ in CH_2Cl_2, with ferrocene/ferrocenium (Fc/Fc^+) as the external standard, using a Pt disk as the working electrode, a Pt plate as the counter electrode, and an Ag wire as the reference electrode).

The electrochemical properties of DTzG-DCV and GIDTz-DCV were

investigated using cyclic voltammograms, as shown in Figure 4.6. DTzG-DCV and GIDTz-DCV presented clear but irreversible reduction peaks. The LUMO energy levels (E_{LUMO}) were calculated to be -3.68 and -3.55 eV, respectively, based on their reduction onset potentials of -0.70 V for DTzG-DCV and -0.83 V for GIDTz-DCV. Because DTzG-DCV and GIDTz-DCV showed relatively weak oxidation peaks, the HOMO energy levels (E_{HOMO}) were determined from the equation $E_{HOMO} = E_{LUMO} - E_g^{opt}$ to be -5.70 and -5.61 eV, respectively. Compared with the E_{LUMO} of DTzG (-2.27 eV) and GIDTz (-2.36 eV) [85], the E_{LUMO} of DTzG-DCV and GIDTz-DCV were considerably lower (by 1.41 and 1.19 eV, respectively), suggesting that the DCV group possesses strong electron-withdrawing properties.

2.3. Response to nucleophiles

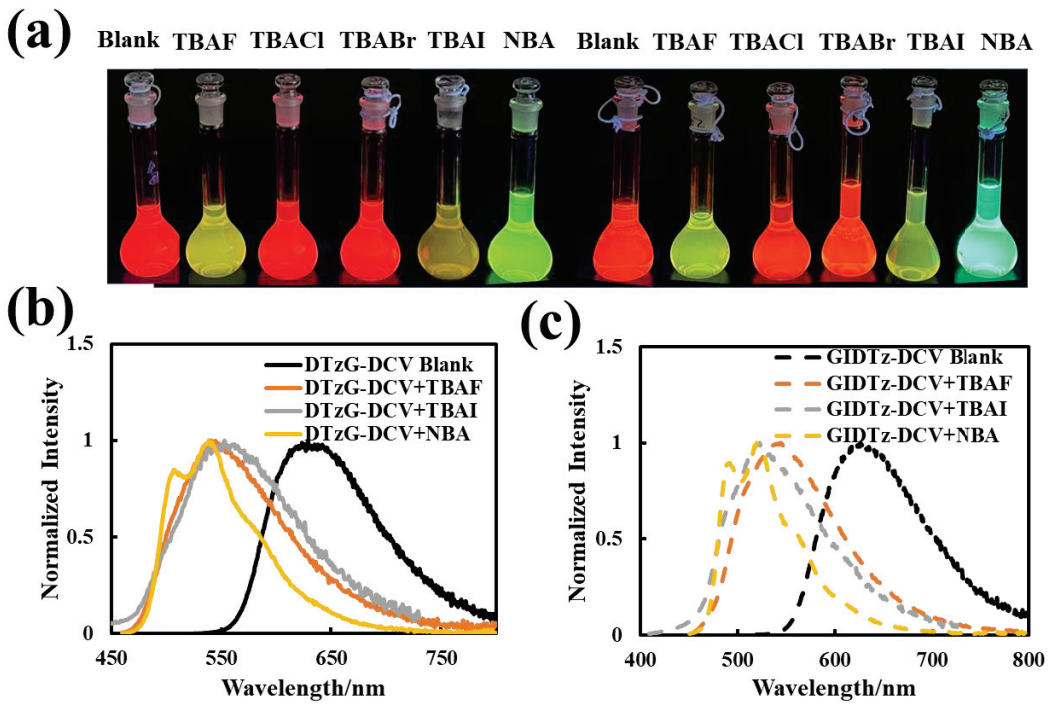

Figure 4.7. Photograph taken under portable UV lamp irradiation at 365 nm (a), and PL spectra (b, c) of DTzG-DCV and GIDTz-DCV in THF (1×10^{-5} M) showing PL color and spectral changes in the presence of TBAF, TBAI, and NBA (1×10^{-2} M).

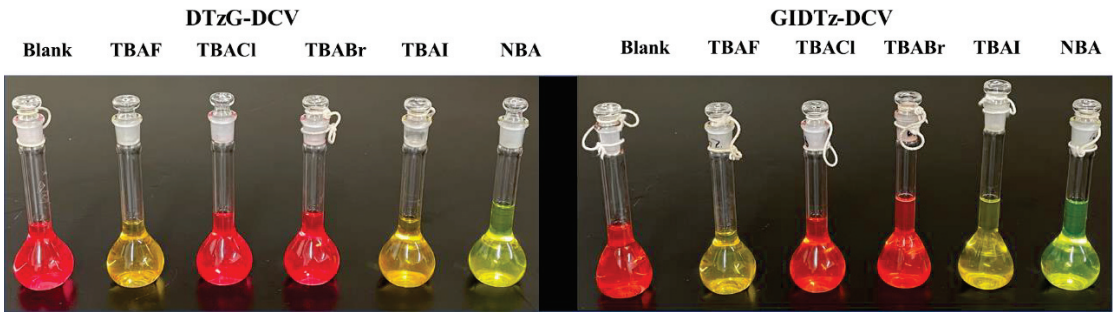

Figure 4.8. Photographs of DTzG-DCV and GIDTz-DCV in THF showing the color changes upon addition of TBAF (2 eq), TBACl (15 eq), TBABr (15 eq), TBAI (15 eq) and NBA (excess) under roomlight.

Given the reactivity of the DCV group toward nucleophiles, DTzG-DCV and GIDTz-DCV were expected to be useful as fluorescent sensors for halogen ions and amines. We first investigated whether PL color changes when halide anions and amines were added to DTzG-DCV and GIDTz-DCV in THF. As shown in Figure 4.7(a), the addition of tetrabutylammonium fluoride (TBAF), tetrabutylammonium iodide (TBAI), and *n*-butylamine (NBA) to the THF solutions of DTzG-DCV and GIDTz-DCV (1×10^{-5} mol/L) induced changes in PL color from red to yellow/green. The PL color changes were observed even under room light (Figure 4.8). These color changes proceeded quickly reaching the steady state within 5 min at room temperature. However, no color changes were observed when tetrabutylammonium chloride (TBACl) and tetrabutylammonium bromide (TBABr) were added, suggesting that DTzG-DCV and GIDTz-DCV can be used for the selective sensing of fluoride and iodide ions. The UV-vis and PL spectra of DTzG-DCV and GIDTz-DCV showed no changes in the presence of TBACl (15 eq) and TBABr (15 eq) (Figure 4.9). In the presence of TBAF (2 eq), TBAI (15 eq), and NBA (excess), however, apparent blue shifts were observed in the UV-vis and PL spectra (Figures 4.7(b), (c) and 4.9). The ^{1}H NMR spectra of DTzG-DCV and GIDTz-DCV measured in the presence of fluoride and iodide ions presented complex signals from which no mechanistic information regarding color and spectral changes could be obtained. However, the mass and infrared (IR) spectra suggested the formation of formyl groups, as shown in Figures 4.10-4.11, possibly by a retro-

Knoevenagel reaction, although the reactions did not complete even after 3 h. A similar reaction of a DCV group by the interaction with TBAF has been already reported [116].

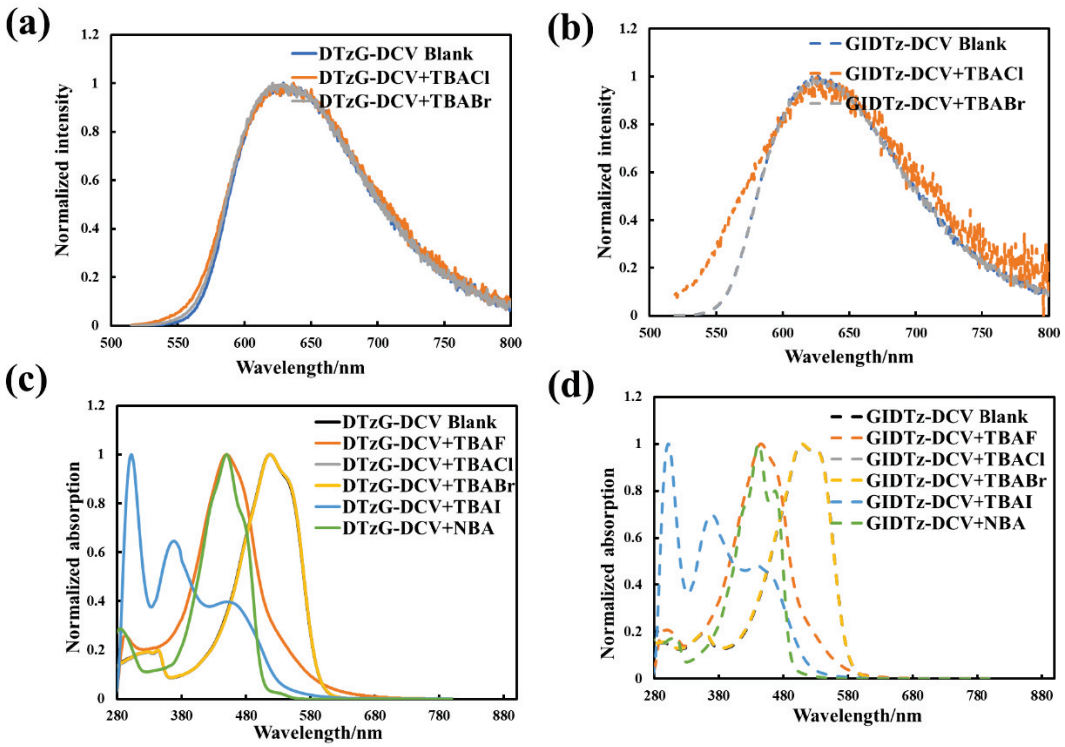

Figure 4.9. PL (a, b) spectra of DTzG-DCV and GIDTz-DCV in THF before and after the addition of TBACl and TBABr. UV-vis (c, d) spectra of DTzG-DCV and GIDTz-DCV in THF before and after the addition of TBAF, TBACl, TBABr, TBAI, and NBA. The spectra of DTzG-DCV/GIDTz-DCV (blank), and those after addition of TBACl, TBABr are overlapped.

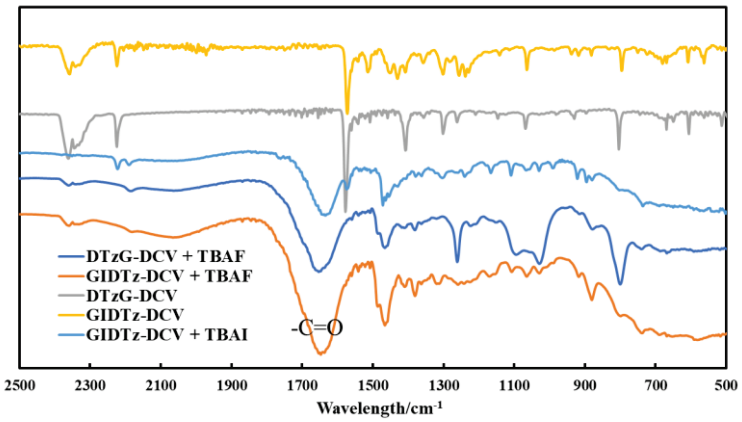

Figure 4.10. IR spectra of DTzG-DCV and GIDTz-DCV on addition of TBAF and TBAI.

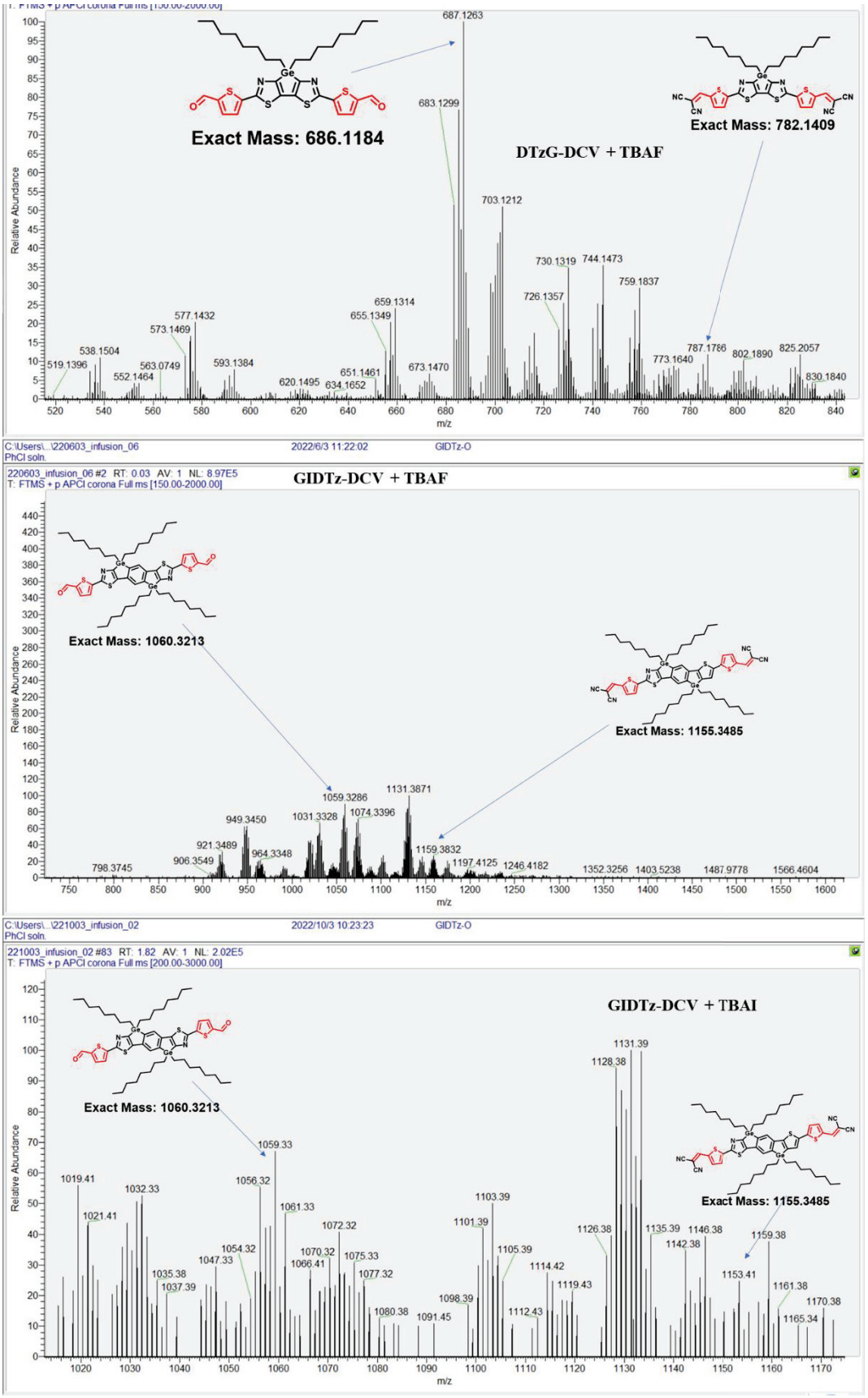

Figure 4.11. Mass spectra of DTzG-DCV and GIDTz-DCV on addition of TBAF and TBAI.

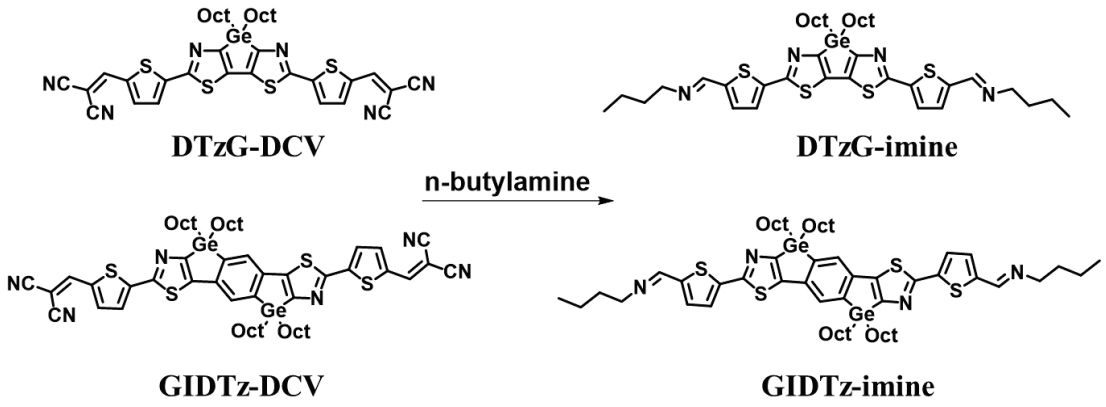

Scheme 4.2. Formation of DTzG-imine and GIDTz-imine.

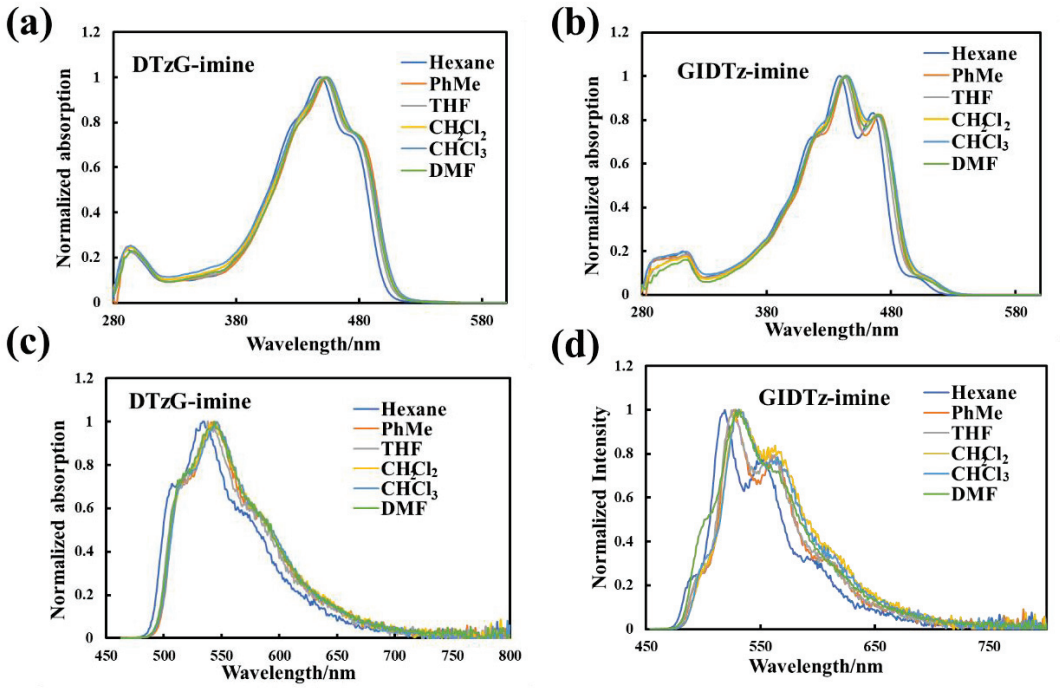

Figure 4.12. UV-vis (a, b) and PL (c, d) spectra of DTzG-imine and GIDTz-imine in various solvents.

The reactions of DTzG-DCV and GIDTz-DCV with NBA proceeded cleanly (Scheme 4.2). DTzG-imine and GIDTz-imine were isolated from large-scale reaction mixtures of DTzG-DCV and GIDTz-DCV with NBA in 92% and 96% yields, respectively. The NMR and mass spectra of the products (i.e., DTzG-imine and GIDTz-imine) revealed that the DCV groups of DTzG-DCV and GIDTz-DCV had been

replaced by imine groups (-C=N), as shown in Figures 4.20-4.23 and 4.26-4.27, respectively. The UV-vis and PL spectra of DTzG-imine and GIDTz-imine measured in different solvents were nearly the same, indicating that no ICT was involved for the cases of DTzG-imine and GIDTz-imine, in contrast to those of DTzG-DCV and GIDTz-DCV, as shown in Figure 4.12 and Table 4.2. This is due to the weaker electron-withdrawing properties of the imine groups than the DCV groups, which is not enough to generate ICT behaviors as reported previously [29]. Moreover, DTzG-imine and GIDTz-imine showed stronger PL quantum yields than their corresponding DCV-capped counterparts, suggesting that DTzG-DCV and GIDTz-DCV can serve as PL turn-on sensors for the detection of primary amines.

2.4. DFT calculations

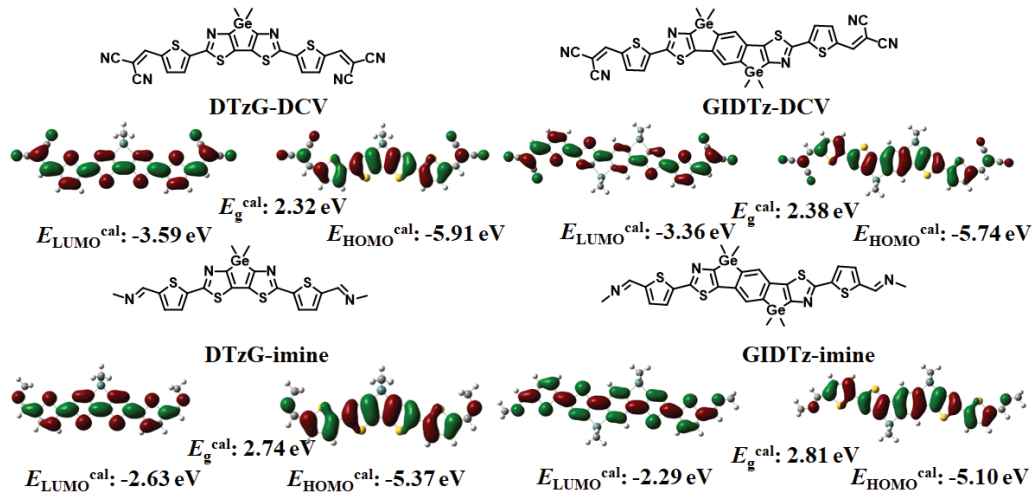

Figure 4.13. LUMO and HOMO diagrams and energy levels of DTzG-DCV, GIDTz-DCV, DTzG-imine, and GIDTz-imine, derived from DFT calculations at the B3LYP/6-31G(d,p) level, with alkyl chains replaced by methyl groups to reduce the calculation time.

To further investigate the ICT behavior of DTzG-imine and GIDTz-imine, DFT calculations were performed at the B3LYP/6-31G(d,p) level of theory on the models in which the alkyl substituents were replaced by short methyl groups. The LUMOs of GIDTz-DCV and DTzG-DCV were more localized on the DCV groups than the

HOMOs, suggesting the ICT behavior (Figure 4.13). In addition, the simulated HOMO and LUMO energy levels E_{LUMO}^{cal} and E_{HOMO}^{cal} of DTzG-DCV (-3.59 and -5.91 eV) and GIDTz-DCV (-3.36 and -5.74 eV) were lower than those of DTzG-imine (-2.63 and -5.37 eV) and GIDTz-imine (-2.29 and -5.10 eV), respectively, possibly owing to the stronger electron-withdrawing properties of the DCV groups than the imine groups. Moreover, compared with the band gaps (E_g^{cal}) of DTzG-DCV (2.32 eV) and GIDTz-DCV (2.38 eV), the E_g^{cal} of DTzG-imine (2.74 eV) and GIDTz-imine (2.81 eV) were increased by 0.42 and 0.43 eV, respectively. This is in good agreement with the experimental E_g^{opt} values of these compounds (Table 4.1). The backbones of these compounds showed good planarity, with a dihedral angle of approximately 0º between the thiophene and thiazologermole units, possibly resulting from the noncovalent interaction between the thiophene S atom and the thiazole N atom, as evidenced by the S–N distance (3.04 Å); this distance is shorter than the sum of the van der Waals radii of the S and N atoms (3.35 Å) [35] (Figure 4.14).

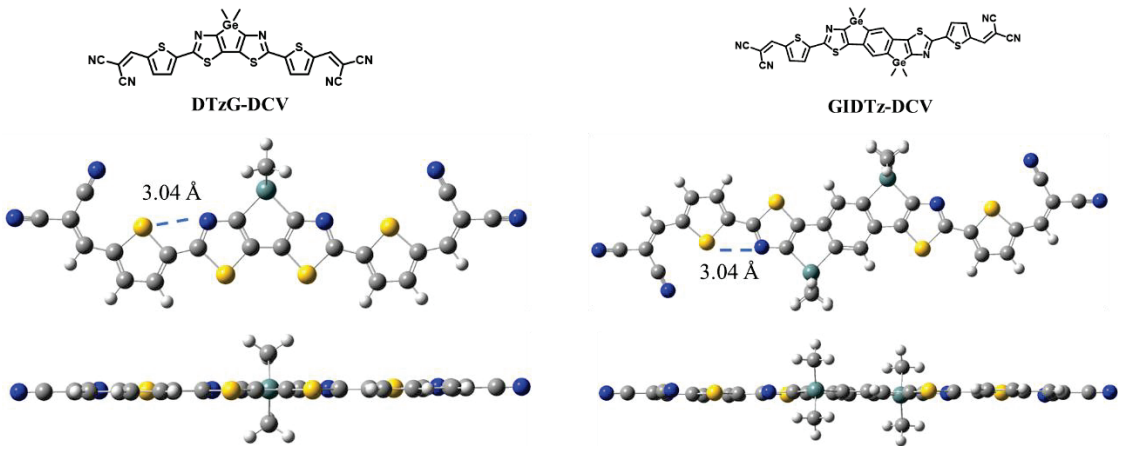

Figure 4.14. Optimized structures of DTzG-DCV and GIDTz-DCV models from different viewing directions.

3. Paper test for alkylamines

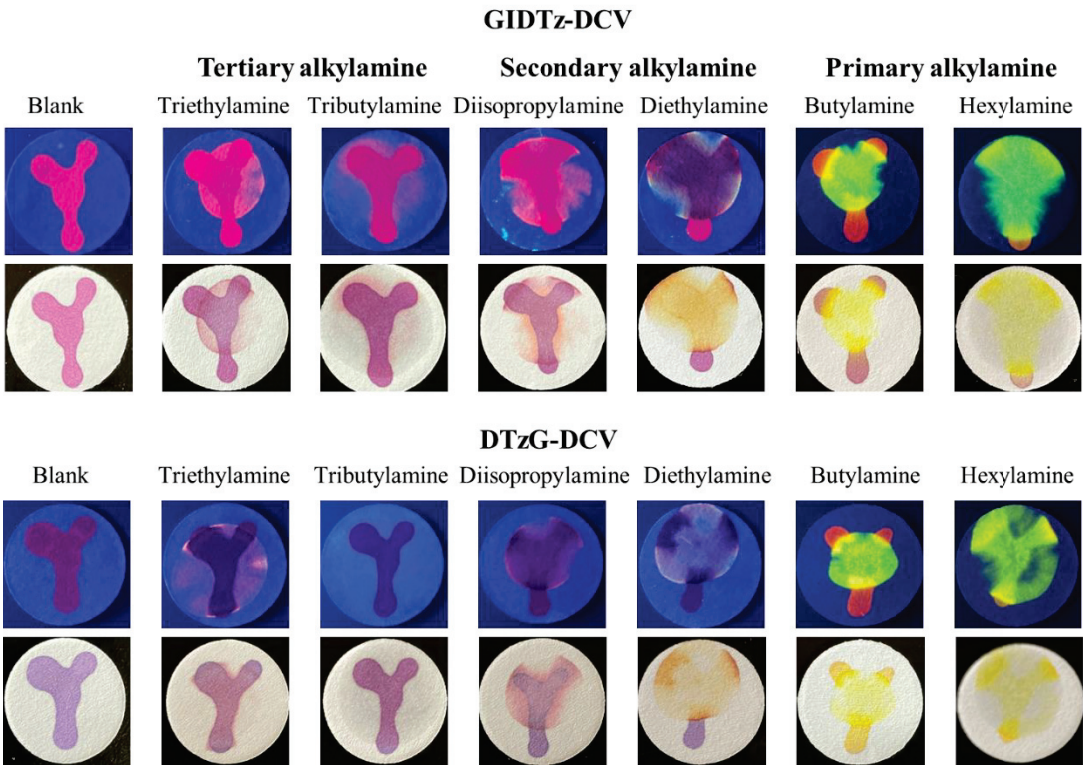

Figure 4.15. DTzG-DCV and GIDTz-DCV on filter papers showing color changes upon addition of tertiary amines, secondary amines, and primary amines under UV light irradiation at 365nm (top) and visible light (bottom).

As amines are common chemical reagents and raw materials used in the chemical industry, it is necessary to recognize quickly the types of amines when they are leaked. As the DCV-capped thiazologermoles DTzG-DCV and GIDTz-DCV readily reacted with primary amines, we examined their direct solid-state reactions for the selective sensing of primary amines, which have many advantages (e.g., solvent-free, simple operation, and low cost). Simple sensors were created by writing the letter "Y" with the solutions of DTzG-DCV and GIDTz-DCV on filter papers (Figure 4.15). After the filter papers were air-dried, a drop of amine was directly added to the "Y" portion of the sensors. Significant changes in PL color were immediately observed by the naked eye, turning from red to yellow/green under UV light irradiation at 365 nm, upon the addition of primary alkylamines. These color changes were also visible under room light. No changes were observed when the filter papers were exposed to amine vapors under ambient conditions. In contrast, no PL color changes were observed when tertiary

and secondary amines, except for diethylamine, were added. As for diethylamine, although the color changes were observed under room light, they were much less obvious than those observed for primary amines under UV light irradiation; thus, it was possible to differentiate diethylamine from butylamine and hexylamine. We suspected that some reactions occurred between diethylamine and DTzG-DCV and GIDTz-DCV in solution, but the ^{1}H NMR and mass spectra of the reaction mixtures were too complex to provide any information on the resulting products.

4. Conclusions

We have synthesized and characterized new DCV-capped PL compounds, DTzG-DCV and GIDTz-DCV, which exhibited remarkable solvatochromism with respect to the PL spectra owing to their ICT behavior in the photo-excited state. The DFT calculations revealed that GIDTz-DCV exhibits enhanced ICT behavior due to the more localized LUMO distribution, compared with DTzG-DCV. In addition, both DTzG-DCV and GIDTz-DCV in solution responded to TBAF, TBAI, and NBA via changes in PL color with a shift from long to short wavelengths, as a result of the nucleophilic reactions of the DCV groups. To obtain more information on the nucleophilic reactions, DTzG-imine and GIDTz-imine were isolated from the reactions of DTzG-DCV and GIDTz-DCV with NBA, respectively; their UV-vis and PL spectra exhibited no apparent solvatochromic behavior. Furthermore, filter papers containing DTzG-DCV and GIDTz-DCV were prepared and used as sensors to examine whether primary amines could be distinguished from secondary and tertiary amines by the change of PL color, which is triggered in response to only primary amines and is observable by the naked eye under irradiation with a portable UV lamp at 365 nm.

General consideration

All reactions were carried out in dry argon. Diethyl ether (Et_2O), *N*,*N*-dimethylformamide (DMF), toluene, and tetrahydrofuran (THF) that were used as the reaction solvents were distilled from CaH_2 and stored over activated molecular sieves in the dark until use. All organic amines and ammonium halides were obtained from Tokyo Chemical Industry Co., Ltd and were used without further purification. DTzG-Sn, GIDTz-Sn and 5-bromo-2-dicyanovinylthiophene were prepared as reported in the literature. NMR spectra were recorded on a Varian 400-MR spectrometer. UV-vis absorption and PL (photoluminescence) spectra were measured on Hitachi U-2910 and HORIBA FluoroMax-4 spectrophotometers, respectively. PL quantum yields were determined on a HORIBA FluoroMax-4 spectrofluorometer using a calibrated integrating sphere system. The Lippert- Mataga plots were constructed by using the relation, $\nu_{fl} = \nu_{ab} - \frac{2\Delta f}{hca^3}(\mu_E - \mu_G)^2 + \text{const}$, where $\Delta f = \frac{\varepsilon-1}{2\varepsilon+1} - \frac{n^2-1}{4n^2+2}$. While the slope is, $Slope = \frac{2\Delta f}{hca^3}(\mu_E - \mu_G)^2$, where a is Onsager cavity radius, n and ε are the refractive index and the dielectric constant of the solvent, ν_{fl} and ν_{ab} are the fluorescence and absorption wavelength (expressed in cm^{-1} unit), μ_E and μ_G the dipole moment (expressed in Debye unit) in the excited and the ground state, respectively. Singlet-singlet annihilation leading to a charge-transfer intermediate in chromophore-end-capped pentaphenylenes. Fourier transform infrared (FTIR) spectroscopy was performed on a Shimadzu IRAffinity-1 spectrometer. APCI-mass spectra were obtained by a Thermo Fisher Scientific LTQ Orbitrap XL spectrometer at N-BARD, Hiroshima University. Melting points of solid products were determined using a Yanaco MP-500P melting point meter. Microwave irradiation for Stille reactions was performed on a Biotage initiator+ microwave reactor. Thermogravimetric analysis (TGA) was conducted using an SII EXSTARTG-DTA6200 thermal analyzer in the temperature range of 25 - 570 ˚C with a rate of 10 ˚C min^{-1} in nitrogen atmosphere.

Synthesis

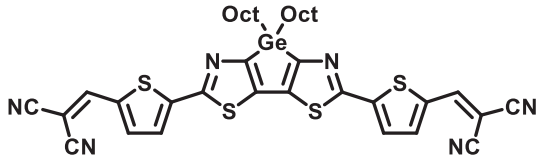

Synthesis of DTzG-DCV

A toluene (6 mL) solution of DTzG-Sn (0.46 g, 0.44 mmol), 5-bromo-2-dicyanovinylthiophene (0.22 g, 0.88 mmol), $Pd_2(dba)_3$ (20 mg, 0.022 mmol), and P(*o*-tolyl)$_3$ (16 mg, 0.053 mmol) was placed in a tightly sealed tube with a rubber stopper. The sealed tube was heated at 140 ºC for 4 h by microwave irradiation. The reaction mixture was allowed to room temperature. Then, the solvent was removed under reduced pressure and the crude products were purified by column chromatography on silica gel with chloroform as the eluent to obtain the target compound in 50% yield (green solid, 172 mg, mp = 204-209 °C). ^{1}H NMR ($CDCl_3$) δ 7.80 (s, 2H), 7.75 (d, *J* = 4.0 Hz, 2H), 7.60 (d, *J* = 4.0 Hz, 2H), 1.53-1.43 (m, 8H), 1.33-1.14 (m, 20H), 0.82 (t, *J* = 6.4 Hz, 6H). ^{13}C NMR ($CDCl_3$) δ 166.90, 160.08, 149.94, 147.35, 140.10, 138.84, 135.82, 126.69, 113.87, 113.01, 78.38, 32.51, 31.77, 29.17, 29.00, 25.11, 22.62, 14.20, 14.08. HRMS (APCI) calcd for $C_{38}H_{40}GeN_6S_4$ [M^+] 782.1429, found 782.1409.

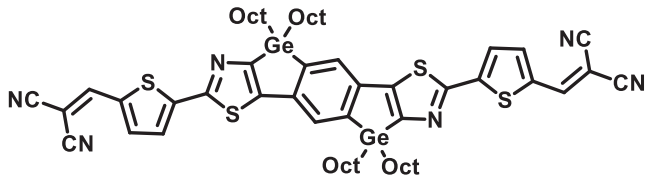

Synthesis of GIDTz-DCV

A toluene (5 mL) solution of GIDTz-Sn (0.39 g, 0.27 mmol), 5-bromo-2-dicyanovinylthiophene (0.13 g, 0.55 mmol), $Pd_2(dba)_3$ (10 mg, 0.025 mmol), and P(*o*-tolyl)$_3$ (10 mg, 0.033 mmol) was placed in a tightly sealed tube with a rubber stopper. The sealed tube was heated at 140 ºC for 4 h by microwave irradiation. The reaction mixture was allowed to room temperature. Then, the solvent was removed under reduced pressure and the crude products were purified by column chromatography on silica gel with chloroform as the eluent to obtain the target compound (0.22 g ,0.19 mmol) was obtained in 70% yield as a dark red solid, mp = 179-182 °C. ^{1}H NMR ($CDCl_3$) δ 7.80 (s, 2H), 7.76 (d, *J* = 4.0 Hz 2H), 7.63-7.53 (m, 4H), 1.54-1.13 (m, 56H),

0.83 (t, J = 6.4 Hz, 12H); ^{13}C NMR ($CDCl_3$) δ 164.82, 160.04, 151.01, 150.01, 148.21, 144.85, 139.55, 138.80, 135.46, 128.35, 126.55, 114.00, 113.09, 77.96, 32.78, 31.81, 29.22, 29.04, 25.24, 22.64, 14.30, 14.09. HRMS (APCI) calcd for $C_{60}H_{76}Ge_2N_6S_6$ [M^+] 1156.3438, found 1156.3485.

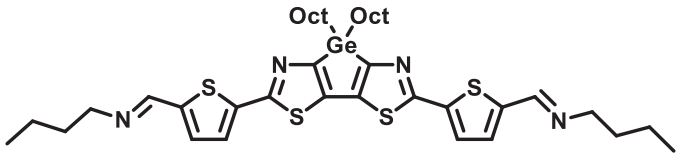

Synthesis of DTzG-imine

Excess NBA was added to the flask containing DTzG-DCV (11.4 mg, 0.015 mmol) without solvent. After 5 min, the mixture was directly purified by column chromatography on silica gel with hexane/Et_3N as the eluent to obtain the target compound (11.0 mg, 0.014 mmol) in 92% yield as a viscous yellow oil. ^{1}H NMR ($CDCl_3$) δ 8.32 (s, 2H), 7.47 (d, J = 4.0 Hz, 2H), 7.24 (d, J = 4.0 Hz, 2H), 3.60 (t, J = 6.8 Hz, 4H), 1.68 (quint, J = 7.2 Hz, 4H), 1.54-1.33 (m, 12H), 1.31-1.10 (m, 20H), 0.95 (t, J = 7.2 Hz, 6H), 0.82 (t, J = 7.2 Hz, 6H); ^{13}C NMR ($CDCl_3$) δ 164.23, 161.75, 153.28, 143.96, 139.62, 138.19, 129.96, 125.88, 61.05, 32.92, 32.47, 31.77, 29.14, 29.02, 25.12, 22.57, 20.39, 14.18, 13.97, 13.79. HRMS (APCI) calcd for $C_{40}H_{58}Ge_2N_4S_4$ [M^+] 796.2756, found 796.2832.

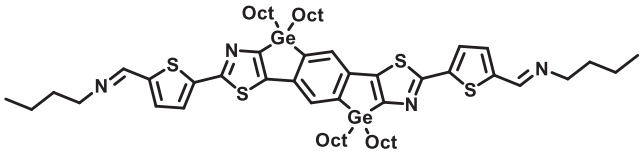

Synthesis of GIDTz-imine

Excess NBA was added to the flask containing GIDTz-DCV (14.5 mg, 0.013 mmol) without solvent. After 5 min, the mixture was directly purified by column chromatography on silica gel with hexane/Et_3N as the eluent to obtain the target compound (14.0 mg, 0.012 mmol) in 96% yield as a viscous yellow oil. ^{1}H NMR ($CDCl_3$) δ 8.33 (s, 2H), 7.52 (s, 2H), 7.50 (d, J = 4.0 Hz, 2H), 7.25 (d, J = 4.0 Hz, 2H), 3.60 (t, J = 7.2 Hz, 4H), 1.73-1.64 (quint, 4H), 1.57-1.47 (m, 8H), 1.43-1.16 (m, 52H),

0.95 (t, J = 7.2 Hz, 6H), 0.83 (t, J = 7.2 Hz, 12H); ^{13}C NMR ($CDCl_3$) δ 163.00, 162.25, 153.33, 148.80, 143.99, 143.78, 140.12, 139.53, 129.94, 127.73, 125.86, 61.05, 32.94, 32.74, 31.79, 31.52, 29.17, 29.04, 25.24, 20.39, 14.33, 13.97, 13.80. HRMS (APCI) calcd for $C_{62}H_{94}Ge_2N_4S_4$ [M^+] 1168.4794, found 1168.4889.

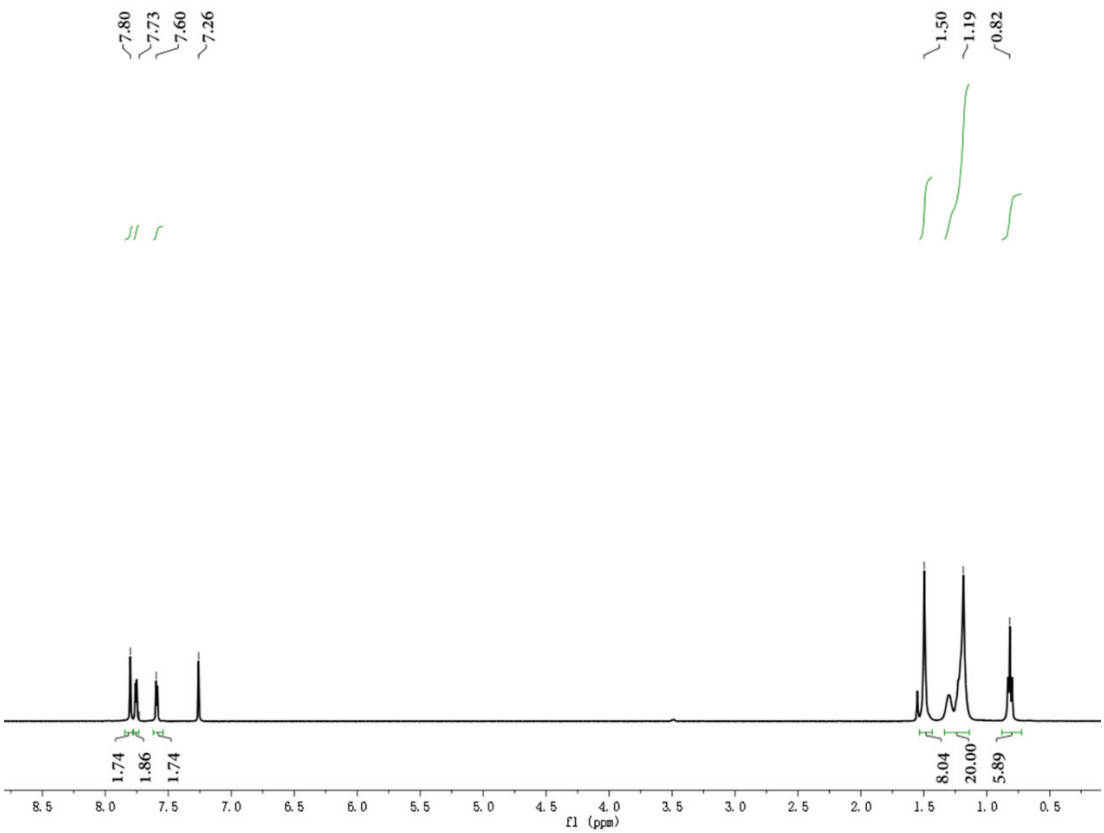

Figure 4.16. ^{1}H NMR spectrum of DTzG-DCV.

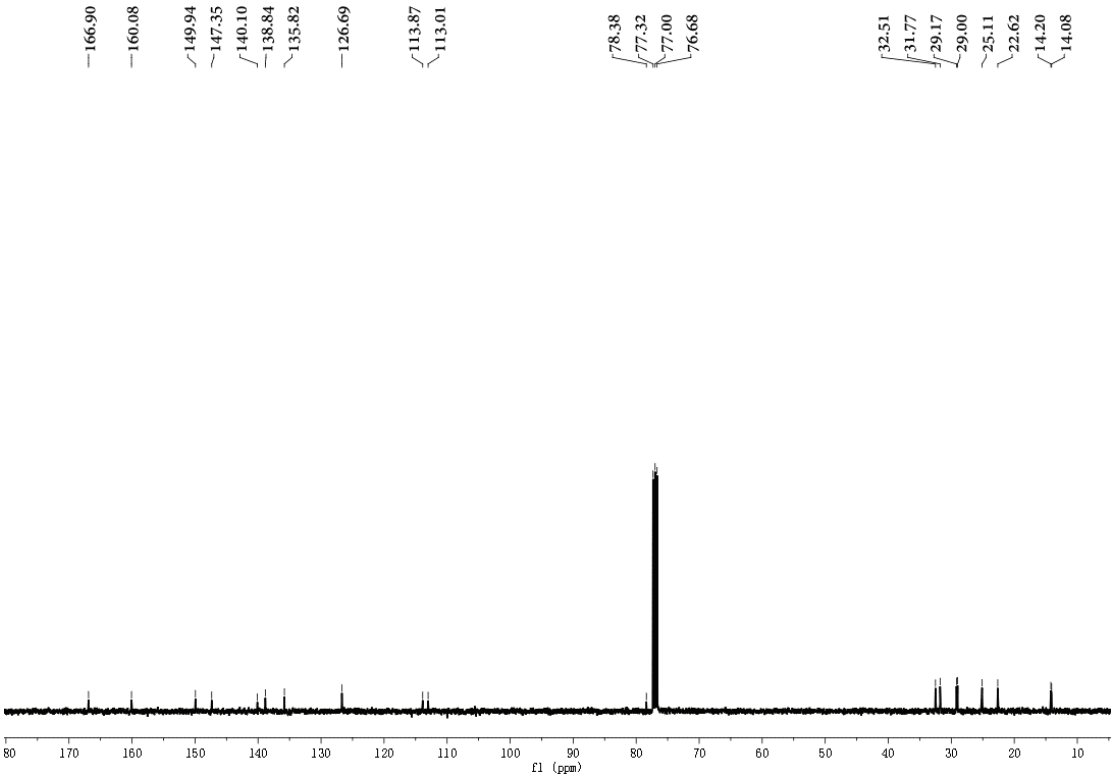

Figure 4.17. ^{13}C NMR spectrum of DTzG-DCV.

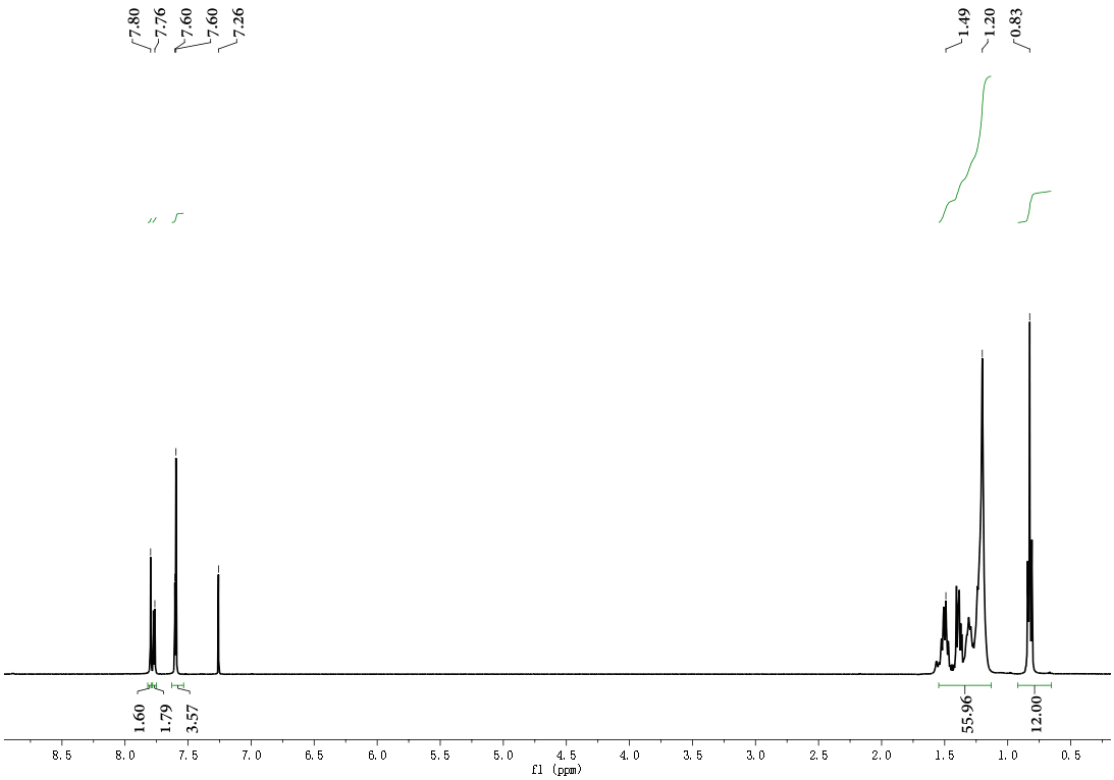

Figure 4.18. ^{1}H NMR spectrum of GIDTz-DCV.

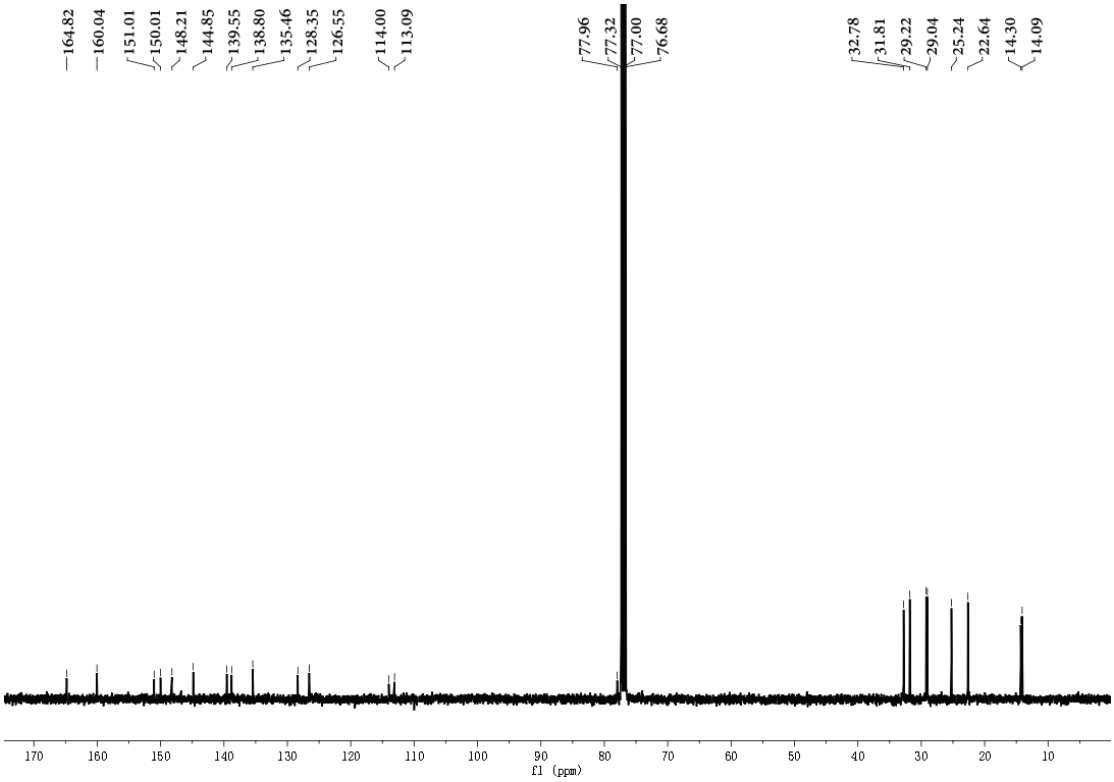

Figure 4.19. ^{13}C NMR spectrum of GIDTz-DCV.

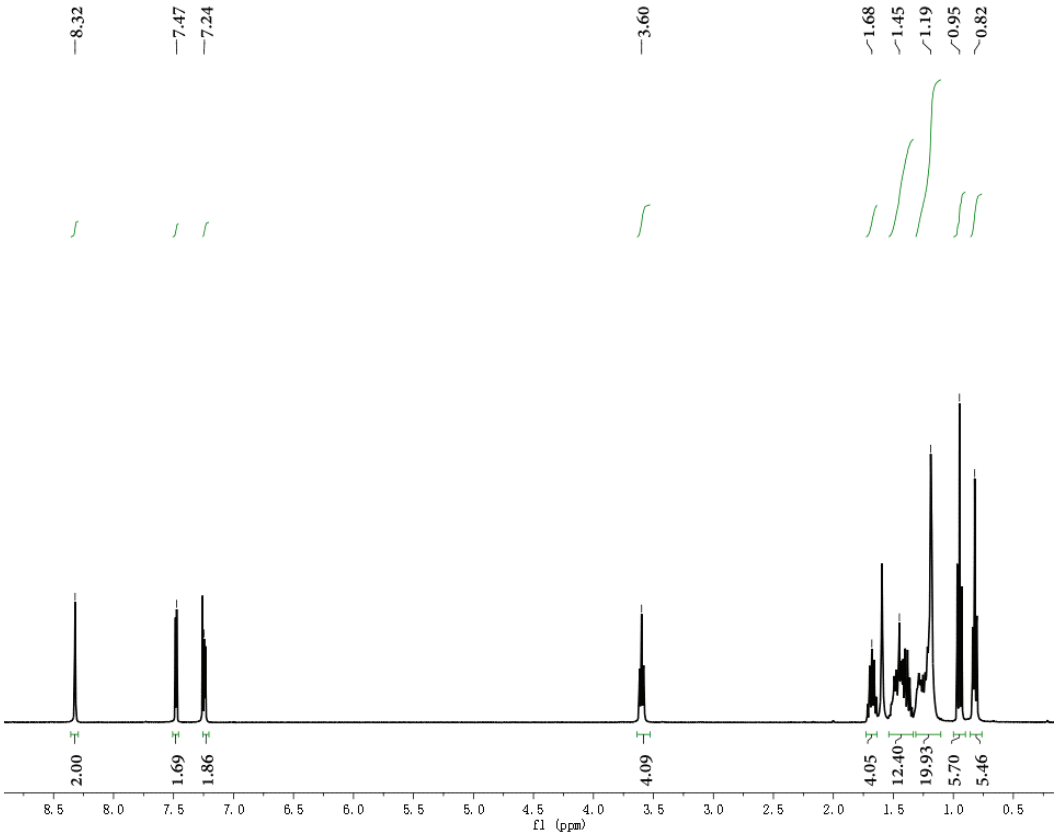

Figure 4.20. ^{1}H NMR spectrum of DTzG-imine.

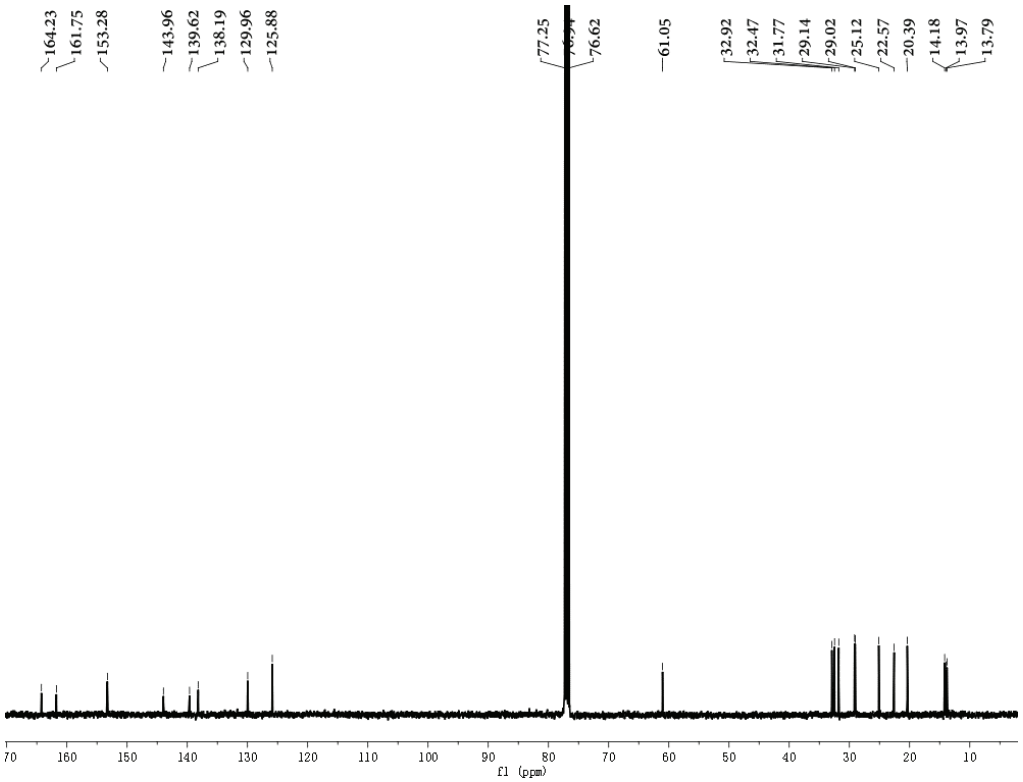

Figure 4.21. ^{13}C NMR spectrum of DTzG-imine.

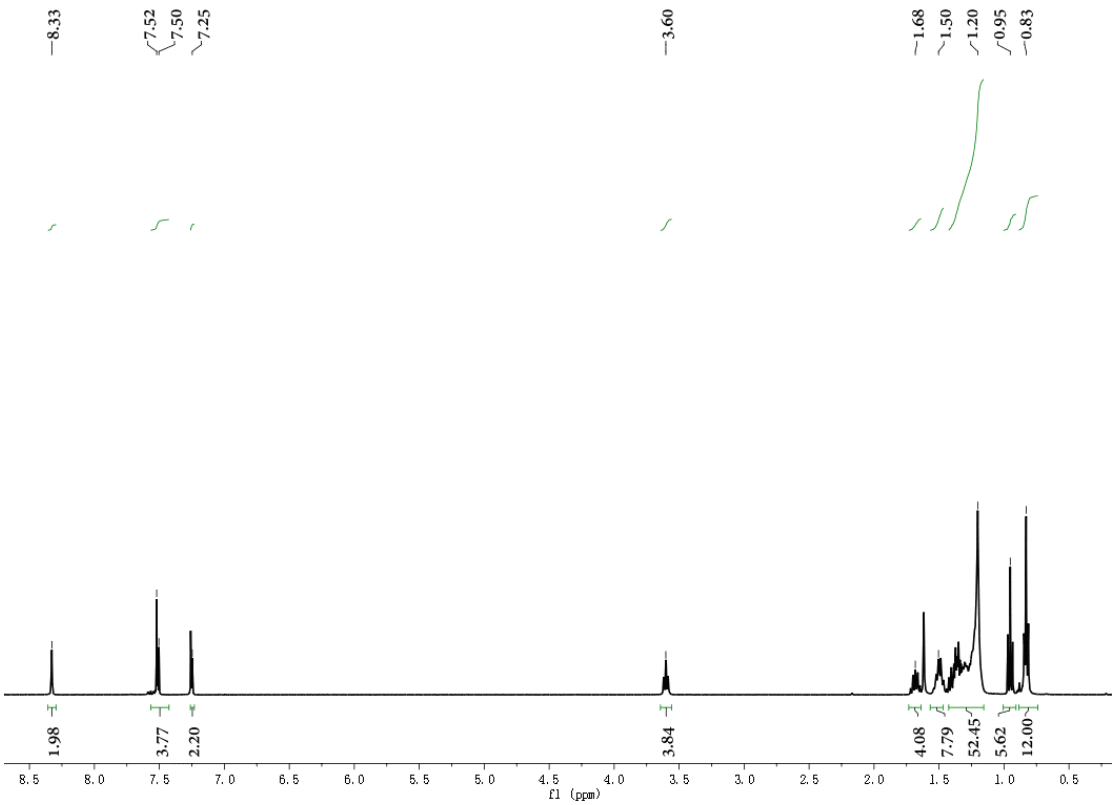

Figure 4.22. ^{1}H NMR spectrum of GIDTz-imine.

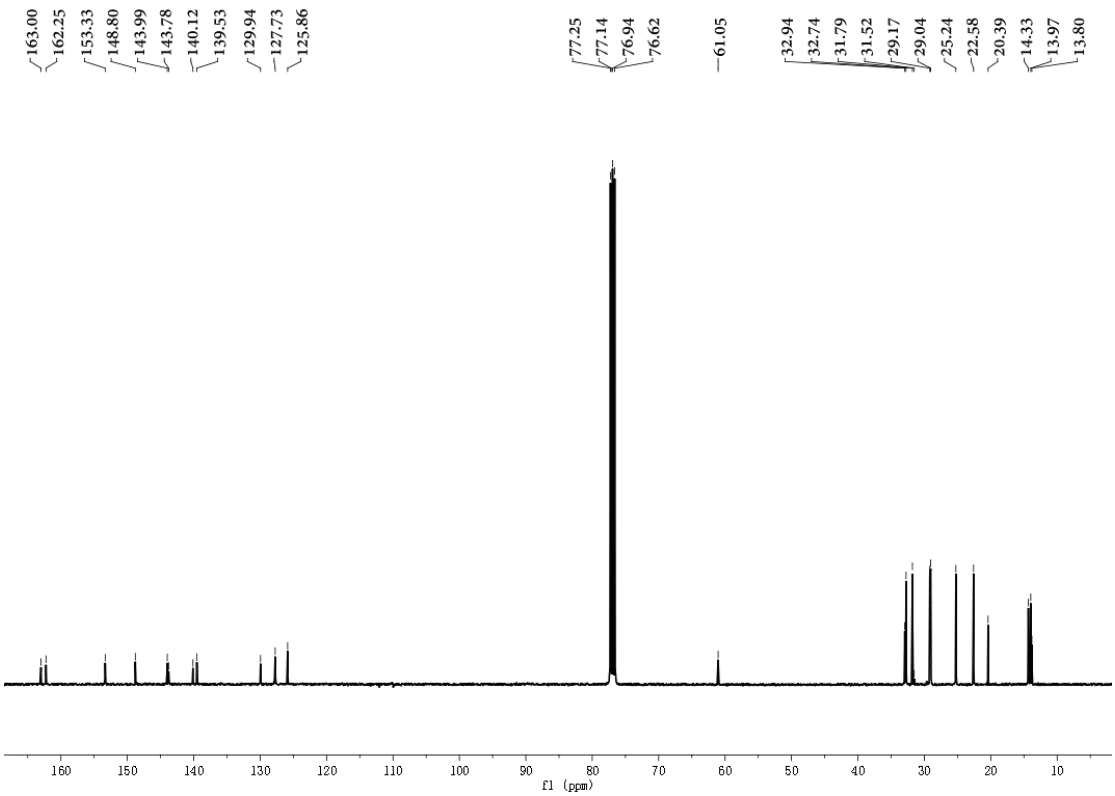

Figure 4.23. ^{13}C NMR spectrum of GIDTz-imine.

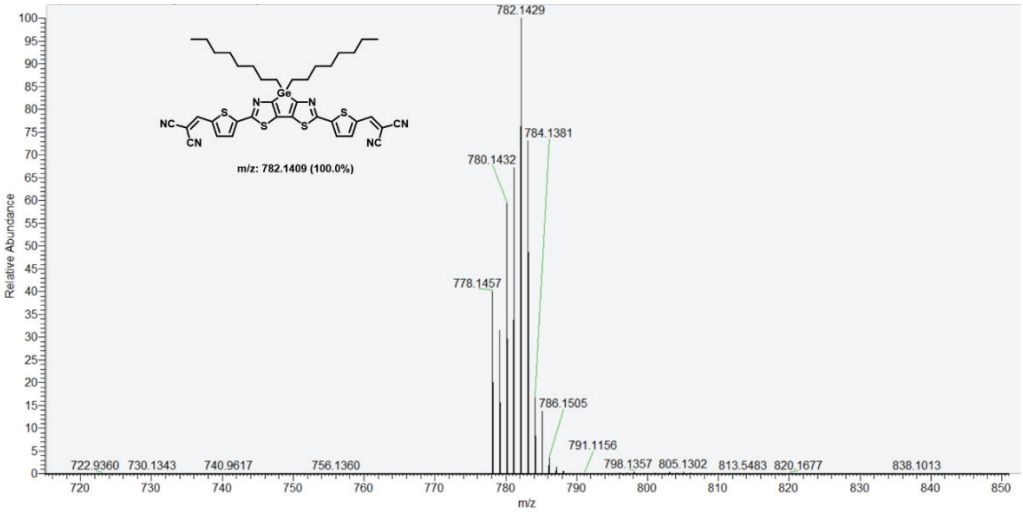

Figure 4.24. APCI-TOF mass spectrum of DTzG-DCV.

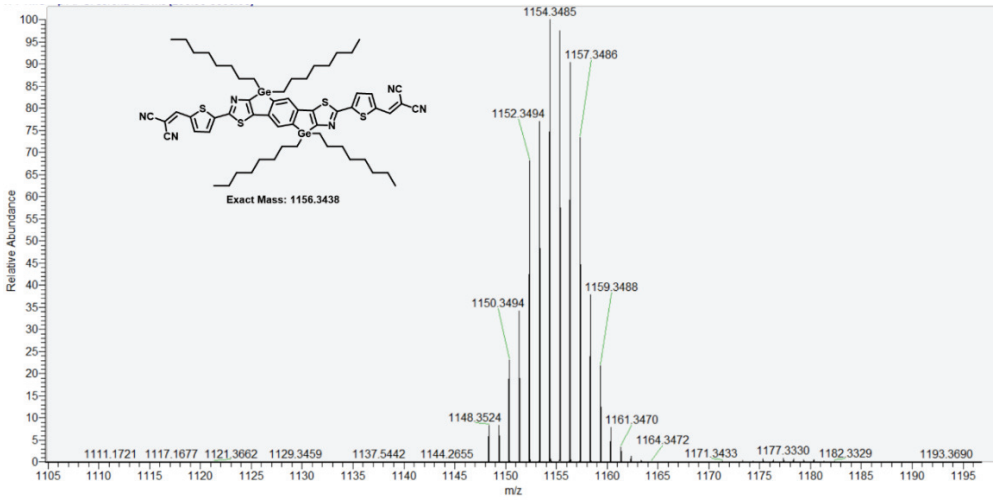

Figure 4.25. APCI-TOF mass spectrum of GIDTz-DCV.

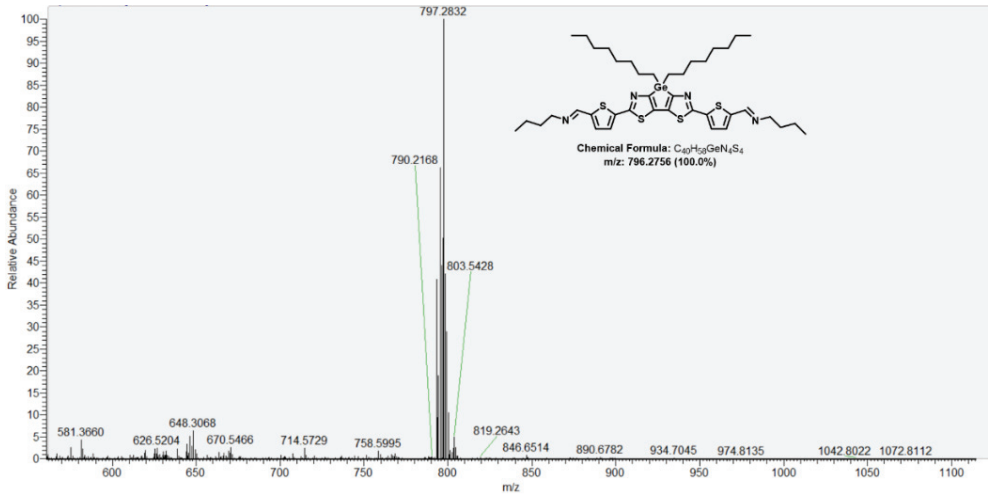

Figure 4.26. APCI-TOF mass spectrum of DTzG-imine.

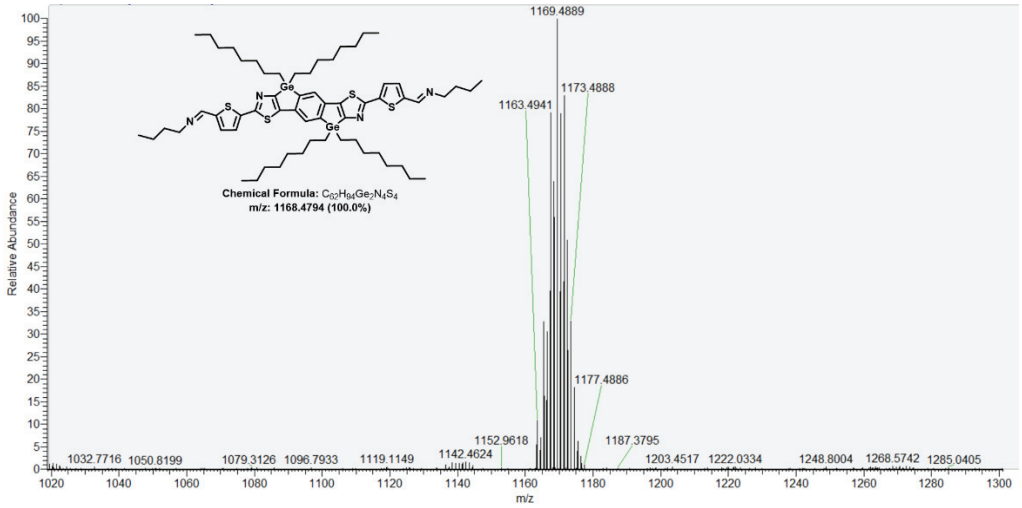

Figure 4.27. APCI-TOF mass spectrum of GIDTz-imine.

Chapter 5: Conclusions

In conclusion, the author proposed new strategies to synthesize weak electron-donor compounds by replacing thiophene units of conventional conjugated systems by thiazole. Thiazole-condensed germoles (DTzG and GIDTz) thus prepared are basically electron donors but showed enhanced electron-withdrawing properties compared with the parent thiophene compounds. DTzG and GIDTz were applied for the synthesis of new n-type conjugated polymers and fluorescent sensing materials.

In Chapter 2, the author successfully prepared dithiazole-condensed single germole and double germole compounds and investigated their electrochemical and optical properties. The single-crystal structure of brominated GIDTz exhibits close intermolecular stacking. DFT calculations revealed that the HOMO and LUMO energy levels of the thiazole-condensed germoles are low in comparison with those of the thiophene-condensed germole congeners reported previously.

In Chapter 3, the author prepared new D-A type polymers containing thiazole-condensed germoles as the donor and BT and DTzBT as the acceptor and investigated their optical and electrochemical properties. The ICT behaviors of these polymers were also examined by PL measurements in different solvents. DFT calculations revealed that the HOMO/LUMO energy levels of DTzG- and GIDTz-based polymers are lower than those of previously reported thiophene-based congeners. In addition, DTzG/GIDTz and the adjacent BT unit exhibited high coplanarity because of intramolecular noncovalent S–N and N–H interactions. It was also indicated that replacing cyclopentadiene by germole and introducing thiazole units in place of thiophene units markedly lowered the HOMO/LUMO energy levels, revealing the possible tuning of the electronic states of the polymers by element-based molecular design. PGIDTz-BT, PDTzG-BT, PGIDTz-DTzBT, and PDTzG-DTzBT with low-lying FMOs are excellent candidates for n-type semiconductor materials.

In Chapter 4, the author synthesized and characterized new DCV-capped PL compounds, DTzG-DCV and GIDTz-DCV, which exhibited remarkable

solvatochromism with respect to the PL spectra owing to their ICT behavior in the photo-excited state. In addition, both DTzG-DCV and GIDTz-DCV in solution responded to TBAF, TBAI, and NBA via changes in PL color with a shift from long to short wavelengths, as a result of the nucleophilic reactions of the DCV groups. To obtain more information on the nucleophilic reactions, DTzG-imine and GIDTz-imine were isolated from the reactions of DTzG-DCV and GIDTz-DCV with NBA, respectively; their UV-vis and PL spectra exhibited no apparent solvatochromic behavior. Furthermore, filter papers containing DTzG-DCV and GIDTz-DCV were prepared and used as sensors to examine whether primary amines could be distinguished from secondary and tertiary amines by the change of PL color, which is triggered in response to only primary amines and is observable by the naked eye under irradiation with a portable UV lamp at 365 nm.

On the basis of the abovementioned results, the author developed strategies to enhance the electron-withdrawing properties of germoles-based compounds by the introduction of thiazole units appropriately. The resultant compounds all showed lower LUMO energy levels than previously reported thiophene-based congeners. These are expected as weak donors for the construction of optoelectronic materials with weak donor-acceptor interaction for enhancing the n-type semiconducting properties and tuning the fluorescent behaviors.

References

[1] Mishra A. Material perceptions and advances in molecular heteroacenes for organic solar cells. Energy Environ Sci 2020;13:4738-93.

[2] Mishra A, Bauerle P. Small molecule organic semiconductors on the move: promises for future solar energy technology. Angew Chem Int Ed 2012;51:2020-67.

[3] Shi Y, Guo H, Huang J, Zhang X, Wu Z, Yang K, et al. Distannylated Bithiophene Imide: Enabling High-Performance n-Type Polymer Semiconductors with an Acceptor-Acceptor Backbone. Angew Chem Int Ed 2020;59:14449-57.

[4] Teshima Y, Saito M, Fukuhara T, Mikie T, Komeyama K, Yoshida H, et al. Dithiazolylthienothiophene Bisimide: A Novel Electron-Deficient Building Unit for N-Type Semiconducting Polymers. ACS Appl Mater Interfaces 2019;11:23410-6.

[5] Lin Y, Fan H, Li Y, Zhan X. Thiazole-based organic semiconductors for organic electronics. Adv Mater 2012;24:3087-106, 1.

[6] Feng K, Guo H, Wang J, Shi Y, Wu Z, Su M, et al. Cyano-Functionalized Bithiophene Imide-Based n-Type Polymer Semiconductors: Synthesis, Structure-Property Correlations, and Thermoelectric Performance. J Am Chem Soc 2021;143:1539-52.

[7] J. Ohshita, M. Nodono, H.Kai, T. Watanabe, A. Kunai, K. Komaguchi, et al. Synthesis and Optical, Electrochemical, and Electron-Transporting Properties of Silicon-Bridged Bithiophenes. Organometallics 1999;18:1453-9.

[8] Ohshita J, Matsui S, Yamamoto R, Mizumo T, Ooyama Y, Harima Y, et al. Synthesis of Dithienobismoles as Novel Phosphorescence Materials. Organometallics 2010;29:3239-41.

[9] Yabusaki Y, Ohshima N, Kondo H, Kusamoto T, Yamanoi Y, Nishihara H. Versatile synthesis of blue luminescent siloles and germoles and hydrogen-bond-assisted color alteration. Chem Eur J 2010;16:5581-5.

[10] Ohshita J, Fujita R, Tanaka D, Ooyama Y, Kobayashi N, Higashimura H, et al. Synthesis and Optical Properties of Dithienostiboles. Chem Lett 2012;41:1002-3.

[11] Tanaka D, Ohshita J, Ooyama Y, Kobayashi N, Higashimura H, Nakanishi T, et al.

Synthesis, Optical Properties, and Crystal Structures of Dithienostannoles. Organometallics 2013;32:4136-41.

[12] Ohshita J, Murakami K, Tanaka D, Ooyama Y, Mizumo T, Kobayashi N, et al. Synthesis of Group 14 Dipyridinometalloles with Enhanced Electron-Deficient Properties and Solid-State Phosphorescence. Organometallics 2014;33:517-21.

[13] Ohshita J, Yamaji K, Ooyama Y, Adachi Y, Nakamura M, Watase S. Synthesis, Properties, and Complex Formation of Antimony- and Bismuth-Bridged Bipyridyls. Organometallics 2019;38:1516-23.

[14] Huang H, Youn J, Ponce Ortiz R, Zheng Y, Facchetti A, Marks T. Very Large Silacylic Substituent Effects on Response in Silole-Based Polymer Transistors. Chem Mater 2011;23:2185-200.

[15] Yamaguchi S, Tamo K. Theoretical Study of the Electronic structure of 2,2'-Bisilole in Comparison with 1,1'-Bi-1,3-cyclopentadiene: σ*-π* Conjugation and a Low-Lying LUMO as the Origin of the Unusual Optical Properties of 3,3',4,4'-Tetraphenyl-2,2'-bisilole. Bull Chem Soc Jpn 1996;69:2327-34.

[16] Amb CM, Chen S, Graham KR, Subbiah J, Small CE, So F, et al. Dithienogermole as a fused electron donor in bulk heterojunction solar cells. J Am Chem Soc 2011;133:10062-5.

[17] Gendron D, Morin P-O, Berrouard P, Allard N, Aïch BR, Garon CN, et al. Synthesis and Photovoltaic Properties of Poly(dithieno[3,2-b:2′,3′-d]germole) Derivatives. Macromolecules 2011;44:7188-93.

[18] Ohshita J, Nakamura M, Ooyama Y. Preparation and Reactions of Dichlorodithienogermoles. Organometallics 2015;34:5609-14.

[19] Fei Z, Kim JS, Smith J, Domingo EB, Anthopoulos TD, Stingelin N, et al. A low band gap co-polymer of dithienogermole and 2,1,3-benzothiadiazole by Suzuki polycondensation and its application in transistor and photovoltaic cells. J Mater Chem 2011;21:16257.

[20] Sasaki H, Akioka I, Imoto H, Naka K. Arsenic-Bridged Silafluorene and Germafluorene as a Novel Class of Mixed-Heteroatom-Bridged Heterofluorenes. Eur J Org Chem 2021;2021:1390-5.

[21] Ohshita J, Hwang Y-M, Mizumo T, Yoshida H, Ooyama Y, Harima Y, et al. Synthesis of Dithienogermole-Containing π-Conjugated Polymers and Applications to Photovoltaic Cells. Organometallics 2011;30:3233-6.

[22] Patra D, Comí M, Zhang X, Kini GP, Udayakantha M, Kalin AJ, et al. Design, synthesis and characterization of fused bithiazole- and dithiophene-based low bandgap thienylenevinylene copolymers. Polym Chem 2021;12:5942-51.

[23] J. Hou, H-Y. Chen, S Zhang, G. Li, Y. Yang. Synthesis, characterization, and photovoltaic properties of a low band gap polymer based on silole-containing polythiophenes and 2,1,3-benzothiadiazole. J Am Chem Soc 2008;130:16144-5.

[24] G. Lu, H. Usta, C. Risko, L. Wang, A. Facchetti, M. A. Ratner, et al. Synthesis, Characterization, and Transistor Response of Semiconducting Silole Polymers with Substantial Hole Mobility and Air Stability. Experiment and Theory. J Am Chem Soc 2008;130:7670-85.

[25] Ohshita J, Adachi Y, Sagisaka R, Nakashima M, Ooyama Y, Kunugi Y. Synthesis of dithienogermole-containing polythiophenes. Synth Met 2017;227:87-92.

[26] Wang J-Y, Hau SK, Yip H-L, Davies JA, Chen K-S, Zhang Y, et al. Benzobis(silolothiophene)-Based Low Bandgap Polymers for Efficient Polymer Solar Cells. Chem Mater 2010;23:765-7.

[27] Fei Z, Ashraf RS, Huang Z, Smith J, Kline RJ, D'Angelo P, et al. Germaindacenodithiophene based low band gap polymers for organic solar cells. Chem Commun (Camb) 2012;48:2955-7.

[28] Zhang M, Guo X, Wang X, Wang H, Li Y. Synthesis and Photovoltaic Properties of D–A Copolymers Based on Alkyl-Substituted Indacenodithiophene Donor Unit. Chem Mater 2011;23:4264-70.

[29] Zhang Y, Liu Z, Shan T, Wang Y, Zhu L, Li T, et al. Tuning the molecular geometry and packing mode of non-fullerene acceptors by altering the bridge atoms towards efficient organic solar cells. Mater Chem Front 2020;4:2462-71.

[30] Wadsworth A, Chen H, Thorley KJ, Cendra C, Nikolka M, Bristow H, et al. Modification of Indacenodithiophene-Based Polymers and Its Impact on Charge Carrier Mobility in Organic Thin-Film Transistors. J Am Chem Soc 2020;142:652-64.

[31] Usta H, Sheets WC, Denti M, Generali G, Capelli R, Lu S, et al. Perfluoroalkyl-Functionalized Thiazole–Thiophene Oligomers as N-Channel Semiconductors in Organic Field-Effect and Light-Emitting Transistors. Chem Mater 2014;26:6542-56.

[32] Kudla CJ, Dolfen D, Schottler KJ, Koenen J-M, Breusov D, Allard S, et al. Cyclopentadithiazole-Based Monomers and Alternating Copolymers. Macromolecules 2010;43:7864-7.

[33] Barłóg M, Zhang X, Kulai I, Yang DS, Sredojevic DN, Sil A, et al. Indacenodithiazole-Ladder-Type Bridged Di(thiophene)-Difluoro-Benzothiadiazole-Conjugated Copolymers as Ambipolar Organic Field-Effect Transistors. Chem Mater 2019;31:9488-96.

[34] Chavez P, Ngov C, de Fremont P, Leveque P, Leclerc N. Synthesis by direct arylation of thiazole-derivatives: regioisomer configurations-optical properties relationship investigation. J Org Chem 2014;79:10179-88.

[35] Shi Y, Guo H, Qin M, Wang Y, Zhao J, Sun H, et al. Imide-Functionalized Thiazole-Based Polymer Semiconductors: Synthesis, Structure–Property Correlations, Charge Carrier Polarity, and Thin-Film Transistor Performance. Chem Mater 2018;30:7988-8001.

[36] Guo X, Quinn J, Chen Z, Usta H, Zheng Y, Xia Y, et al. Dialkoxybithiazole: a new building block for head-to-head polymer semiconductors. J Am Chem Soc 2013;135:1986-96.

[37] Cao Y, Lei T, Yuan J, Wang J-Y, Pei J. Dithiazolyl-benzothiadiazole-containing polymer acceptors: synthesis, characterization, and all-polymer solar cells. Polym Chem 2013;4:5228-36.

[38] Ohshita J, Nodono M, Kai H, Watanabe T, Kunai A, Komaguchi K, et al. Synthesis and Optical, Electrochemical, and Electron-Transporting Properties of Silicon-Bridged Bithiophenes. Organometallics 1999;18:1453-9.

[39] Zhang Y, Peng J, Li M, Saiz E, Wolf SE, Cheng Q. Bioinspired Supertough Graphene Fiber through Sequential Interfacial Interactions. ACS Nano 2018;12:8901-8.

[40] Getmanenko YA, Tongwa P, Timofeeva TV, Marder SR. Base-catalyzed halogen

dance reaction and oxidative coupling sequence as a convenient method for the preparation of dihalo-bisheteroarenes. Org Lett 2010;12:2136-9.

[41] Usta H, Lu G, Facchetti A, Marks TJ. Dithienosilole- and Dibenzosilole-Thiophene Copolymers as Semiconductors for Organic Thin-Film Transistors. J Am Chem Soc 2006;128:9034-5.

[42] Wang CK, Jiang BH, Su YW, Jeng RJ, Wang YJ, Chen CP, et al. Si-Bridged Ladder-Type Small-Molecule Acceptors for High-Performance Organic Photovoltaics. ACS Appl Mater Interfaces 2019;11:1125-34.

[43] Hou J, Chen HY, Zhang S, Li G, Yang Y. Synthesis, Characterization, and Photovoltaic Properties of a Low Band Gap Polymer Based on Silole-Containing Polythiophenes and 2,1,3-Benzothiadiazole. J Am Chem Soc 2008;130:16144-5.

[44] Huo L, Chen HY, Hou J, Chen TL, Yang Y. Low band gap dithieno[3,2-b:2',3'-d]silole-containing polymers, synthesis, characterization and photovoltaic application. Chem Commun (Camb) 2009:5570-2.

[45] Huo L, Hou J, Chen HY, Zhang S, Jiang Y, Chen TL, et al. Bandgap and Molecular Level Control of the Low-Bandgap Polymers Based on 3,6-Dithiophen-2-yl-2,5-dihydropyrrolo[3,4-c]pyrrole-1,4-dione toward Highly Efficient Polymer Solar Cells. Macromolecules 2009;42:6564-71.

[46] Gendron D, Morin PO, Berrouard P, Allard N, Aïch BR, Garon CN, et al. Synthesis and Photovoltaic Properties of Poly(dithieno[3,2-b:2′,3′-d]germole) Derivatives. Macromolecules 2011;44:7188-93.

[47] Ashraf RS, Chen Z, Leem DS, Bronstein H, Zhang W, Schroeder B, et al. Silaindacenodithiophene Semiconducting Polymers for Efficient Solar Cells and High-Mobility Ambipolar Transistors. Chem Mater 2010;23:768-70.

[48] Chen H, Wadsworth A, Ma C, Nanni A, Zhang W, Nikolka M, et al. The Effect of Ring Expansion in Thienobenzo[b]indacenodithiophene Polymers for Organic Field-Effect Transistors. J Am Chem Soc 2019;141:18806-13.

[49] Tseng CA, Wu JS, Lin TY, Kao WS, Wu CE, Hsu SL, et al. A pentacyclic nitrogen-bridged thienyl-phenylene-thienyl arene for donor-acceptor copolymers: synthesis, characterization, and applications in field-effect transistors and polymer solar cells.

Chem Asian J 2012;7:2102-10.

[50] Love JA, Nagao I, Huang Y, Kuik M, Gupta V, Takacs CJ, et al. Silaindacenodithiophene-based molecular donor: morphological features and use in the fabrication of compositionally tolerant, high-efficiency bulk heterojunction solar cells. J Am Chem Soc 2014;136:3597-606.

[51] Ie Y, Ueta M, Nitani M, Tohnai N, Miyata M, Tada H, et al. Air-Stable n-Type Organic Field-Effect Transistors Based on 4,9-Dihydro-s-indaceno[1,2-b:5,6-b′]dithiazole-4,9-dione Unit. Chem Mater 2012;24:3285-93.

[52] Tian H, Deng Y, Pan F, Huang L, Yan D, Geng Y, et al. A feasibly synthesized ladder-type conjugated molecule as the novel high mobility n-type organic semiconductor. J Mater Chem 2010;20:7998-8004.

[53] He X, Woo AY, Borau-Garcia J, Baumgartner T. Dithiazolo[5,4-b:4',5'-d]phosphole: a highly luminescent electron-accepting building block. Chem Eur J 2013;19:7620-30.

[54] Green JP, Cryer SJ, Marafie J, White AJP, Heeney M. Synthesis of a Luminescent Arsolo[2,3-d:5,4-d′]bis(thiazole) Building Block and Comparison to Its Phosphole Analogue. Organometallics 2017;36:2632-6.

[55] Li S-B, Duan Y-A, Geng Y, Gao H-Z, Qiu Y-Q, Su Z-M. Theoretical design and characterization of pyridalthiadiazole-based chromophores with fast charge transfer at donor/acceptor interface toward small molecule organic photovoltaics. RSC Adv 2015;5:29401-11.

[56] Getmanenko YA, Risko C, Tongwa P, Kim EG, Li H, Sandhu B, et al. Mono- and dicarbonyl-bridged tricyclic heterocyclic acceptors: synthesis and electronic properties. J Org Chem 2011;76:2660-71.

[57] Liang J, Pan M, Chai G, Peng Z, Zhang J, Luo S, et al. Random Polymerization Strategy Leads to a Family of Donor Polymers Enabling Well-Controlled Morphology and Multiple Cases of High-Performance Organic Solar Cells. Adv Mater 2020;32:e2003500.

[58] Xiong Y, Wu Q, Li J, Wang S, Gao X, Li H. Electron-rich pyrroloindacenodithiophenes: synthesis, characterization, and spectroscopic studies. J

Org Chem 2013;78:752-6.

[59] Mitsudo K, Tanaka S, Isobuchi R, Inada T, Mandai H, Korenaga T, et al. Rh-catalyzed dehydrogenative cyclization leading to benzosilolothiophene derivatives via Si-H/C-H bond cleavage. Org Lett 2017;19:2564-7.

[60] Mouri K, Wakamiya A, Yamada H, Kajiwara T, Yamaguchi S. Ladder distyrylbenzenes with silicon and chalcogen bridges: synthesis, structures, and properties. Org Lett 2006;9:93-6.

[61] Martinez JI, Mora-Fuentes JP, Carini M, Saeki A, Melle-Franco M, Mateo-Alonso A. Dibenzoanthradiquinone building blocks for the synthesis of nitrogenated polycyclic aromatic hydrocarbons. Org Lett 2020;22:4737-41.

[62] Patra D, Lee J, Lee J, Sredojevic DN, White AJP, Bazzi HS, et al. Synthesis of low band gap polymers based on pyrrolo[3,2-d:4,5-d′]bisthiazole (PBTz) and thienylenevinylene (TV) for organic thin-film transistors (OTFTs). J Mater Chem C 2017;5:2247-58.

[63] Yuan J, Zhang Y, Zhou L, Zhang G, Yip H-L, Lau T-K, et al. Single-Junction Organic Solar Cell with over 15% Efficiency Using Fused-Ring Acceptor with Electron-Deficient Core. Joule 2019;3:1140-51.

[64] Lu G, Usta H, Risko C, Wang L, Facchetti A, Ratner MA, et al. Synthesis, characterization, and transistor response of semiconducting silole polymers with substantial hole mobility and air stability. experiment and theory. J Am Chem Soc 2008;130:7670-85.

[65] Guo X, Ortiz RP, Zheng Y, Hu Y, Noh YY, Baeg KJ, et al. Bithiophene-imide-based polymeric semiconductors for field-effect transistors: synthesis, structure-property correlations, charge carrier polarity, and device stability. J Am Chem Soc 2011;133:1405-18.

[66] Yang J, Zhao Z, Geng H, Cheng C, Chen J, Sun Y, et al. Isoindigo-Based Polymers with Small Effective Masses for High-Mobility Ambipolar Field-Effect Transistors. Adv Mater 2017;29.

[67] Sun H, Yu H, Shi Y, Yu J, Peng Z, Zhang X, et al. A Narrow-Bandgap n-Type Polymer with an Acceptor-Acceptor Backbone Enabling Efficient All-Polymer Solar

Cells. Adv Mater 2020;32:e2004183.

[68] Sun W, Wang J, Shi Y, Wu Z, Tang Y, Feng K, et al. Terpolymer acceptors based on bithiophene imide for all-polymer solar cells. Dyes Pigm 2021;186.

[69] Yan H, Chen Z, Zheng Y, Newman C, Quinn JR, Dotz F, et al. A high-mobility electron-transporting polymer for printed transistors. Nature 2009;457:679-86.

[70] Wang C, Dong H, Hu W, Liu Y, Zhu D. Semiconducting pi-conjugated systems in field-effect transistors: a material odyssey of organic electronics. Chem Rev 2012;112:2208-67.

[71] Yi Z, Jiang Y, Xu L, Zhong C, Yang J, Wang Q, et al. Triple Acceptors in a Polymeric Architecture for Balanced Ambipolar Transistors and High-Gain Inverters. Adv Mater 2018;30:e1801951.

[72] Yang K, Li X, Huang Y-F, Bhatta RS, Liu J, Tsige M, et al. Investigation of hydrogen-bonding mediated molecular packing of diketopyrrolopyrrole based donor-acceptor oligomers in the solid state. Polymer 2019;160:238-45.

[73] Panidi J, Paterson AF, Khim D, Fei Z, Han Y, Tsetseris L, et al. Remarkable Enhancement of the Hole Mobility in Several Organic Small-Molecules, Polymers, and Small-Molecule:Polymer Blend Transistors by Simple Admixing of the Lewis Acid p-Dopant B(C6F5)3. Adv Sci (Weinh) 2018;5:1700290.

[74] Paterson AF, Lin Y-H, Mottram AD, Fei Z, Niazi MR, Kirmani AR, et al. The Impact of Molecular p-Doping on Charge Transport in High-Mobility Small-Molecule/Polymer Blend Organic Transistors. Adv Electron Mater 2018;4.

[75] Sun H, Guo X, Facchetti A. High-Performance n-Type Polymer Semiconductors: Applications, Recent Development, and Challenges. Chem 2020;6:1310-26.

[76] Usta H, Facchetti A, Marks TJ. n-Channel Semiconductor Materials Design for Organic Complementary Circuits. Acc Chem Res 2011;44:501-10.

[77] Benincori T, Consonni V, Gramatica P, Pilati T, Rizzo S, Sannicolo F, et al. Steric Control of Conductivity in Highly Conjugated Polythiophenes. Chem Mater 2001;13:1665-73.

[78] Ohshita J. Conjugated Oligomers and Polymers Containing Dithienosilole Units. Macromol Chem Phys 2009;210:1360-70.

[79] Wang M, Ford M, Phan H, Coughlin J, Nguyen TQ, Bazan GC. Fluorine substitution influence on benzo[2,1,3]thiadiazole based polymers for field-effect transistor applications. Chem Commun (Camb) 2016;52:3207-10.

[80] Beaujuge P M, Pisula W, Tsao H N, Ellinger S, Mu¨ llen K, Reynolds J R. Tailoring Structure-Property Relationships in Dithienosilole-Benzothiadiazole Donor-Acceptor Copolymers. J Am Chem Soc 2009;131:7514-5.

[81] Wong K-T, Chao T-C, Chi L-C, Chu Y-Y, Balaiah A, Chiu S-F, et al. Syntheses and Structures of Novel Heteroarene-Fused Coplanar π-Conjugated Chromophores. Org Lett 2006;8:5033-6.

[82] Li Y, Meng H, Li Y, Pang B, Luo G, Huang J. Adjusting the energy levels and bandgaps of conjugated polymers via Lewis acid–base reactions. New J Chem 2018;42:18961-8.

[83] Yuan J, Ford MJ, Zhang Y, Dong H, Li Z, Li Y, et al. Toward Thermal Stable and High Photovoltaic Efficiency Ternary Conjugated Copolymers: Influence of Backbone Fluorination and Regioselectivity. Chem Mater 2017;29:1758-68.

[84] Zhang W, Smith J, Watkins S E, Gysel R, McGehee M, Salleo A, et al. Indacenodithiophene semiconducting polymers for high-performance, air-stable transistors. J Am Chem Soc 2010;132:11437–9.

[85] Sun W, Adachi Y, Ohshita J. Synthesis of thiazole-condensed germoles with enhanced electron-deficient properties. Dyes Pigm 2022;203:110333.

[86] Lee JY, Song KW, Song HJ, Moon DK. Synthesis and photovoltaic property of donor–acceptor type conjugated polymer containing carbazole and 4,7-dithiazolylbenzothiadiazole moiety utilized as a promising electron withdrawing unit. Synth Met 2011;161:2434-40.

[87] Kotadiya NB, Mondal A, Blom PWM, Andrienko D, Wetzelaer GAH. A window to trap-free charge transport in organic semiconducting thin films. Nat Mater 2019;18:1182-6.

[88] Hergue N, Mallet C, Savitha G, Allain M, Frere P, Roncali J. Facile Synthesis of 3-Alkoxy-4-cyanothiophenes As New Building Blocks for Donor-Acceptor Conjugated Systems. Org Lett 2011;13:1762–5.

[89] Xu Z, Kim SK, Yoon J. Revisit to imidazolium receptors for the recognition of anions: highlighted research during 2006-2009. Chem Soc Rev 2010;39:1457-66.

[90] Zhang Q, Zhang J, Zuo H, Wang C, Shen Y. A novel colorimetric and fluorescent sensor for cyanide anions detection based on triphenylamine and benzothiadiazole. Tetrahedron 2016;72:1244-8.

[91] Wang L, Ran X, Tang H, Cao D. Recent advances on reaction-based amine fluorescent probes. Dyes Pigm 2021;194:109634.

[92] Ruiz-Capillas C, Herrero AM. Impact of Biogenic Amines on Food Quality and Safety. Foods 2019;8.

[93] Bu L, Rémond M, Colinet P, Jeanneau E, Le Bahers T, Chaput F, et al. Sensitive 1,1-dicyanovinyl push-pull dye for primary amine sensing in solution by fluorescence. Dyes Pigm 2022;202:110258.

[94] Wang Y-Y, Song L, Tang S-Y, Dai Z-Q, Guo J-Y, Shen H-Y, et al. Highly sensitive and selective gas sensing of methylamine and aniline with a new ternary europium complex material. Mater Today Commun 2022;32:104054.

[95] Chen B, Sun X, Li X, Ågren H, Xie Y. TICT based fluorescence “turn-on” hydrazine probes. Sens and Actuators B Chem 2014;199:93-100.

[96] Shabnam Virji, Richard B. Kaner, Weiller BH. Hydrazine Detection by Polyaniline Using Fluorinated Alcohol Additives. Chem Mater 2005;17:1256-60.

[97] Yuan MS, Wang Q, Wang W, Wang DE, Wang J, Wang J. Truxene-cored pi-expanded triarylborane dyes as single- and two-photon fluorescent probes for fluoride. Analyst 2014;139:1541-9.

[98] Al-Zahrani FAM, El-Shishtawy RM, Asiri AM, Al-Soliemy AM, Mellah KA, Ahmed NSE, et al. A new phenothiazine-based selective visual and fluorescent sensor for cyanide. BMC Chem 2020;14.

[99] Long L, You M, Wang H, Wang Y, Yang R. A fluorescent sensing membrane for iodine based on intramolecular excitation energy transfer of anthryl appended porphyrin. Sci China Ser B 2009;52:793-801.

[100] Danchuk AI, Komova NS, Mobarez SN, Doronin SY, Burmistrova NA, Markin AV, et al. Optical sensors for determination of biogenic amines in food. Anal Bioanal

Chem 2020;412:4023-36.

[101] Li L, Li W, Ran X, Wang L, Tang H, Cao D. A highly efficient, colorimetric and fluorescent probe for recognition of aliphatic primary amines based on a unique cascade chromophore reaction. Chem Commun (Camb) 2019;55:9789-92.

[102] Seo H, An M, Kim B-Y, Choi J-H, Helal A, Kim H-S. Highly selective fluorescent probe for sequential recognition of copper(II) and iodide ions. Tetrahedron 2017;73:4684-91.

[103] Zayed MEM, El-Shishtawy RM, Elroby SA, Al-Footy KO, Al-Amshany ZM. Experimental and theoretical study of donor-pi-acceptor compounds based on malononitrile. Chem Cent J 2018;12:26.

[104] Fan J, Hu M, Zhan P, Peng X. Energy transfer cassettes based on organic fluorophores: construction and applications in ratiometric sensing. Chem Soc Rev 2013;42:29-43.

[105] Zhang Y, Yuan L, Jia S, Liu X, Zhao J, Yin G. Dicyanovinyl substituted push-pull chromophores: effects of central C[double bond, length as m-dash]C/phenyl spacers, crystal structures and application in hydrazine sensing. Phys Chem Chem Phys 2019;21:3218-26.

[106] Orrego-Hernandez J, Portilla J. Synthesis of Dicyanovinyl-Substituted 1-(2-Pyridyl)pyrazoles: Design of a Fluorescent Chemosensor for Selective Recognition of Cyanide. J Org Chem 2017;82:13376-85.

[107] Chen Z, Li J, Wang J, Yang K, Zhang J, Wang Y, et al. Imide-Functionalized Fluorenone and Its Cyanated Derivative Based n-Type Polymers: Synthesis, Structure-Property Correlations, and Thin-Film Transistor Performance. Angew Chem Int Ed 2022;61:e202205315.

[108] Ie Y, Uchida A, Kawaguchi N, Nitani M, Tada H, Kakiuchi F, et al. Electron-Accepting pi-Conjugated Molecules with Fluorine-Containing Dicyanovinylidene as Terminal Groups: Synthesis, Properties, and Semiconducting Characteristics. Org Lett 2016;18:4320-3.

[109] Slodek A, Zych D, Kotowicz S, Szafraniec-Gorol G, Zimosz S, Schab-Balcerzak E, et al. “Small in size but mighty in force” – The first principle study of the impact of

A/D units in A/D-phenyl-π-phenothiazine-π-dicyanovinyl systems on photophysical and optoelectronic properties. Dyes Pigm 2021;189:109248.

[110] Percino MJ, Ceron M, Venkatesan P, Perez-Gutierrez E, Santos P, Ceballos P, et al. A low molecular weight OLED material: 2-(4-((2-hydroxyethyl)(methyl)amino)benzylidene)malononitrile. Synthesis, crystal structure, thin film morphology, spectroscopic characterization and DFT calculations. RSC Adv 2019;9:28704-17.

[111] Rout Y, Misra R, Singhal R, Biswas S, Sharma GD. Phenothiazine-based small-molecule organic solar cells with power conversion efficiency over 7% and open circuit voltage of about 1.0 V using solvent vapor annealing. Phys Chem Chem Phys 2018;20:6321-9.

[112] Wadsworth A, Bristow H, Hamid Z, Babics M, Gasparini N, Boyle CW, et al. End Group Tuning in Acceptor–Donor–Acceptor Nonfullerene Small Molecules for High Fill Factor Organic Solar Cells. Adv Funct Mater 2019;29:1808429.

[113] Gong J, Han J, Liu Q, Ren X, Wei P, Yang L, et al. An ideal platform of light-emitting materials from phenothiazine: facile preparation, tunable red/NIR fluorescence, bent geometry-promoted AIE behaviour and selective lipid-droplet (LD) tracking ability. J Mater Chem C 2019;7:4185-90.

[114] Chen B, Ding Y, Li X, Zhu W, Hill JP, Ariga K, et al. Steric hindrance-enforced distortion as a general strategy for the design of fluorescence "turn-on" cyanide probes. Chem Commun (Camb) 2013;49:10136-8.

[115] Zhang G, Loch AS, Kistemaker JCM, Burn PL, Shaw PE. Dicyanovinyl-based fluorescent sensors for dual mechanism amine sensing. J Mater Chem C 2020;8:13723-32.

[116] Kimura Y, Kawajiri I, Ueki M, Morimoto T, Nishida J-i, Ikeda H, et al. A new fluorophore displaying remarkable solvatofluorochromism and solid-state light emission, and serving as a turn-on fluorescent sensor for cyanide ions. Org Chem Front 2017;4:743-9.

[117] Saravanakumar M, Umamahesh B, Selvakumar R, Dhanapal J, Ashok kumar SK, Sathiyanarayanan KI. A colorimetric and ratiometric fluorescent sensor for biogenic

primary amines based on dicyanovinyl substituted phenanthridine conjugated probe. Dyes Pigm 2020;178:108346.

[118] Shi L, Fu Y, He C, Zhu D, Gao Y, Wang Y, et al. A mild and catalyst-free conversion of solid phase benzylidenemalononitrile/benzylidenemalonate to N-benzylidene-amine and its application for fluorescence detection of primary alkyl amine vapor. Chem Commun (Camb) 2014;50:872-4.

[119] Fu Y, Xu W, He Q, Cheng J. Recent progress in thin film fluorescent probe for organic amine vapour. Sci China Chem 2015;59:3-15.

[120] Liu T, Yang L, Feng W, Liu K, Ran Q, Wang W, et al. Dual-Mode Photonic Sensor Array for Detecting and Discriminating Hydrazine and Aliphatic Amines. ACS Appl Mater Interfaces 2020;12:11084-93.

[121] Li Y, Cai Z, Liu S, Zhang H, Wong STH, Lam JWY, et al. Design of AIEgens for near-infrared IIb imaging through structural modulation at molecular and morphological levels. Nat Commun 2020;11.

[122] Su HL, Sredojevic DN, Bronstein H, Marks TJ, Schroeder BC, Al-Hashimi M. Bithiazole: An Intriguing Electron-Deficient Building for Plastic Electronic Applications. Macromol Rapid Commun 2017;38:1600610.

[123] Saito M, Osaka I, Suda Y, Yoshida H, Takimiya K. Dithienylthienothiophenebisimide, a Versatile Electron-Deficient Unit for Semiconducting Polymers. Adv Mater 2016;28:6921-5.

[124] Sun W, Adachi Y, Ohshita J. Preparation of D-A Copolymers Based on Dithiazologermole and Germaindacenodithiazole as Weak Electron Donor Units. Polym J;55:797-805.

[125] Vijay Kumar C, Cabau L, Koukaras EN, Sharma GD, Palomares E. Synthesis, optical and electrochemical properties of the A-pi-D-pi-A porphyrin and its application as an electron donor in efficient solution processed bulk heterojunction solar cells. Nanoscale 2015;7:179-89.

[126] Fron E, Schweitzer G, Jacob J, Van Vooren A, Beljonne D, Mullen K, et al. Singlet-singlet annihilation leading to a charge-transfer intermediate in chromophore-end-capped pentaphenylenes. ChemPhysChem 2007;8:1386-93.

List of publications

Chapter 2:

Synthesis of thiazole-condensed germoles with enhanced electron-deficient properties.

Weipeng Sun, Yohei Adachi, Joji Ohshita

Dyes and Pigments, 2022, 203, 110333.

Chapter 3:

Preparation of D-A copolymers based on dithiazologermole and germaindacenodithiazole as weak electron donor units.

Weipeng Sun, Yohei Adachi, Joji Ohshita

Polymer Journal, 2023, 55, 797-805.

Chapter 4:

Dicyanovinyl-capped thiazologermoles with moderate donor-acceptor interaction as visible photoluminescence turn-on sensors for primary amines.

Weipeng Sun, Yohei Adachi, Joji Ohshita

Dyes and Pigments, 2023, In press.

Other papers not included in this thesis

Bis(benzofurano)pyrrole and Hybrid thienopyrrole Derivatives for Organic Thin-Film Transistors

Weipeng Sun, Cong-Huan Wang, Su-Fang Lv, Jian-Xiong Jiang, Xugang Guo and Fei-Bao Zhang

Organic Electronics, 2020, 105548.

Terpolymer acceptors based on bithiophene imide for all-polymer solar cells

Weipeng Sun, Junwei Wang, Yongqiang Shi, Ziang Wu, Yumin Tang, Kui Feng, Han Young Woo, Xugang Guo, Fei-Bao Zhang

Dyes and Pigments, 2021, 186, 109049.

Sulfur-Containing Bent N-Heteroacenes

Fangwei Ding, Debin Xia, **Weipeng Sun**, Wei Chen, Yulin Yang, Kaifeng Lin, Feibao Zhang, Xugang Guo

Chemistry - A European Journal, .2019, 25, 15106–15111

Imide-functionalized acceptor–acceptor copolymers as efficient electron transport layers for high-performance perovskite solar cells

Yongqiang Shi, Wei Chen, Ziang Wu, Yang Wang, **Weipeng Sun**, Kun Yang, Yumin Tang, Han Young Woo, Ming Zhou, Aleksandra B. Djurišić, Zhubing He and Xugang Guo

Journal of Materials Chemistry A. 2020, 8, 13754-62.

Acknowledgements

This thesis is a summary of my studies from 2020 to 2023 under the direction of Professor Joji Ohshita at Hiroshima University.

I would like to express my sincere gratitude to my supervisor, Professor Joji Ohshita for his kind and helpful advice and encouragement. I also would like to thank Assistant Professor Yohei Adachi, Dr. Zhang Dian and Dr. Sakino Takase for their useful advices and helps. Furthermore, I am grateful to a scholarship from the China Scholarship Council (CSC) to support my living expenses.

I would like to thank, Ms. Wang Conghuan, Mr. Kei Oshima, Ms. Maho Kurihara, Mr. Mitsuru Sakabe, Mr. Kohei Yamada, Mr. Arata Tanaka, Mr. Takumi Hasegawa, Mr. Tsubasa Yoshio, Mr. Lin Zhixin, Mr. Shota Terao, Mr. Ryuji Matsuura, Mr. Ryuto Miyazaki, Mr. Kosuke Tsutsui, Mr. Toshiki Kaneko, Ms. Kanaka Sasaki, Ms. Riho Tanaka, Mr. Yuto Hattori, Mr. Kazuki Hara for their kindness and collaboration.